Rational Design for Advanced Functional Materials

Based on POSS

Jong-Hwan Jeon

2013

Department of Polymer Chemistry

Graduate School of Engineering

Kyoto University

Preface

The study presented in this thesis has been carried out under the direction of Professor Yoshiki Chujo at the Department of Polymer Chemistry, Graduate School of Engineering, Kyoto University from October 2010 to September 2013 as a regular student for doctor course. The studies are concerned with "Rational Design for Advanced Functional Materials Based on Polyhedral Oligomeric Silsesquioxanes (POSS)".

The author wishes to express his sincerest gratitude to Professor Yoshiki Chujo for his kind guidance, valuable suggestions and warm encouragement throughout this work. The author also wishes to express his gratitude to Lecturer Yasuhiro Morisaki and Assistant Professor Kazuo Tanaka for valuable advices and helpful discussions during the course of this work. The author is deeply grateful to Mr. Fumiyasu Ishiguro, Mr. Tatsuhiro Hiraoka, and Mr. Masahiro Murakami for their great contribution to this work. The author is also grateful to Mr. Ryousuke Yoshii, Mr. Hiroyuki Okada, and Mr. Takuya Matsumoto for valuable discussions and critical comments and is indebted to all his colleagues for their active collaborations.

Furthermore, the author appreciates Associate Professor Kyung-Min Kim at the Department of Polymer Science and Engineering, Chung-Ju National University for opening a good chance of studying in Japan, kind support, and valuable suggestions.

Finally, the author expresses his heartfelt thanks to his parents, Mr. Jung-Sik Jeon and Mrs. Min-Ja Jeong for their constant financial support, encouragement, and deep affection.

Jong-Hwan Jeon

Department of Polymer Chemistry
Kyoto University
September 2013

Contents

General Introduction

General Introduction

Background

1. Organic-Inorganic Hybrid Materials

The design of new materials with enhanced properties continues to be a driver for the investigation of hybrid materials. As hybrid materials are synthetic products based on inorganic and organic components, they display enhanced properties by bridging the property space between two dissimilar types of materials.[1–8] Organic–inorganic hybrid materials are generally prepared with solution or sol-gel processing methods, in situ polymerization techniques, and solid-state reactions. They can be readily prepared in diverse forms such as monolithic structures, thin films, fibers, particles, and powders. These versatile and mild approaches to materials with new or enhanced properties makes hybrids attractive candidates for optical devices, separations media, catalysts and catalyst supports, microelectronic coatings, sensor coatings, and structural materials. Because of such large potential, organic–inorganic hybrid materials are the subjects with intense interests from industrial and academic researchers. Typical hybrid materials contain a cross-linked inorganic phase bound covalently with an organic phase or organic phase incorporated into the inorganic matrix by physical interactions of two phases. One of key factors for controlling the material functions is the regulation of the domain sizes involved in the hybrids. A combination of organic and inorganic materials in the molecular level is promised to generate the enhanced bulk properties. That is, the structures of organic–inorganic hybrids or bioactive components in a
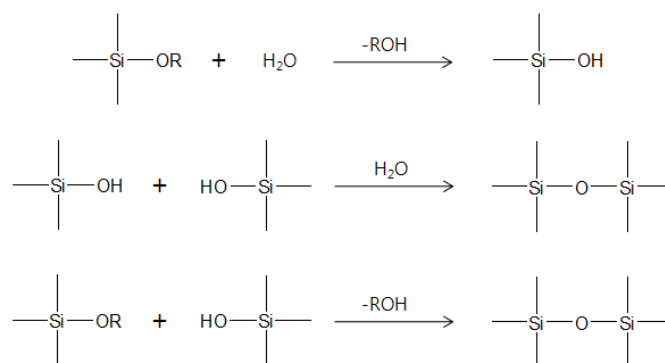
**Scheme 1.** Sol-gel reactions of alkoxysilanes.

single material engineered at the molecular or nanometer scale have made accessible to an immense new area in materials science and innovative advanced materials for promising applications. For example, a polymer hybrid with inorganic fillers can be functional materials that show the processability and flexibility, thermal stability, high modulus, and oxidation resistance of inorganic ceramics.[9–11]

   As mentioned above, one of the effective methods for preparing hybrid materials is the sol-gel process involved inorganic precursors that undergo various reactions resulting in the formation of a three dimensional molecular network.[12] A common example is the hydrolysis and condensation reactions of silicon alkoxide to form the silica gel (Scheme 1). The reaction allows low-temperature fabrication of networks facilitating the introduction of organic elements without deterioration of their functionalities, and the resulting hybrids possess high glass transition temperature, low beam propagation loss, and high uniformity and are more stable because of the greater rigidity and higher thermal stability of silica than organic polymers.[13,14] Theses hybrid materials capitalize on the unique properties offered by the two components to generate novel materials with desired characteristics. Chujo *et al.* have

explored the development of new preparative methods for novel organic–inorganic polymer hybrids by utilizing the sol-gel technique. Main focus is to create the organic–inorganic polymer hybrids not using covalent bonding but using physical bonding between organic and inorganic components. The hydrogen bonding interaction with residual silanol groups from sol-gel process under the acidic condition and organic polymers having strong hydrogen acceptor groups such as poly(2-methyl-2-oxazoline), poly(*N*-vinylpyrrolidone), and poly(*N,N*-dimethylacrylamide) results in the molecular dispersion of organic polymers in the silica matrix.[15-21] In this sense, other interactions such as aromatic (π-π)[22,23] or ionic[24] interactions can be used in the preparation of homogeneous polymer hybrids. Homogeneous interpenetrating network polymer hybrids were prepared by applying an in situ polymerization method.[25-28] In this connection, recently, new concept of "compatibilizer" between organic polymers and silica gel is applied to obtain transparent polymer hybrids by utilizing cyclodextrin[29] or amphiphilic solvents (dimethylformamide (DMF) and dimethylacetamide (DMAC)[30]) as a compatibilizer by the Chujo group.

In addition, organic–inorganic polymer hybrids with responsive functions to various external stimuli such as light[31], heat[32], or the polarity of microenvironment[33] were accomplished. Thus, the field of organic–inorganic hybrid materials is vigorous and innovative. New synthetic inorganic and organic precursors tailored for more precise structural control and chemistry are discovered regularly. Novel polymerization and processing techniques still have been developed to prepare advanced functional hybrid materials.
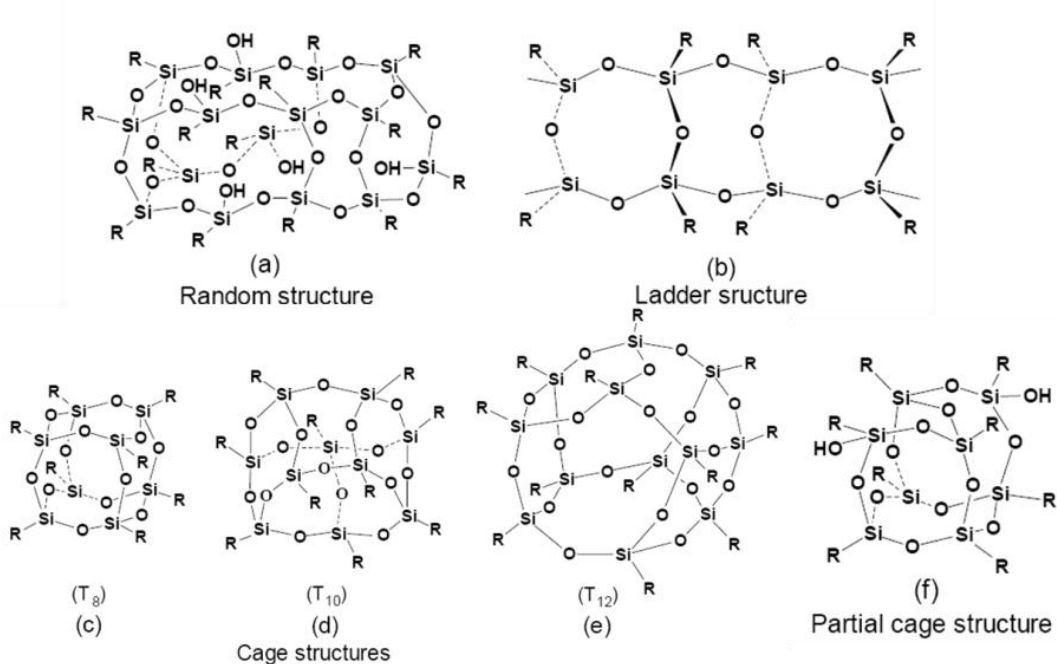
Figure 1. Structures of silsesquioxanes.

2. Silsesquioxanes

The term silsesquioxanes are the general name for organosiloxide species with the empirical formulas $(RSiO_{3/2})_n$ (R=H, hydrocarbon) and closely related compounds. The structures of silsesquioxanes have been known as irregular, ladder, cage, and partial cage structures, as illustrated in Figure 1.[34] Most of the precursors to silsesquioxanes find their origin in trichlorosilanes. These are frequently prepared from the silicone industry's direct process reaction of methyl chloride or hydrogen chloride with silicon metal, catalyzed with copper. Alkyl group larger than methyl and organo-functional groups are formed by platinum-catalyzed hydrosilylation reactions with trichlorosilane or by organometallic coupling reactions with chlorosilane.[35]

The chemistry of the silsesquioxane and its derivatives has been a subject with intense interests for more than a half century. Such examples include poly(phenylsilsesquioxane)

(PPSQ)[36], poly(methylsilsesquioxane) (PMSQ)[37], and poly(hydrosilsesquioxane) (PHSQ)[38]. Especially, PPSQ having a rigid ladder-like structure from phenyltrichlorosilane or phenyltrialkoxysilane can be used for a variety of applications due to excellent properties such as solubility in a common solvent, thermal stability, mechanical strength, oxidative resistance, and electrical insulation. The use of PPSQ has been focused in various fields of industry such as coating films for semiconductor devices, liquid crystal display elements, magnetic recording media, optical fiber coatings, gas separation membranes, binders for ceramics, and carcinostatic drugs.[39] Furthermore, the application fields of PSSQ have been extended to the blend or block copolymerization with organic polymers.[40]

3. Polyhedral Oligomeric Silsesquioxane (POSS)

Over the past decade, POSS molecules have attracted considerable interest as "self-healing" high-temperature nanocomposites and space-survivable coatings[41], low-k dielectric materials[42], and as templates for the preparation of nanostructured materials such as liquid crystalline polymers[43], catalyst[44], and dendrimers[45]. POSS compounds embody a truly hybrid (organic–inorganic) architecture, which contains an inner inorganic framework made up of silicon and oxygen $(SiO_{3/2})_n$, that is externally covered by organic substituents. These cage structures can be regarded as small three-dimensional pieces of silica as their oligomerization is sufficient to result in rigid structures that resemble, for example, crystalline forms of silica such as β-cristobalite or β-tridymite, whereas their organic substituents allow solubility in the most common organic solvents. POSS reagents are nanostructured with the sizes of 1–3 nm and can be thought of as the smallest particles of silica possible. However, unlike silica, silicones, or fillers, each POSS molecule may contain organic substituents on its outer surface that make the POSS nanostructures compatible with polymers, biological systems, or surfaces.
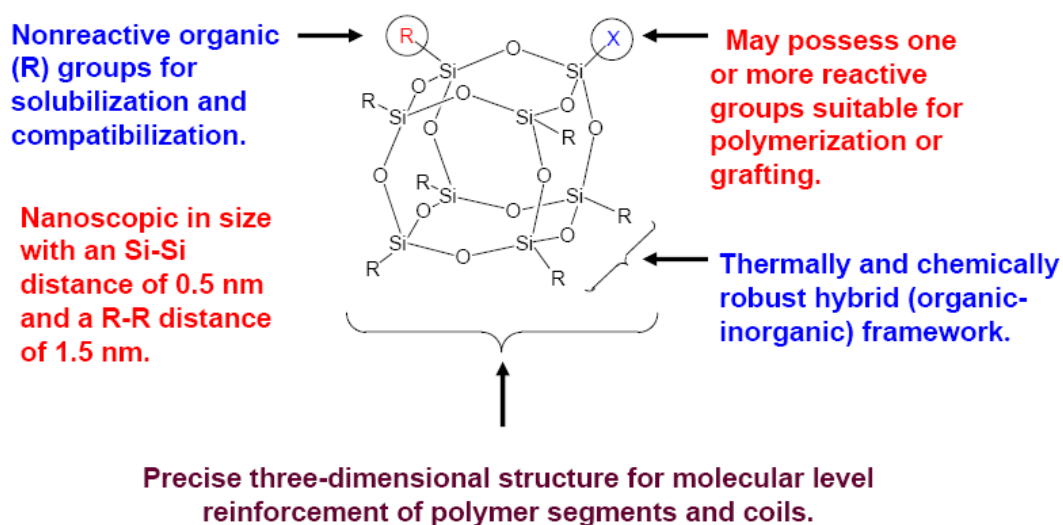
**Figure 2.** Polyhedral oligomeric silsesqioxane (POSS)

A variety of POSS nanostructured chemicals which contain one or more covalently bonded reactive functionalities that are suitable for polymerization or grafting has been prepared.[46] Nanostructured POSS chemicals can be easily incorporated into common plastics via copolymerization, grafting, or blending.[47] Since unlike traditional organic compounds, POSS chemicals release no volatile organic components, they are odorless and environmentally friendly. The incorporation of POSS into polymeric materials often results in dramatic improvements in polymer properties which include, but are not limited to, increases in use temperature, oxidation resistance, surface hardening, and improved mechanical properties as well as reductions in flammability and heat evolution. These enhancements have been shown to apply to a wide range of thermoplastic and a few thermoset systems.[48,49]

Many interesting works based on well-defined POSS have been conducted by some groups. Feher and coworkers discovered a new methodology for preparing discrete Si/O frameworks with well-defined structures, particularly functionalized frameworks from fully-condensed frameworks using base or acid catalyzed cleavage.[50] Laine and coworkers investigated various octa-functional cubes with polymerizable moieties that offer access to

highly cross-linked (thermoset) nanocomposites.[51] Duchateau *et al.* proposed the usefulness and drawbacks of silsesquioxanes as model supports in developing silica-supported olefin polymerization catalysts.[52] Lichtenhan *et al.* reported the utilization of POSS macromonomers or graftable agents as the building units for the construction of organic–inorganic hybrid structure.[53,54]

4. Survey of This Thesis

The author prepared a series of studies including various advanced functional materials using POSS that are described in this thesis: In Chapter 1, the author describes the POSS-based ionic liquid crystal which has the extremely-high thermal stability. The series of POSS ionic liquid crystal were prepared by acid-base neutralization using octa-carboxy POSS (POSS-$(COOH)_8$) and 1-methyl-3-alkyl-imidazolium$^+$OH$^-$ (alkyl: C_4 to C_{18}) (Chart 1). The decreases of the melting temperatures were observed by tethering the ion pairs to the POSS core. Notably, the significant enhancement on the temperature range of the liquid crystal was received: The isotropic phase of the obtained POSS salt was not detected until the decomposition occurred during the heating. The thermal stabilizing by the POSS core extremely stabilized the deformation of the liquid crystal.
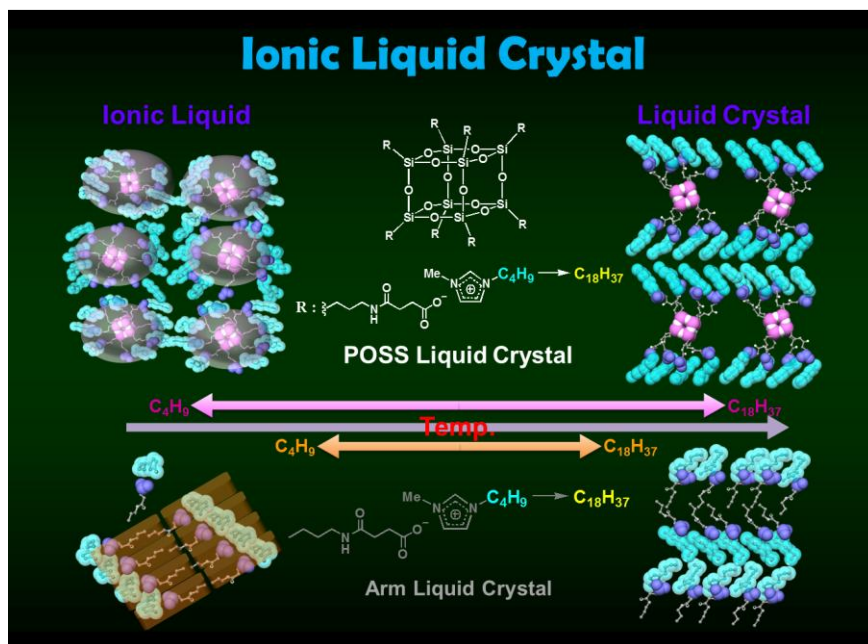
Chart 1.

In Chapter 2, the author demonstrates the ability of POSS-based filler for improving thermal properties of ionic liquids (ILs). The homogeneous IL mixtures containing the octa-carboxy POSS (POSS-(COOH)$_8$) as a filler were prepared by the solution process (Chart 2).
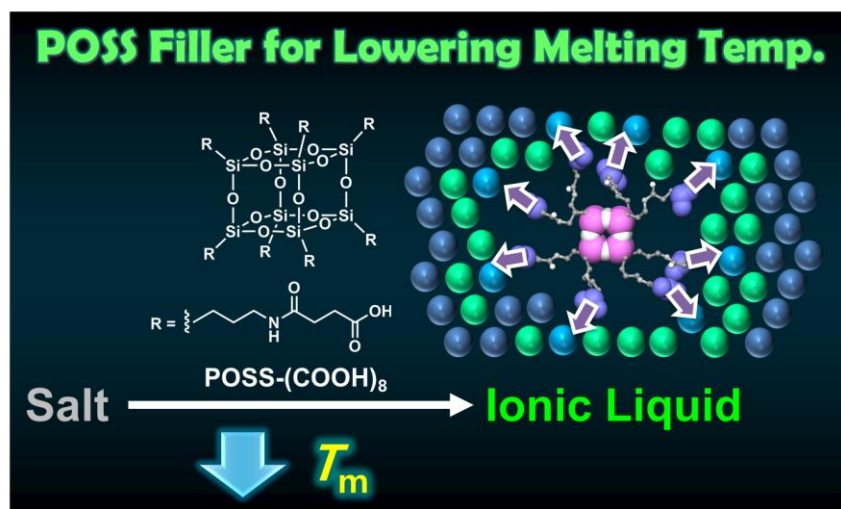
Chart 2.

13

The melting temperatures of the ionic pairs were lowered by adding the POSS filler. Based on this effect, some of ionic salts were transformed to an IL by adding the POSS filler. Moreover, the reinforcement of thermal stability was also observed from the salts which have intrinsically a low decomposition temperature.

In Chapter 3, the author shows the synthesis of the novel POSS derivative as the octa-substituted POSS with sulfonic acid groups. From the series of the measurements, POSS filler showed the large enhancement to the thermal stability and the lowering effect on the melting temperatures of a wide variety of ILs (Chart 3). In particular, some of ion salts can be transformed to the liquids by adding the POSS filler. The mechanism can be explained by thermodynamic phenomenon that the introduction of the POSS fillers significantly reduced both the fusion enthalpy and entropy via the robust hydrogen bonds between the sulfonic acid groups and ion pairs.

Chart 3.

14
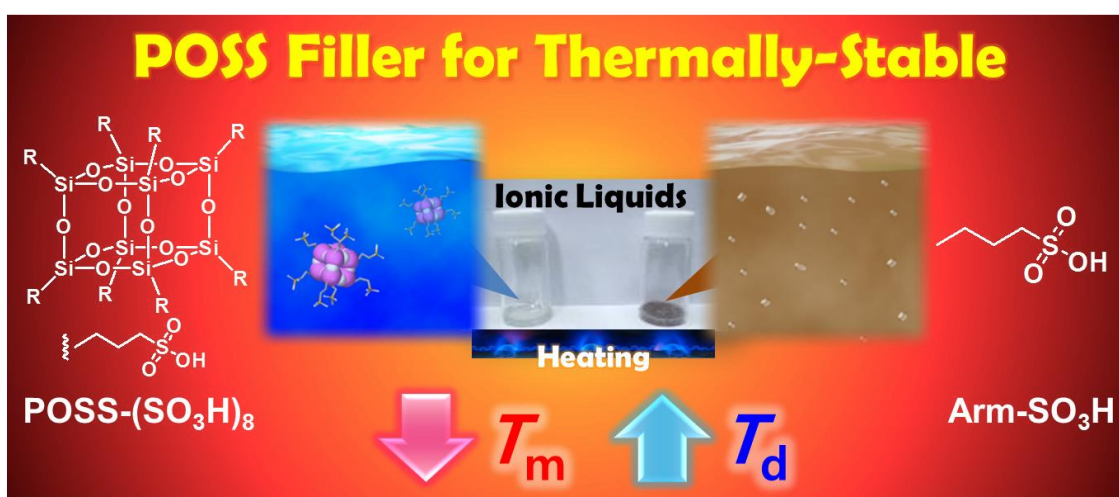
In Chapter 4, the author illustrates the development of efficient molecular fillers using POSS-based dual functional molecules for lowering refractive indices and improving thermomechanical properties of polymeric matrices (Chart 4). The composite films were prepared by solution mixing of conventional polymers (PMMA and PS) with various kinds of the POSS fillers. Refractive indices of polymer composites were decreased by adding all POSS fillers. In addition, thermal stabilities and mechanical properties were enhanced by POSS fillers.
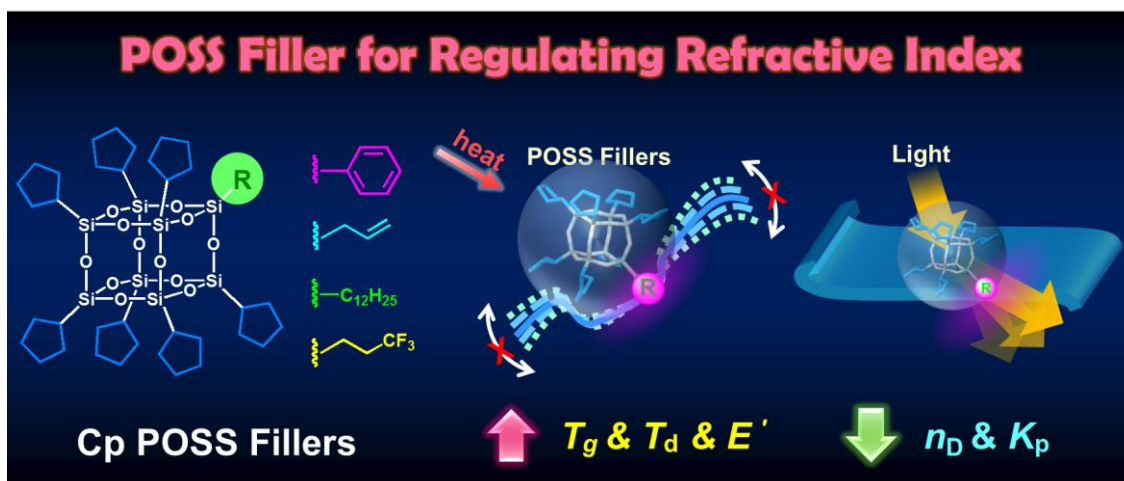
Chart 4.

In Chapter 5, the author explains the synthesis of the modified dendrimers having the cubic silica core and dendrimer/dye complexes as a bioprobe (Chart 5). The unique optical properties were observed from the dyes at the solid–liquid critical surfaces. By the complexation with the dendrimers, the dispersibility of trisvinyl-pyridinium triphenylamine (TP3PY) in the buffer was improved. In addition, fluorescence quantum yields and emission

life times were also enhanced. From the series of studies on the photochemistry of the dyes in the dendrimers, the molecular rotations occurring at the excited state could be suppressed by the complex formation with dendrimers.
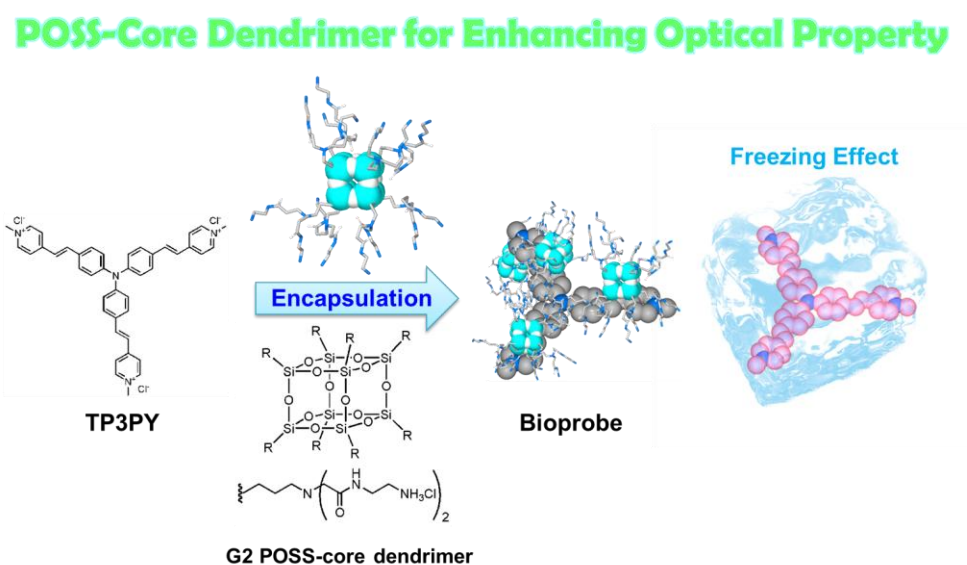
Chart 5.

In Chapter 6, the author demonstrates the selective encapsulation of guanosine triphosphate (GTP) into the POSS-core dendrimer via the complex formation with the naphthyridine derivatives (Chart 6). At the surface of the hydrophobic POSS core inside dendrimer, the complex stability via hydrogen bonds between the guanine moiety of GTP and the naphthyridine derivatives was significantly improved. In addition, the negatively-charged compounds such as triphosphates made a strong interaction with the ammonium groups at the surface dendrimer.
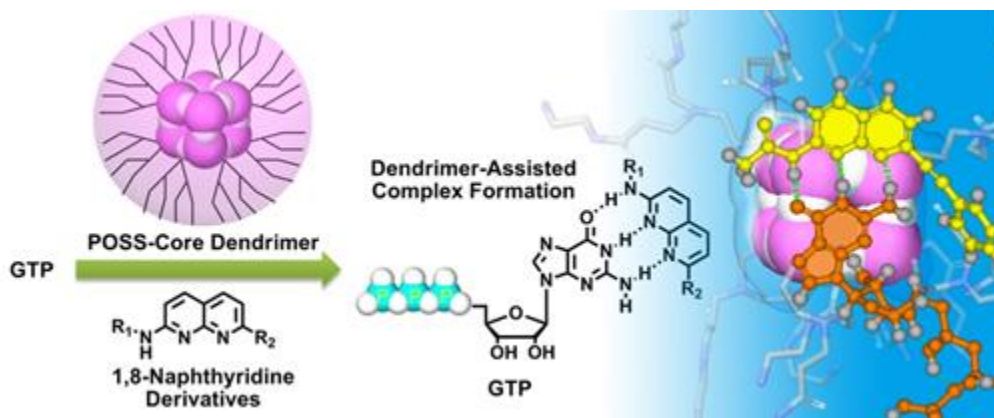
Chart 6.

In Charter 7, the author describes the light-driven artificial enzyme for GTP oxidation. The POSS-based water-soluble network polymers involving the naphthyridine ligands to capture GTP inside the networks and the Ru-complexes to oxidize the captured GTP were synthesized (Chart 7). The complex formation with GTP should occur inside POSS network polymers. Next, the photo-catalytic activity of the naphthyridine ligand and the ruthenium complex-modified POSS network polymers were investigated. The captured GTP was efficiently decomposed by POSS network polymers with the Ru-complexes under light irradiation.
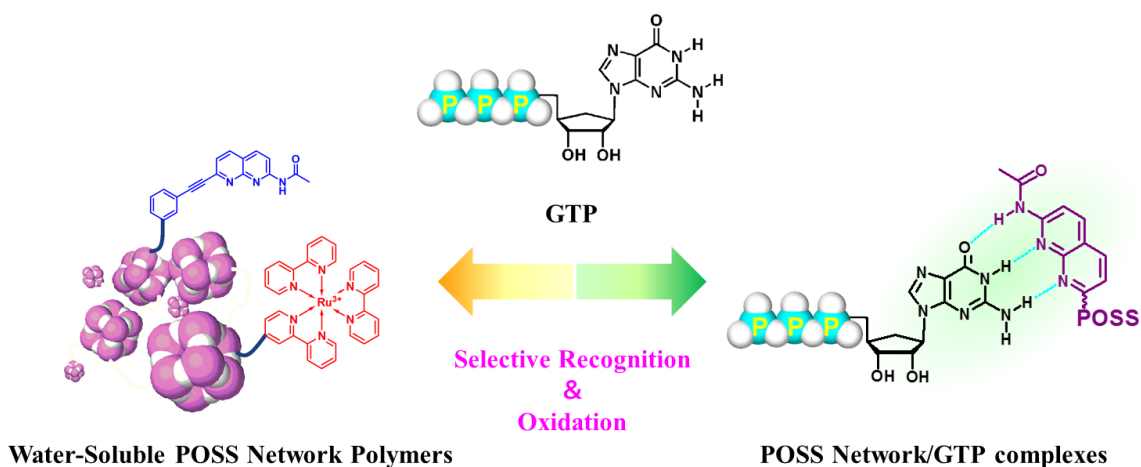
Chart 7.

In Charter 8, the author explains the binding of non-fluorescent nucleotides to the designed ligands in the POSS network polymers. The cytidine triphosphate (CTP)-, adenosine triphosphate (ATP)- and uridine triphosphate (UTP)-selective recognition were accomplished using the water-soluble network polymers composed of POSS (Chart 8). The water-soluble POSS network polymers containing the designed ligands were synthesized for capturing the target base molecules inside the networks. The author observed the designed ligands selectively captured each target molecule. In addition, the affinity of the complexation with nucleoside triphosphate (CTP, ATP, and UTP) by POSS network polymers was enhanced, respectively.
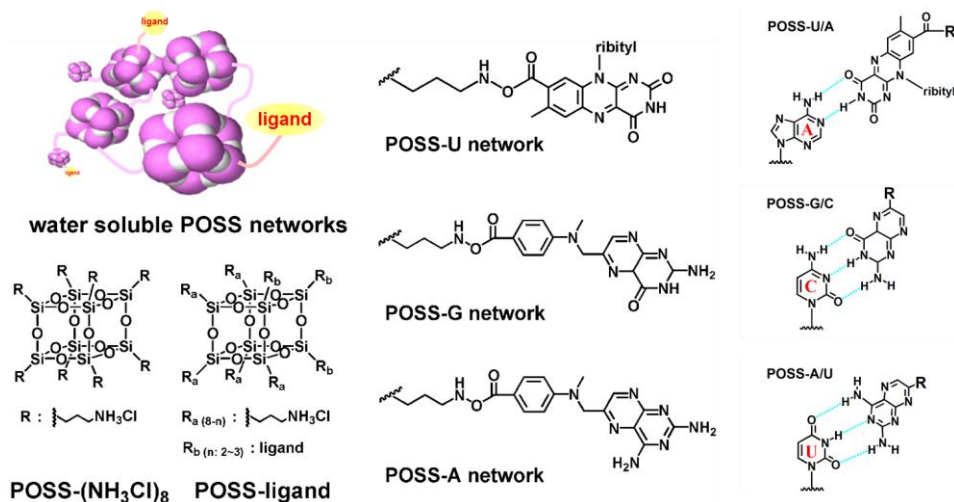
Chart 8.

18

References

1. (a) Andrews, R.; Weisenberger, M. C. *Curr. Opin. Solid State Mater. Sci.* **2004**, *8*, 31. (b) Velasco-Santos, C.; Martinez-Hernandez, A. L.; Castano, V. M. *Compos. Interface* **2005**, *11*, 567.

2. Wen, J.; Wilkes, G.L. *Chem. Mater.* **1996**, *8*, 1667.

3. Mark, J.E. Heterog. *Chem. Rev.* **1996**, *3*, 307.

4. Mackenzie, J. D.; Bescher, E. P. *J. Sol-Gel Sci. Technol.* **1998**, 13,371.

5. Chujo, Y. *Curr. Opin. Solid-State Mater. Sci.* **1996**, *1*, 806.

6. Loy, D. A.; Shea, K. *J. Chem. Rev.* **1995**, *95*, 1431.

7. Sanchez, C.; Lebeau, B.; Ribot, F.; In, M. *J. Sol-Gel Sci. Technol.* **2000**, *19*, 31.

8. Arkles, B. *CHEMTECH* **1999**, *29*, 7.

9. Giannelis, E. P. *Adv. Mater.* **1996**, *8*, 29.

10. Sanchez, C.; Solar-Illia, G. J. De A. A.; Ribot, F.; Lalot, T.; Mayer, C. R.; Cabuil, V. *Chem. Mater.* **2001**,*13*,3061.

11. Carrado, K. A.; Xu, L. *Chem. Mater.* **1998**, *10*, 1440.

12. Kawasumi, M.; Hasegawa, N.; Kato, M.; Usuki, A.; Okada, A. *Macromolecules* **1997**, *30*, 6333.

13. Brinker, C. J.; Scherer, H. W. Sol-Gel Science: The Physics and Chemistry of Sol-Gel Processing; Academic Press: San Diego, 1990

14. Levy, D.; Esquivias, L. *Adv. Mater.* **1995**, *7*, 120.

15. Ikushima, A. J.; Fujiwara, T.; Saito, K. *Jpn. J. Appl. Phys.* **2000**. *88*, 1201.

16. Chujo, Y.; Ihara, E.; Kure, S.; Saegusa, T. *Macromolecules* **1993**, *26*, 5681.

17. Chujo, Y. *POLYM. Mater. Encyclopedia* **1996**, *6*, 4793.

18. Chujo, Y.; Matsuki, H.; Kure, S.; Saegusa, T.; Yazawa, T. *J. Chem. Soc. Chem. Commun.* **1994**, 635.

19. Saegusa, T.; Chujo, Y. Makromol. *Chem. Marcromol. Symp.* **1991**, *51*, 1.

20. Saegusa, T.; Chujo, Y. Makromol. *Chem. Marcromol. Symp.* **1992**, *64*, 1.

21. Tamaki, R.; Chujo, Y. *Comp. Interfaces* **1999**, *6*, 259.

22. Tamaki, R.; Chujo, Y.; Yazawa, T.; Kuraoka, K. *J. Mater. Chem.* **1999**, *9*, 1741.

23. Tamaki, R.; Samura, K.; Chujo, Y. *Chem. Commun.* **1998**, 1131.

24. Tamaki, R.; Han, S. Y.; Chujo, Y. *Polym. Prep. Jpn.* **1998**, 47, 1016.

25. Tamaki, R.; Chujo, Y. *Chem. Mater.* **1999**, *11*, 1719.

26. Tamaki, R.; Chujo, Y. *Bull. Chem. Soc. Jpn.* **1998**, *71*, 2749.

27. Tamaki, R.; Chujo, Y. *J. Mater. Chem.* **1998**, *8*, 1113.

28. Ogoshi, T.; Itoh, H.; Kim, K. M.; Chujo, Y. *Macromolecules* **2002**, *35*, 334.

29. Ogoshi, T.; Itoh, H.; Kim, K. M.; Chujo, Y. *Polym. J.* **2003**, *35*, 178.

30. Ogoshi, T.; Chujo, Y. *Macromolecules* **2003**, *36*, 654.

31. Ogoshi, T.; Chujo, Y. *submitted to Chem. Mater*.

32. Imai, Y.; Naka, K.; Chujo, Y. *Macromolecules* **1998**, *31*, 532.

33. Imai, Y.; Itoh, H.; Naka, K.; Chujo, Y. *Macromolecules* **2000**, *12*, 4343.

34. Imai, Y.; Chujo, Y. *Macromolecules* **2000**, *33*, 3059.

35. Baney, R. H.; Itoh, M.; Sakakibara, A.; Suzuki, T. *Chem. Rev.* **1995**, *95*, 1409.

36. West, R.; Barton, T. J. *J. Chem. Educ.* **1980**, *57*, 165.

37. Lee, E. C.; Kimura, Y. *Polym. J.* **1998**, *30*, 234.

38. Maciel, G. M.; Sullivan, M. J.; Sindorf, D. W. *Macromolesules* **1981**, *14*, 1607.

39. Frye, C. L.; Collins, W. T. *J. Am. Chem. Soc.* **1970**, *92*, 5586.

40. Gozdz, A. S. *Polym. Adv. Technol.* **1994**, *5*, 70.

41. Coleman, M. M.; Pehlert, G. J.; Painter, P. C. *Macromolecules* **1996**, *29*, 6820.

42. Gonzalez, R. I.; Phillips, S. H.; Hoflund, G. B. *J. Spacer. Rockets* **2000**, *37*, 463.

43. Hacker, N. P. *MRS Bull.* **1997**, *22*, 33.

44. Laine, R. M.; Zhang, C.; Sellinger, A.; Viculis, L. *Appl. Organomet. Chem.* **1998**, *12*, 715.

45. Feher, F. J.; Newman, D. A.; Walzer, J. F. *F. Am. Chem. Soc.* **1989**, *111*, 1741.

46. Ropartz, L.; Foster, D. F.; Morris, R. E.; Slawin, A. M. Z.; Cole-Hamilton, D. J. *J. Chem. Soc., Dalton Trans.* **2002**, 1997.

47. Lichtenhan, J. D.; Schwab, J. J.; Reinerth, W. A., Sr. *Chem. Innovation* **2001**, *1*, 3.

48. Haddad, T. S.; Stapleton, R.; Jeon, H. G.; Mather, P. T.; Lichtenhan, J. D.; Plillips, S. *Polym. Prepr.* **1999**, *40*, 496.

49. Ellsworth, M. W.; Gin, D. L. *Polym. News* **1999**, *24*, 331.

50. Feher, F. J.; Weller, K. J. *Inorg. Chem.* **1991**, *30*, 880.

51. Zhang, C.; Babonneau, F.; Bonhomme, C.; Laine, R. M.; Soles, C. L.; Hristov, H. A.; Yee, A. F. *J. Am. Chem. Soc.* **1998**, *120*, 8380.

52. Duchateau, R. *Chem. Rev.* **2002**, *102*, 3525.

53. Haddad, T. S.; Lichtenhan, J. D. *J. Inorg. Organometal. Polym.* **1995**, *5*, 237.

54. Gilman, J. W.; Schlitzere, D. S.; Lichtenhan, J. D. *J. Appl. Polym. Sci.* **1996**, *60*, 591.

Chapter 1

POSS Ionic Liquid Crystals

Chapter 1

POSS Ionic Liquid Crystals

Abstract : This chapter shows the POSS-based ionic liquid crystal which has the extremely-high thermal stability. The author synthesized the POSS-based imidazolium salts with various lengths of alkyl chains possessed melting temperature below 100 °C and turned to be ILs. Corresponding to the results, by tethering the ion pairs to the POSS core, the decreases of the melting temperatures were observed. Moreover, over the whole range of the alkyl chains with n = 4－18, POSS-based ILs showed higher thermal stability than corresponding ILs not connected to POSS. These phenomena can be explained by the decrease of fusion enthalpy. In contrast to the lowering effect on melting temperatures, POSS-C_{18}Im showed much higher mesophase stability. Such stabilization effect caused by connecting to POSS can be illustrated by the restriction of free molecular motions derived from anchoring molecules to rigid core and the tendency of POSS molecule to form spindle orientation.

Introduction

Ionic liquid (IL) crystals are the latest topic with high relevance because there are much possibility to receive the significant properties originated from each factor and the combination of the characteristics of ILs and the optical properties of liquid crystals.[1-4] For example, it has been reported that small amount of ionic chiral sources can efficiently induce the enatiomeric bulk structures.[5-7] By using electrostatic interaction originated among ionic moieties, robust chiral structures can be produced. As another instance, based on the formation of regularly-ordered structures, the ionic moieties should be also restrictedly aligned. These well-ordered ionic moieties are promised to work as an efficient cation carrier and a scaffold for ordering cations. These materials have abundant possibility to express the intriguing optical and magnetic properties. Thus, the preparation and formation of stable liquid crystalline with ionic species is of great importance to develop advanced materials.[8-12]

The concept of supported ionic liquid phase (SILP) has been recently proposed, and several materials based on SILP and their significant characteristics were presented. Silica-supported liquid crystalline showed high thermal stability and effective catalytic activity.[13-19] Carmichael *et al.* have demonstrated the silicon wafer-assisted SILP materials in their early works. The thermal stability was greatly enhanced owing to rigidity of silica moiety. Inspired by their works, Wasserscheid *et al.* have reported the SILP materials using silicon-nanoparticles as a support for preparing the mesoporous structures.[20] These are the successful and representative examples to demonstrate unique properties of SILP materials. To construct the advanced materials based on the concept of SILP materials, fine-tunings of the properties are required according to the preprogramed designs at the molecular level. Recently, Chujo *et al.* have reported the polyhedral oligomeric silsesquioxane (POSS)-based ionic liquids.[16,17] By tethering the multiple ion pairs composed of imidazolium cation and carboxylate to the vertices of POSS core, the decrease of the melting temperatures and the increase of the

25

thermal stability are simultaneously observed due to the structural characteristics of POSS. Finally, the author presented the room-temperature ILs using POSS. Next interests have shifted to apply the unique thermal properties of POSS for realizing the optical materials. In particular, the author aimed to construct the unique optical materials from SILP materials based on the structural features of POSS.

In this chapter, the author presents the POSS-based ionic liquid crystal which has the extremely-high thermal stability. The author designed and synthesized the ionic liquid crystals based on the POSS-carboxylate and imidazolium ion pairs. Corresponding to the results as the author obtained, by tethering the ion pairs to the POSS core, the decreases of the melting temperatures were observed. Notably, the significant enhancement on the temperature range of the liquid crystal was received: The isotropic phase of the obtained POSS-IL was not detected until the decomposition occurred during the heating. The thermal stabilizing by the POSS core extremely stabilized the deformation of the liquid crystal. This is the first example to detect the significant enhancement to the liquid crystal formation by the structural characteristics of the molecular cube and to offer the unique thermally-stable materials as a liquid crystal.

Experimental Section

General. ^{1}H NMR and ^{13}C NMR spectra were measured with a JEOL EX–400 (400 MHz for ^{1}H and 100 MHz for ^{13}C) spectrometer. ^{29}Si NMR spectra were measured with a JEOL JNM– A400 (80 MHz) spectrometer. Coupling constants (*J* value) are reported in hertz. The chemical shifts are expressed in ppm downfield from tetramethylsilane, using residual chloroform ($\delta = 7.24$ in ^{1}H NMR, $\delta = 77.0$ in ^{13}C NMR) or residual DMSO ($\delta = 2.49$ in ^{1}H NMR, $\delta = 39.5$ in ^{13}C NMR) as an internal standard. MASS spectra were obtained on a JEOL

JMS–SX102A. Water abundances were evaluated with a Karl–Fischer Moisture Titrator MKC–501, Kyoto Electronics Manufacturing, Co., Ltd. (Kyoto, Japan).

General procedure for the preparation of 1-alkyl-3-methylimidazolium bromide 1, [C$_n$mim]Br.[23] Freshly distilled 1-bromoalkane (0.400 mol) was dropped to the distilled 1-methylimidazole (0.200 mol) with vigorous stirring under nitrogen at 0 °C. The mixture was stirred under nitrogen for least 1 week at ambient temperature. After the reaction was completed, the excessive phase-separated 1-bromoalkane was decanted. Then, the molten salt was washed with ethyl acetate and dried *in vacuo* at 50 °C for 24 h to obtain **1** as the white solids (96–98%).

The compound 3, POSS-(NH$_3$Cl)$_8$. (3-Aminopropyl)triethoxysilane (100 mL, 0.427 mol) and conc. hydrochloric acid (35–37%, 135 mL) in methanol (800 mL) produced **3** as a white precipitate after 5 days at room temperature. The product was obtained after filtration, washing with cold methanol, and dried. The compound **3** was spectroscopically pure in 30% yield (18.8 g). ^{1}H NMR (DMSO-d_6) δ 8.23 (s, 24H), 2.76 (t, 16H), 1.71 (m, 16H), 0.72 (t, 16H). ^{13}C NMR (DMSO-d_6) δ 40.53, 20.13, and 7.96. ^{29}Si NMR (DMSO-d_6) δ −66.4 (s).

The compound 4, POSS-(COOH)$_8$. To a solution of **3** (20.0 g, 17.0 mmol) and triethylamine (20 mL, 14.4 mmol) in methanol (1 L), succinic anhydride (80 g, 0.80 mol) was added, and the reaction mixture was stirred at room temperature for 2 h and then condensed by evaporation. Chloroform was poured into the reaction solution, and the white precipitate was collected via filtration and washed with chloroform and tetrahydrofuran. Subsequently, the product was resolved in 60 mL of formic acid and reprecipitated by the addition of 1 L of water. The white precipitate was filtered and washed by water until the filtrate indicated pH 7.

The desired product **4** was obtained as a white solid after dried *in vacuo* (19.2 g, 11.4 mmol, 67%). ^{1}H NMR (DMSO-d_6) δ 0.59 (br, 2H), 1.44 (br, 2H), 2.30 (br, 2H), 2.41 (br, 2H), 3.02 (br, 2H). ^{13}C NMR (DMSO-d_6) δ 8.74, 22.48, 29.15, 29.98, 41.00, 170.92, and 173.89. ^{29}Si NMR (DMSO-d_6) δ −65.3. LRMS (NBA) [(M+H)$^+$] calcd. 1680, found 1680. HRMS (NBA) [M+H$^+$] calcd. 1680.4081, found 1680.4041.

The compound 6, Arm-COOH. Succinic anhydride (60.0 g, 0.6 mol) was dissolved into 200 mL of dioxane and propylamine (35.4 g, 0.6 mol) in 200 mL of dioxane was slowly added. The solution was warmed to 80 °C and stirred for 40 min. The succinamic acid was crystallized by cooling after the reaction. The white crystal **6** was filtered, dried and recrystallized from dioxane (76.2 g, 0.48 mol, 80%). ^{1}H NMR (DMSO-d_6) δ 0.79 (t, 3H, J = 7.43 Hz), 1.37 (m, 2H), 2.28 (t, 2H, J = 6.76 Hz), 2.40 (t, 2H, J = 6.76 Hz), 2.97 (m, 2H). ^{13}C NMR (DMSO-d_6) δ 11.37, 22.37, 29.20, 30.00, 40.29, 170.74, 173.84. LRMS (NBA) [(M+H)$^+$] calcd. 160, found 160. HRMS (NBA) [M+H$^+$] calcd. 160.0974, found 160.0978. Anal. Calcd. for $C_7H_{13}NO_3$: C, 52.82; H, 8.23; N, 8.80; O, 30.15. Found: C, 52.71; H, 8.08; N, 8.80; O, 29.99.

General procedure for the preparation of the ILs (5a-h, 7a-h). Desired equivalent mole of bromide anion **1** to the hydroxyl groups was converted into **2** by anion exchange resin (Amberlite–IRA400) in water, and neutralized with each carboxyl compound suspended in methanol (2 L). The aqueous solution was concentrated by a rotary evaporator and the residual liquid was freeze dehydrated to give the white solid. The solid was dried *in vacuo* and stored in a glove box.

POSS-C_4Im, **5a**: ^{1}H NMR (DMSO-d_6) δ 0.53 (t, 16H, J = 8.16Hz), 0.88 (t, 24H, J = 7.31Hz), 1.23 (m, 16H), 1.38 (br, 16H), 1.75 (m, 16H), 2.05 (t, 16H, J = 7.09 Hz), 2.18 (t, 16H, J =

7.09 Hz), 2.94 (m, 16H), 3.87 (s, 24H), 4.17 (t, 16H, J = 7.19 Hz), 7.74 (s, 8H), 7.81 (s, 8H), 8.98 (s, 8H), 9.59 (s, 8H). ^{13}C NMR (DMSO-d_6) δ 8.88, 13.26, 18.77, 22.68, 31.39, 33.51, 34.74, 35.54, 40.83, 48.30, 122.09, 123.41, 137.28, 173.12, 174.76. ^{29}Si NMR (DMSO-d_6) δ –66.2. LRMS (NBA) [(M+H)$^+$] calcd. 2787, found 2787. Anal. Calcd. for $C_{120}H_{208}N_{24}O_{36}Si_8$: C, 51.70; H, 7.52; N, 12.06; Br, 0. Found: C, 45.21; H, 7.70; N, 11.30; Br, 0.

POSS-C$_6$Im, **5b**: ^{1}H NMR (DMSO-d_6) δ 0.54 (br, 16H), 0.82 (t, 24H, J = 6.70Hz), 1.23 (m, 48H), 1.40 (br, 16H), 1.76 (m, 16H), 2.09 (t, 16H, J = 6.94 Hz), 2.18 (t, 16H, J = 6.94 Hz), 2.94 (m, 16H), 3.88 (s, 24H), 4.20 (t, 16H, J = 6.94 Hz), 7.80 (s, 8H), 7.87 (s, 8H), 8.90 (s, 8H), 9.86 (s, 8H). ^{13}C NMR (DMSO-d_6) δ 8.84, 13.76, 21.84, 22.66, 25.13, 29.40, 30.53, 33.34, 34.50, 35.49, 40.87, 48.58, 122.21, 123.53, 137.51, 173.20, 175.15. ^{29}Si NMR (DMSO-d_6) δ –66.2. Anal. Calcd. for $C_{136}H_{240}N_{24}O_{36}Si_8$: C, 54.23; H, 8.03; N, 11.16; Br, 0. Found: C, 48.34; H, 8.20; N, 10.40; Br, 0.

POSS-C$_8$Im, **5c**: ^{1}H NMR (DMSO-d_6) δ 0.53 (t, 16H, J = 8.16Hz), 0.83 (t, 24H, J = 6.94Hz), 1.22 (m, 80H), 1.36 (br, 16H), 1.77 (m, 16H), 2.02 (m, 16H), 2.15 (m, 16H), 2.93 (m, 16H), 3.86 (s, 24H), 4.16 (t, 16H, J = 7.19 Hz), 7.75 (s, 8H), 7.81 (s, 8H), 8.99 (s, 8H), 9.60 (s, 8H). ^{13}C NMR (DMSO-d_6) δ 8.80, 13.52, 21.99, 22.45, 25.69, 28.40, 28.46, 29.68, 31.10, 33.16, 34.04, 35.62, 41.10, 48.76, 121.27, 123.30, 137.81, 173.95, 177.87. ^{29}Si NMR (DMSO-d_6) δ –67.0. Anal. Calcd. for $C_{152}H_{272}N_{24}O_{36}Si_8$: C,56.41; H, 8.47; N, 10.39; Br, 0. Found: C, 52.93; H, 8.80; N, 10.15; Br, 0.

POSS-C$_{10}$Im, **5d**: ^{1}H NMR (DMSO-d_6) δ 0.53 (t, 16H, J = 8.16Hz), 0.83 (t, 24H, J = 6.94Hz), 1.22 (m, 80H), 1.36 (br, 16H), 1.77 (m, 16H), 2.02 (m, 16H), 2.15 (m, 16H), 2.93 (m, 16H), 3.86 (s, 24H), 4.16 (t, 16H, J = 7.19 Hz), 7.75 (s, 8H), 7.81 (s, 8H), 8.99 (s, 8H), 9.60 (s, 8H). ^{13}C NMR (DMSO-d_6) δ 8.80, 13.52, 21.99, 22.45, 25.69, 28.40, 28.46, 29.68, 31.10, 33.16, 34.04, 35.62, 41.10, 48.76, 121.27, 123.30, 137.81, 173.95, 177.87. ^{29}Si NMR (DMSO-d_6) δ

–67.0. Anal. Calcd. for $C_{168}H_{304}N_{24}O_{36}Si_8$: C, 58.30; H, 8.85; N, 9.71; Br, 0. Found: C, 55.77; H, 8.64; N, 9.59; Br, 0.

POSS-C_{12}Im, **5e**: ^{1}H NMR (DMSO-d_6) δ 0.54 (br, 16H), 0.85 (t, 24H, J = 6.82Hz), 1.23 (m, 144H), 1.39 (br, 16H), 1.77 (m, 16H), 2.03 (m, 16H), 2.15 (m, 16H), 2.94 (m, 16H), 3.86 (s, 24H), 4.14 (t, 16H, J = 7.19Hz), 7.75 (s, 8H), 7.81 (s, 8H), 9.00 (s, 8H), 9.56 (s, 8H). ^{13}C NMR (DMSO-d_6) δ 8.91, 13.87, 22.12, 22.67, 25.59, 28.49, 28.76, 28.92, 29.02, 29.06, 29.08 29.55, 31.33, 33.35, 34.53, 35.53, 40.95, 48.63, 122.21, 123.57, 137.48, 173.25, 175.41. ^{29}Si NMR (DMSO-d_6) δ −66.2.

POSS-C_{14}Im, **5f**: ^{1}H NMR (DMSO-d_6) δ 0.54 (br, 16H), 0.85 (t, 24H, J = 6.84Hz), 1.23 (m, 176H), 1.39 (br, 16H), 1.76 (m, 16H), 2.04 (m, 16H), 2.16 (m, 16H), 2.94 (m, 16H), 3.86 (s, 24H), 4.14 (t, 16H, J = 7.21Hz), 7.76 (s, 8H), 7.82 (s, 8H), 9.00 (s, 8H), 9.61 (s, 8H). ^{13}C NMR (DMSO-d_6) δ 9.25, 13.95, 22.49, 22.90, 26.13, 28.88, 29.16, 29.23, 29.37, 29.43 29.46, 29.47, 29.50, 30.10, 31.72, 33.65, 34.50, 36.02, 41.42, 49.60, 121.26, 123.46, 138.10, 174.24, 178.11. ^{29}Si NMR (DMSO-d_6) δ −66.8. Anal. Calcd. for $C_{200}H_{368}N_{24}O_{36}Si_8$: C,61.44; H, 9.49; N, 8.60; Br, 0. Found: C, 58.72; H, 9.49; N, 8.40; Br, 0.

POSS-C_{16}Im, **5g**: ^{1}H NMR (DMSO-d_6) δ 0.53 (br, 16H), 0.84 (t, 24H, J = 6.82Hz), 1.22 (m, 208H), 1.38 (br, 16H), 1.76 (m, 16H), 2.02 (m, 16H), 2.15 (m, 16H), 2.93 (m, 16H), 3.85 (s, 24H), 4.15 (t, 16H, J = 7.07Hz), 7.74 (s, 8H), 7.80 (s, 8H), 8.97 (s, 8H), 9.57 (s, 8H). ^{13}C NMR (DMSO-d_6) δ 8.81, 13.59, 22.14, 22.51, 25.80, 28.57, 28.82, 28.94, 29.07, 29.12 29.18, 29.77, 31.38, 33.22, 34.08, 35.07, 41.20, 49.24, 121.21, 123.40, 137.16, 174.06, 177.91. ^{29}Si NMR (DMSO-d_6) δ −66.9. Anal. Calcd. for $C_{216}H_{400}N_{24}O_{36}Si_8$: C,62.75; H, 9.75; N, 8.13; Br, 0. Found: C, 60.33; H, 9.63; N, 7.94; Br, 0.

POSS-C_{18}Im, **5h**: ^{1}H NMR (DMSO-d_6) δ 0.53 (br, 16H), 0.84 (t, 24H, J = 6.58Hz), 1.22 (m, 176H), 1.36 (br, 16H), 1.76 (m, 16H), 2.02 (m, 16H), 2.15 (m, 16H), 2.92 (m, 16H), 3.85 (s, 24H), 4.15 (t, 16H, J = 7.19Hz), 7.74 (s, 8H), 7.80 (s, 8H), 9.00 (s, 8H), 9.56 (s, 8H). ^{13}C

NMR (DMSO-d_6) δ 8.94, 13.95, 22.16, 22.65, 25.64, 28.54, 28.78, 28.97, 29.08, 29.13 29.58, 31.37, 33.38, 34.48, 35.68, 41.03, 48.79, 122.24, 123.61, 137.03, 173.39, 175.66. ^{29}Si NMR (DMSO-d_6) δ –66.3. Anal. Calcd. for $C_{232}H_{432}N_{24}O_{36}Si_8$: C, 63.93; H, 9.99; N, 7.71; Br, 0. Found: C, 61.72; H, 10.43; N, 7.63; Br, 0.

Arm-C$_4$Im,**7a**: ^{1}H NMR (DMSO-d_6) δ 0.82 (t, 3H, J = 7.43 Hz), 0.90 (t, 3H, J = 7.31Hz), 1.25 (m, 2H), 1.35 (m, 2H), 1.74 (m, 2H), 2.01 (t, 2H, J = 6.76 Hz), 2.13 (t, 2H, J = 6.76 Hz), 2.94 (m, 2H), 3.85 (s, 3H), 4.16 (t, 2H, J = 7.19 Hz), 7.71 (m, 1H), 7.78 (m, 1H), 9.04 (s, 1H), 9.31 (s, 1H). ^{13}C NMR (DMSO-d_6) δ 11.41, 13.25, 18.76, 22.47, 31.38, 33.80, 34.90, 35.59, 40.12, 48.36, 122.21, 123.55, 137.24, 173.38, 174.70. LRMS (NBA) $[(M + [Bmim^+])^+]$ calcd. 436, found 436. HRMS (NBA) $[(M + [Bmim^+])^+]$ calcd. 436.3282, found 436.3297. Anal. Calcd. for $C_{15}H_{27}N_3O_3$: C, 60.58; H, 9.15; N, 14.13; Br, 0. Found: C, 57.26; H, 9.40; N, 13.43; Br, 0.

Arm-C$_6$Im,**7b**: ^{1}H NMR (DMSO-d_6) δ 0.81 (t, 3H, J = 7.43 Hz), 0.84 (t, 3H, J = 7.07Hz), 1.25 (m, 6H), 1.34 (m, 2H), 1.76 (m, 2H), 2.00 (t, 2H, J = 6.70 Hz), 2.13 (t, 2H, J = 6.70 Hz), 2.93 (m, 2H), 3.85 (s, 3H), 4.15 (t, 2H, J = 7.19 Hz), 7.71 (m, 1H), 7.78 (m, 1H), 9.00 (s, 1H), 9.47 (s, 1H). ^{13}C NMR (DMSO-d_6) δ 11.33, 13.70, 21.79, 22.41, 25.09, 29.33, 30.48, 33.80, 34.96, 35.45, 40.13, 48.52, 122.03, 123.34, 137.35, 173.15, 174.59. HRMS (NBA) $[(M+[C_6Im^+])^+]$ calcd. 492.7171, found 492.3890. Anal. Calcd. for $C_{17}H_{31}N_3O_3$: C,62.74; H, 9.60; N, 12.91; Br, 0. Found: C,60.80; H, 10.27; N, 12.56; Br, 0.

Arm-C$_8$Im,**7c**: ^{1}H NMR (DMSO-d_6) δ 0.81 (t, 3H, J = 7.33 Hz), 0.85 (t, 3H, J = 6.60Hz), 1.25 (m, 10H), 1.34 (m, 2H), 1.74 (m, 2H), 2.00 (m, 2H), 2.12 (m, 2H), 2.93 (m, 2H), 3.84 (s, 3H), 4.14 (t, 2H, J = 7.21 Hz), 7.69 (m, 1H), 7.76 (m, 1H), 9.06 (s, 1H), 9.28 (s, 1H). ^{13}C NMR (DMSO-d_6) δ 11.28, 13.74, 21.95, 22.41, 25.48, 28.30, 28.41, 29.45, 31.08, 33.67, 34.84, 35.38, 40.04, 48.50, 122.06, 123.35, 137.58, 173.07, 174.85. HRMS (NBA)

[(M+[C$_8$Im$^+$])$^+$] calcd. 548.8234, found 548.4554. Anal. Calcd. for C$_{19}$H$_{35}$N$_3$O$_3$: C, 64.56; H, 9.98; N, 11.89; Br, 0. Found: C, 62.66; H, 10.86; N, 11.59; Br, 0.

Arm-C$_{10}$Im,**7d**: ^{1}H NMR (DMSO-d_6) δ 0.81 (t, 3H, J = 7.33 Hz), 0.85 (t, 3H, J = 6.60Hz), 1.25 (m, 10H), 1.34 (m, 2H), 1.74 (m, 2H), 2.00 (m, 2H), 2.12 (m, 2H), 2.93 (m, 2H), 3.84 (s, 3H), 4.14 (t, 2H, J = 7.21 Hz), 7.69 (m, 1H), 7.76 (m, 1H), 9.06 (s, 1H), 9.28 (s, 1H). ^{13}C NMR (DMSO-d_6) δ 11.33, 13.81, 21.99, 22.41, 25.45, 28.31, 28.56, 28.75, 28.80, 29.37, 31.18, 33.80, 34.93, 35.46, 40.00, 48.54, 122.02, 123.32, 137.26, 173.14, 174.52. HRMS (NBA) [(M+[C$_{10}$Im$^+$])$^+$] calcd. 04.5156, found 604.5180. Anal. Calcd. for C$_{21}$H$_{39}$N$_3$O$_3$: C, 66.10 H, 10.30; N, 11.01; Br, 0. Found: C, 65.23; H, 10.18; N, 10.77; Br, 0.

Arm-C$_{12}$Im,**7e**: ^{1}H NMR (DMSO-d_6) δ 0.81 (t, 3H, J = 7.33 Hz), 0.84 (t, 3H, J = 6.84Hz), 1.23 (m, 18H), 1.34 (m, 2H), 1.75 (m, 2H), 1.99 (m, 2H), 2.12 (m, 2H), 2.93 (m, 2H), 3.84 (s, 3H), 4.14 (t, 2H, J = 7.21 Hz), 7.70 (m, 1H), 7.76 (m, 1H), 9.08 (s, 1H), 9.29 (s, 1H). ^{13}C NMR (DMSO-d_6) δ 11.27, 13.73, 22.06, 22.44, 25.56, 28.46, 28.71, 28.88, 28.98, 29.01, 29.04, 29.57, 31.28, 33.68, 34.93, 35.35, 40.13, 48.48, 122.22, 123.50, 137.88, 173.27, 175.22. HRMS (NBA) [(M+[C$_{12}$Im$^+$])$^+$] calcd. 660.5786, found 660.5786. Anal. Calcd. for C$_{23}$H$_{43}$N$_3$O$_3$: C, 67.44; H, 10.58; N, 10.26; Br, 0. Found: C, 66.08; H, 10.86; N, 10.05; Br, 0.

Arm-C$_{14}$Im,**7f**: ^{1}H NMR (DMSO-d_6) δ 0.81 (t, 3H, J = 7.33 Hz), 0.84 (t, 3H, J = 6.72Hz), 1.22 (m, 22H), 1.34 (m, 2H), 1.75 (m, 2H), 1.99 (m, 2H), 2.12 (m, 2H), 2.93 (m, 2H), 3.84 (s, 3H), 4.14 (t, 2H, J = 7.21 Hz), 7.70 (m, 1H), 7.76 (m, 1H), 9.07 (s, 1H), 9.28 (s, 1H). ^{13}C NMR (DMSO-d_6) δ 11.33, 13.82, 22.03, 22.44, 25.50, 28.38, 28.66, 28.82, 28.92, 28.97, 29.01, 29.44, 31.25, 33.77, 34.91, 35.49, 40.04, 48.57, 122.16, 123.48, 137.42, 173.33, 174.83. HRMS (NBA) [(M+[C$_{14}$Im$^+$])$^+$] calcd. 716.6412, found 716.6411. Anal. Calcd. for C$_{25}$H$_{47}$N$_3$O$_3$: C, 68.61; H, 10.82; N, 9.60; Br, 0. Found: C, 66.68; H, 10.56; N, 9.36; Br, 0.

Arm-C$_{16}$Im,**7g**: ^{1}H NMR (DMSO-d_6), δ 0.81 (t, 3H, J = 7.45 Hz), 0.84 (t, 3H, J = 6.72Hz), 1.22 (m, 26H), 1.34 (m, 2H), 1.75 (m, 2H), 1.99 (m, 2H), 2.12 (m, 2H), 2.93 (m, 2H), 3.84 (s,

3H), 4.14 (t, 2H, J = 7.21 Hz), 7.69 (m, 1H), 7.76 (m, 1H), 9.05 (s, 1H), 9.27 (s, 1H). ^{13}C

NMR (DMSO-d_6) δ 11.33,   13.81, 22.04, 22.44, 15.51, 28.40, 28.68, 28.84, 28.95, 28.98, 29.02, 29.45, 31.26, 33.74, 34.85, 35.49, 40.04, 48.56, 122.16, 123.47, 137.44, 173.29, 174.84. HRMS (NBA) [(M+[C_{16}Im$^+$])$^+$] calcd. 772.7038, found 772.7021. Anal. Calcd. for $C_{27}H_{51}N_3O_3$: C, 69.63; H, 11.04; N, 9.02; Br, 0. Found: C, 68.21; H, 10.94; N, 9.72; Br, 0.

Arm-C_{18}Im,**7h**: ^{1}H NMR (DMSO-d_6) δ 0.81 (t, 3H, J = 7.45 Hz), 0.84 (t, 3H, J = 6.84Hz), 1.22 (m, 30H), 1.34 (m, 2H), 1.75 (m, 2H), 2.01 (m, 2H), 2.12 (m, 2H), 2.93 (m, 2H), 3.84 (s, 3H), 4.13 (t, 2H, J = 7.21 Hz), 7.69 (m, 1H), 7.76 (m, 1H), 9.00 (s, 1H), 9.22 (s, 1H). ^{13}C

NMR (DMSO-d_6) δ 11.46, 13.97, 22.14, 22.49, 25.57, 28.45, 28.74, 28.90, 29.01, 29.05, 29.08, 29.48, 31.34, 33.55, 34.50, 35.72, 40.19, 48.78, 122.27, 123.61, 136.87, 173.31, 175.04. HRMS (NBA) [(M+[C_{18}Im$^+$])$^+$] calcd. 828.7664, found 828.7673. Anal. Calcd. for $C_{29}H_{55}N_3O_3$: C, 70.54; H, 11.23; N, 8.51; Br, 0. Found: C, 60.16; H, 10.49 N, 7.35; Br, 0.

Differential scanning calorimetry. DSC thermograms were carried out on a SII DSC 6220 instrument by using approximately ~10 mg of exactly weighed samples. The sample on the aluminum open pan was cooled to −130 °C at the rate of 10 °C/min under nitrogen flowing (30 mL/min) and then heated from −130 °C to 80 °C with the same rate. The glass transition (T_g) and melting temperatures (T_m) were determined as the onset of the second curves to eliminate heat history. Fusion enthalpy (ΔH_{fus}) was calculated from the areas of the endothermic peaks at the first cycle with the completely crystallized samples soaked in the liquid nitrogen before the measurements.

Thermogravimetric analysis. TGA was performed on an EXSTAR TG/DTA6220, Seiko Instrument, Inc., with the heating rate of 10 °C/min up to 900 °C under nitrogen flowing (200 mL/min). Residual water was removed by keeping on the platinum pan at 110 °C for 1 h

before the curve profiling. The decomposition temperatures (T_d) were determined from the onset of the weight loss.

Results and Discussion

In previous reports on the POSS ILs, smaller fusion entropies were obtained during the melting process of POSS-tethered ion salts from those of ion salts without POSS. These data represent that the distribution of the ion salts tethered to the POSS core in the crystals should be preserved even after melting. In other words, a star-shaped structure centering around POSS cores should exist before and after melting. Based on these presumptions, the author aimed to align the POSS molecules to form regular structures in the liquid phase. By elongating the length of alkyl chains in the imidazolium cation, the hydrophobic interaction among ion pair-moieties should be enhanced, leading to the formation of well-aligned high-dimensional structure in the POSS ILs. Thus, the series of the POSS-tethered ion pairs with various lengths of alkyl chains in imidazolium cation were synthesized as shown in Scheme 1. From the anion exchange, various 1-alkyl-3-methylimidazolium hydroxides were synthesized, respectively, and the desired products were prepared via neutralization with POSS-$(COOH)_8$. After lyophilization, the products were obtained as colorless and transparent liquids or white solids. To prohibit coloration, all procedures were carried out without heating. The author also prepared the ion pair, Arm-C_nIm, for comparison purposes to evaluate the effects of the connection to the POSS core.

All samples containing the POSS moiety provided single peaks around −66 ppm in the ^{29}Si NMR spectra assigned to the T_8 POSS structure. These data indicate that no degradation of the POSS cage should occur under the detectable level. Integration of the peaks in the ^{1}H-

NMR spectrum indicates the formation of the 1:8 ion pairs of POSS-(COOH)$_8$ and imidazolium cation. All samples were stored in the glove box under argon atmosphere, and water abundance can be kept below 1.5 wt % as determined by the Karl Fischer method. The concentration of residual bromide ion was lower than the detectable level in the elemental analysis. Therefore, the author can conclude that all products were sufficiently pure for the following analyses.

Scheme 1. Synthesis of the ionic compounds^a
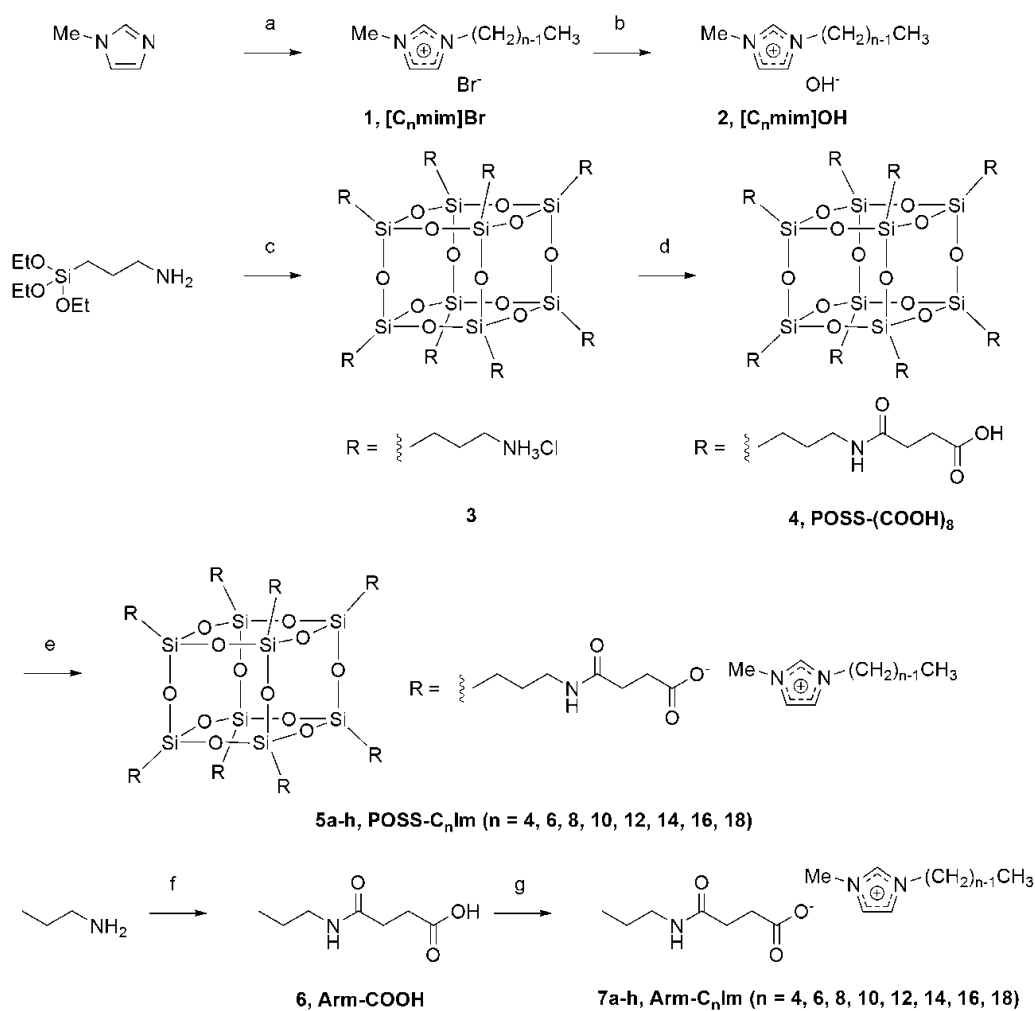
^{a}Reagents and conditions: (a) Alkyl bromide, 0 °C to r.t., at least 1 week, 96–98%; (b) Amberlite–IRA400, water, r.t.; (c) methanol, conc. hydrochloric acid, r.t., 5 days, 30%; (d) succinic anhydride, triethylamine, methanol, r.t., 2 h, 67%; (e) **2**, methanol, r.t.; (f) succinic anhydride, dioxane, 80 °C, 40 min, 80%; (g) **2**, methanol, r.t.

The T_m values of the obtained compounds at the second cycles in DSC analysis with a heating rate of 10 °C/min are listed in Table 1. The most of samples showed the endothermic peaks below 100 °C. Therefore, they were classified to ILs according to a definition.[33] From the comparison of the T_m values of ILs with the same length of alkyl chains, it was obviously shown that POSS contributes to decreasing of the T_m values. These data can be explained by the previous findings that the star-shaped distribution of ion pairs originated from the cubic core could reduce intermolecular interactions among ion pairs. In particular, below n = 14 in POSS-C_nIm, the elongation of the alkyl chain hardly influenced on the T_m values. It was found that POSS-C_{16}Im can be categorized as a room-temperature IL defined as an IL with the T_m below 25 °C. On the other hand, Arm-C_nIm showed lowest temperature at the alkyl length of n = 8, and the introduction of the longer alkyl chain more than n = 10 significantly induced the increase of the T_m values. In general, these T_m dependencies on alkyl chain lengths in imidazolium moieties were observed in other kinds of ILs, and the lowest melting temperatures were mostly found between n = 2 and 8.[34] Similarly as the TGA results, the T_m data imply that the POSS core could significantly dominate the distributions of the ion pairs. Thereby, the formation of the most-thermally-stable structure should be inhibited. Thus, the molecular motions of the remote alkyl chains might be controlled by the POSS core. The alkyl chain length n = 14 of POSS-C_nIm was quite longer than both Arm-C_nIm and typical ILs. To clarify this reason, it could be powerful method to measure and calculate ΔH_{fus} and ΔS_{fus} of fully crystallized samples. However, it was impossible to measure accurate ΔH_{fus} and ΔS_{fus} because POSS-C_nIm with moderate alkyl chain lengths possessed both crystalline phase and glassy phase. Therefore, the dependence of ΔH_{fus} and ΔS_{fus} on the alkyl lengths and the difference of them with or without POSS core are quantitatively considered in the following.

Table 1. Melting temperatures of the ILs determined from the DSC curves

|	4	6	8	10	12	14	16	18
POSS (°C)	23	18	–	–	17	15	22	45
Arm (°C)	51	–	9	31, 47	36, 42	43	52	59

ΔH_{fus} is mainly consisted of Coulomb and van der Walls interactions. On elongating the alkyl chain lengths because of the longer distance between ions and larger steric hindrance, Coulomb interaction should become weaker. On the other hand, van der Waals interaction should be enhanced because of the enlargement of neutral parts.[35, 36] As for ΔS_{fus}, it shows larger value because of the more conformational flexibilities.[35, 36] That is, on elongating alkyl chain lengths, Coulomb interaction and ΔS_{fus} could contribute to decreasing T_m values. On the contrary, van der Waals interaction induces to increase in T_m values. While it was very complicated question which had main contribution, POSS might affect these factors and cause increase of alkyl chain length at the lowest melting temperature.

The thermal stability of the synthetic compounds against pyrolysis was investigated by TGA. Figure 1 shows the TGA profiles of the synthetic compounds. The T_d values evaluated from the onsets of the TGA profiles are summarized in Table 2. Two significant weight losses were observed from all samples. Considering the percentage of weight losses and T_d values, first weight losses were assigned to the degradation of carboxylate anion. On elongating the alkyl chain lengths of imidazolium cation, the T_d values of POSS-C_nIm gradually decreased. On the other hand, those of Arm-C_nIm were approximately constant. It should be mentioned that T_d values of POSS-C_nIm were higher than those of Arm-C_nIm with corresponding length of alkyl chain. These data clearly indicate the stabilization effect of

POSS on T_d regardless of the alkyl chain length in the imidazolium moiety. In particular, even in the POSS salts with long alkyl chains, in which the stabilization effect by the POSS core could be no longer influenced, the T_d values were higher than those of the Arm salts. It is implied that the regular structures originated from the cubic core might be formed, resulting in the increases of the stability by limiting thermal motions of the remote alkyl chains from the POSS core.

Table 2. Degradation temperatures of the ILs determined from the TGA curves

	4	6	8	10	12	14	16	18
POSS (°C)	234	231	216	217	216	216	210	208
Arm (°C)	202	208	205	202	209	205	202	202
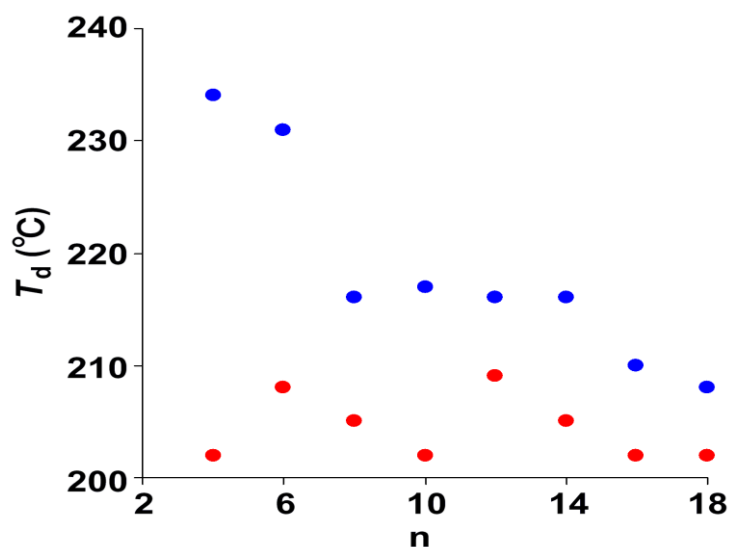
Figure 1. Plots of degradation temperature in Table 2.

By the DSC analysis, phase transition behaviors were investigated with the salts containing $C_{18}Im$. Endothermic transitions at 59 °C (T_{cr-lc}) and 83 °C (T_{lc-iso}) were observed from Arm-$C_{18}Im$. In contrast, remarkably, POSS-$C_{18}Im$ showed endothermic transition only

at 45 °C and showed no other transitions until decomposition temperature. POM observations were performed with the samples containing $C_{18}Im$ (Figure 2). Arm-$C_{18}Im$ exhibited focal-conic fan like texture and POSS-$C_{18}Im$ also showed mesophase of broken or small focal-conic fan like texture. These results indicate that both Arm-C_nIm and POSS-C_nIm formed smectic mesophase. From these data, it is concluded that the connection to POSS can extend the temperature region as a liquid crystalline.

a   **b**
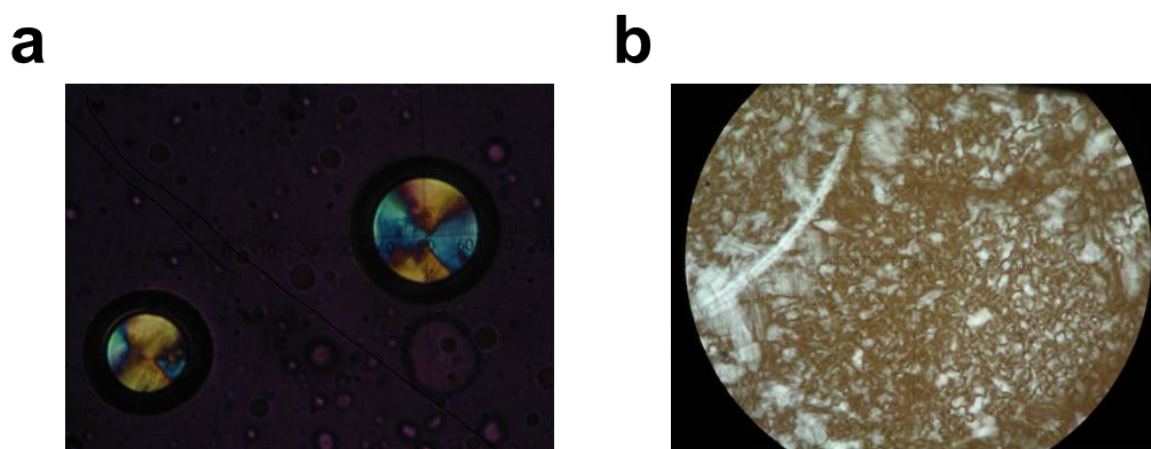
Figure 2. POM textures of (a) Arm-$C_{18}Im$ at 40 °C on the first cooling process and (b) POSS-$C_{18}Im$ at 150 °C on the first cooling process.

VT-PXRD experiments with a rate 1 °C/min were also executed to estimate the liquid crystal structures (Figure 3). In the Arm-$C_{18}Im$ mesophase, two pairs of diffraction peaks were observed at 5.11° and 7.70° at 60 °C, which were attributed to (02) and (03) peaks (*d*-spacing = 34.4 Å) derived from the smectic layer distance. Moreover, a wide angle broad halo peak was also observed around 20.0° (*d*-spacing = 4.4 Å) attributed to molten alkyl chains. In contrast, in the POSS-$C_{18}Im$ mesophase, one diffraction peak was observed at 4.30° and broad halo was observed around 19.7° (*d*-spacing = 4.5 Å) at 100 °C. From the investigation of SAXS experiments (Figure 4), two pairs of diffraction peaks at q = 1.528 nm^{-1} and 3.060

(*d*-spacing = 41.1 Å) derived from smectic layer distance were observed. These values were consistent with the XRD peak attributed to (02) diffraction.
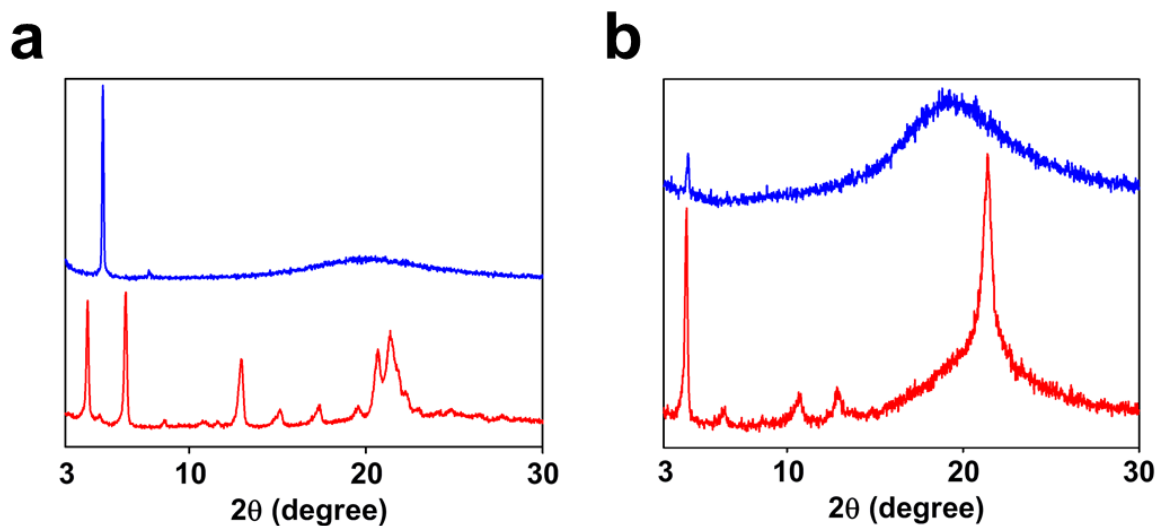
Figure 3. VT-XRD patterns of (a) Arm-C_{18}Im at 30 °C (red line) and at 60 °C (blue line) and (b) POSS-C_{18}Im at 30 °C (red line) and at 100 °C (blue line).
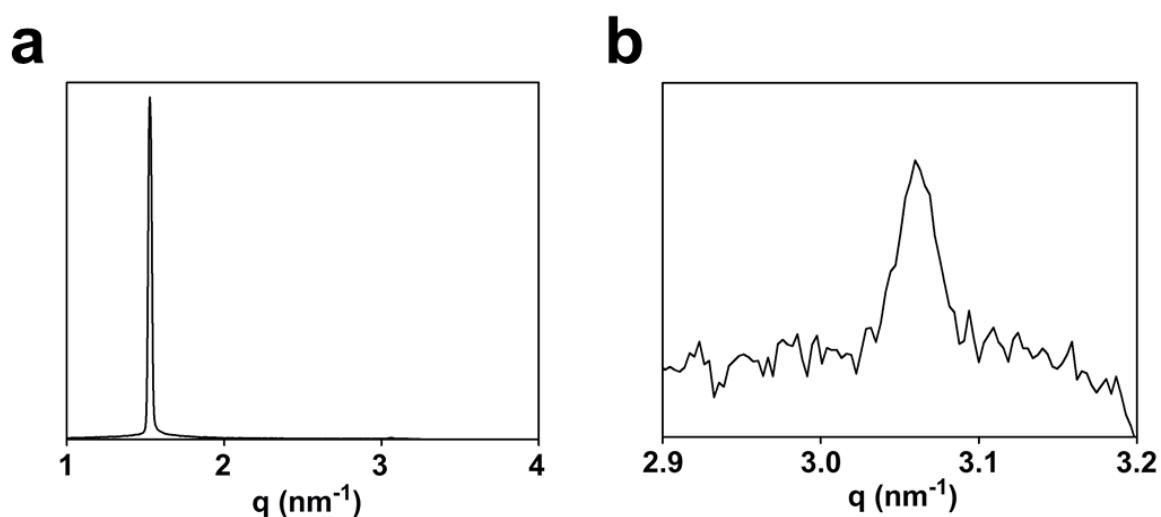
Figure 4. 1-D SAXS patterns of POSS-C_{18}Im at 100 °C.

In summary, it was indicated that POSS-C_{18}Im maintained mesophase until decomposition temperature and showed mesophase stability over much wider temperature range (ΔT = 163 °C) than that of Arm-C_{18}Im (ΔT = 24 °C). Therefore, the connection to POSS should induce greatly enhanced mesophase stability of ILs; higher mesophase stability and lower melting temperature. These significant properties of POSS-C_{18}Im could be explained by the rigid cubic structure and the spindle molecular shape of POSS (Figure 4). Molecular alignment of POSS liquid crystal could be easily formed because the connection of molecular chains to POSS core would make them spindle structure and reduce the entropy of the whole system.[37–40] On the other hand, because of relatively longer arm lengths, the POSS core bulkiness would hardly disturb mesogen packing and would cause little decrease of the enthalpy. According to the basic relationship, $T_{tr} = \Delta H_{tr} / \Delta S_{tr}$, these facts could lead to the increase of the clearing point and enhance the mesophase stability of POSS ILs. Meanwhile, POSS core could be the ideal crystal packing structure and lead to decrease of the fusion enthalpy, resulting in the lower T_m. Therefore, POSS ILs possessed lower T_m and higher clearing temperature.

Conclusion

POSS-based imidazolium salts with various lengths of alkyl chains possessed melting temperature below 100 °C and turned to be ILs. Over the whole range of the alkyl chains with n = 4–18, POSS-based ILs showed higher thermal stability and lower melting temperature than the corresponding ILs not connected to POSS. These phenomena can be explained by the decrease of fusion enthalpy. In contrast to lower melting temperature, POSS-C_{18}Im showed much higher mesophase stability. Such stabilization effect caused by connecting to POSS can be illustrated by the restriction of free molecular motion derived

from anchoring molecules to rigid core and the tendency of POSS molecule to form spindle orientation. These results suggest that POSS core could play much important role in the properties of ILs, and present the new strategies of core-properties relationships.

References

1. Yang, S.; Wu, C.; Tan, H.; Wu, Y.; Liao, S.; Wu, Z.; Shen, G.; Yu, R. *Anal. Chem.* **2013**, *85*, 14.

2. Yoneyama, H.; Tsujimoto, A.; Goto, H. *Macromolecules* **2007**, *40*, 5279.

3. Mendil-Jakani, H.; Baroni, P.; Noirez, L. *Langmuir* **2009**, *25*, 5248.

4. Xin, X.; Li, H.; Kalwarczyk, E.; Kelm, A.; Fiałkowski, M.; Gorecka, E.; Pociecha, D.; Hołyst, R. *Langmuir* **2010**, *26*, 8821.

5. Franke, D.; Vos, M.; Antonietti, M.; A. J. M. Sommerdijk, N.; F. J. Faul, Charl. *Chem. Mater.* **2006**, *18*, 1839.

6. C. Branco, L.; Serbanovic, A.; N. da Ponte, M.; A. M. Afonso, C. *ACS Catal.* **2011**, *1*, 1408.

7. Yu, T.; Yamada, T.; C. Gaviola, G.; G. Weiss, R. *Chem. Mater.* **2008**, *20*, 5337.

8. Yang, J.; Zhang, Q.; Zhu, L.; Zhang, S.; Li, J.; Zhang, X.; Deng, Y. *Chem. Mater.* **2007**, *19*, 2544.

9. Dobbs, W.; Douce, L.; Allouche, L.; Louati, A.; Malbosc, F.; Welter, R. *New J. Chem.* **2006**, *30*, 528.

10. V. Axenov, K.; Laschat, S. *Materials* **2011**, *4*, 206.

11. Binnemans, K. *Chem. Rev.* **2005**, *105*, 4148.

12. Lu, J-T.; Lee, C-K.; J. B. Lin, Ivan. *Soft Matter* **2011**, *7*, 3491.

13. a) Riisager, A.; Wasserscheid, P.; van Hal, R.; Fehrmann, R. *J. Catal.* **2003**, *219*, 452; b) Riisager, A.; Eriksen, K. M.; Wasserscheid, P.; Fehrmann, R. *Catal. Lett.* **2003**, *90*, 149.

14. Ruta, M.; Yuranov, I.; Dyson, P. J.; Laurenczy, G.; Kiwi-Minsker, L. *J. Catal.* **2007**, *247*, 269.

15. Haumann, M.; Jakuttis, M.; Werner, S.; Wasserscheid, P. *J. Catal.* **2009**, *263*, 321.

16. Jimenez, O. T.; Mller, E.; Sievers, C.; Spirkl, A.; Lercher, J. A. *Chem. Commun.* **2006**, *28*, 2974.

17. Riisager, A.; Jorgensen, B.; Wasserscheid, P.; Fehrmann, R. *Chem. Commun.* **2006**, *9*, 994.

18. Werner, S.; Szesni, N.; Fischer, R. W.; Haumann, M.; Wasserscheid, P. *Phys. Chem. Chem. Phys.* **2009**, *11*, 10817.

19. Kohler, F.; Roth, D.; Kuhlmann, E.; Wasserscheid, P.; Haumann, M. *Green Chem.* **2010**, *12*, 979.

20. T. U. Kohler, F.; Morain, B.; Weiß, A.; Laurin, M.; Libuda, J.; Wagner, V.; U. Melcher, B.; Wang, X.; Meyer, K.; Wasserscheid, P. *ChemPhysChem* **2011**, *12*, 3539.

21. Tanaka, K.; Ishiguro, F.; Chujo, Y.; *Polym. J.* **2011**, *43*, 708.

22. Tanaka, K.; Ishiguro, F.; Chujo, Y. *J. Am. Chem. Soc.* **2010**, *132*, 17649.

23. Asuncion, M. Z.; Ronchi, M.; Abu-Seir, H.; Laine, R. M.; *C. R. Chim.* **2010**, *13*, 270.

Chapter 2

POSS Fillers for Modulating Thermal Properties of Ionic Liquids

Chapter 2

POSS Fillers for Modulating Thermal Properties of Ionic Liquids

Abstract : This chapter reports a polyhedral oligomeric silsesquioxane (POSS)-based filler for improving the thermal properties of ionic liquids (ILs). The author prepared homogeneous mixtures containing the octa-substituted carboxy-POSS as a filler via a solution process. Initially, it was found that the melting temperatures of the ionic pairs were lowered by adding the POSS filler. Based on this effect, some of ionic salts were transformed into ILs by adding the POSS filler. Reinforcement of thermal stability was also observed from the salts which have an intrinsically low decomposition temperature. According to the thermodynamic parameters in melting, the introduction of the POSS filler significantly reduces both the fusion enthalpy and entropy. Furthermore, from experiments on the substituent effect on POSS, it was found that only octa-carboxy POSS had an effect on the modulation of the thermal properties of ion salts.
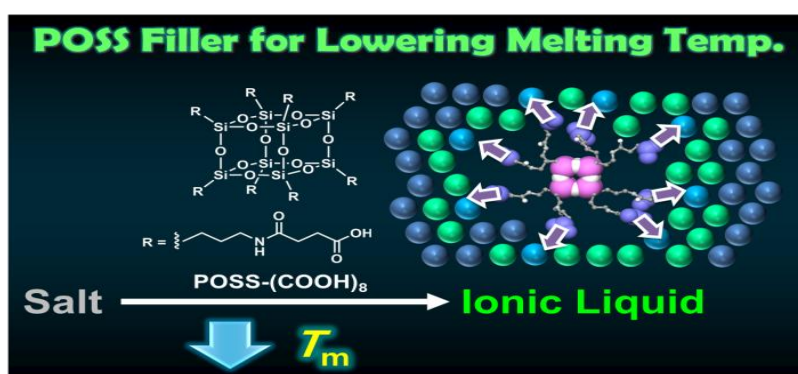
Introduction

Ionic liquids (ILs), which are defined as a pure salt with a melting temperature below 100 °C, are attractive materials because of their intriguing fundamental chemistry on molecular dynamics,[1–7] and useful properties in industrial applications, *e.g.* as ion conductors,[8–11] solvents,[12–16] and electrolytes.[17–23] Therefore, new ILs have been explored vigorously. However, in the development of new ILs, there are few methods available to modulate the properties of ILs such as the alteration of the chemical structures of the components based on organic synthetic procedures. Thus, the development of simple procedures to modulate the characteristics of ion pairs is beneficial in the production of highly functional ILs. In particular, decreasing the melting temperature of ion pairs is crucial since the lowering of melting temperatures generally induces the improvement of various properties such as ion conductivity[24–31] and viscosity.[32–36]

The introduction of fillers is a simple and valid strategy to modulate material properties.[37,38] It can modulate a single property or provide other functions without changing the intrinsic parameters of the materials. There are several examples about the modulation of IL properties by fillers. For example, by adding a small portion of water to the cellulose-dissolved ILs, the enzymatic activity of cellulase can be enhanced in ILs.[39–42] The solvation of cellulose and the rate of digestion to glucose can be improved. However, there are very few examples to show a filler which effectively regulates the thermal properties of conventional ILs.

Polyhedral oligomeric silsesquioxane (POSS)-based materials show unique characteristics originating from their structural features.[43,44] Recently, a series of POSS-based ILs and their significant thermal properties were reported.[45,46] The author found that by connecting the POSS core to ionic salts, the thermal properties of the ion pairs are positively changed as an IL. Decreased melting temperatures and increased thermal stabilities were

simultaneously obtained. These behaviors were explained by the structural features of POSS. Since POSS adopts a globular conformation, such structural features can contribute to reducing the packing density and isolating the distal ion pairs.[38] Consequently, the suppression of interactions between ion pairs and the formation of a highly symmetrical distribution of ion pairs around the POSS core could occur, leading to the decrease in melting temperatures and increase in thermal stabilities, simultaneously.[47] The author's next interest is to realize the effects of POSS on the thermal properties of ILs via non-covalent bonding.

In this chapter, the author describes the use of POSS fillers to modulate the thermal properties of ILs. The author found that octa-substituted carboxy-POSS has a significant effect, decreasing the melting temperature without loss of thermal stability. From a thermodynamic study on the melting process, it is suggested that the thermal characteristics originate from the structural features of POSS, *i.e.* decreasing fusion enthalpies and entropies could be transmitted to surrounding ionic pairs. In addition, the author also mentions the crucial role of carboxyl groups in the effect of POSS on melting temperatures.

Experimental Section

General. ^{1}H NMR and ^{13}C NMR spectra were measured using a JEOL EX-400 (400 MHz for ^{1}H and 10 MHz for ^{13}C) spectrometer. ^{29}Si NMR spectra were measured using a JEOL JNM-A400 (80 MHz) spectrometer. Coupling constants (*J* value) are reported in Hertz. The chemical shifts are expressed in ppm downfield from tetramethylsilane, using residual chloroform ($\delta = 7.24$ in ^{1}H NMR, $\delta = 77.0$ in ^{13}C NMR) or residual DMSO ($\delta = 2.49$ in ^{1}H NMR, $\delta = 39.5$ in ^{13}C NMR) as an internal standard. Mass spectra were obtained using a JEOL JMS–SX102A. Differential scanning calorimetry (DSC) thermograms were carried out using a SII DSC 6220 instrument by using *ca.* 10 mg of exactly weighed samples at a heating

rate of 10 °C min^{-1}. Thermogravimetric analysis (TGA) was performed using an EXSTAR TG/DTA 6220, Seiko Instrument, Inc., with a heating rate of 10 °C min^{-1} up to 500 °C under a nitrogen atmosphere. Residual methanol was removed by keeping the samples in a vacuum oven at 100 °C for 1 h before the TGA measurements. Water abundances were evaluated with a Karl Fischer Moisture Titrator MKC-501, Kyoto Electronics Manufacturing, Co., Ltd. (Kyoto, Japan). POSS derivatives and the control compound, Arm-COOH, were prepared according to the previous reports.[45,46]

Preparation of 1-eicosyl-3-methylimidazolium bromide, C$_{20}$MIM-Br[47]. Freshly distilled 1-bromoeicosane (0.400 mol) was dropped into distilled 1-methylimidazole (0.200 mol) with vigorous stirring under nitrogen at 0 °C. The mixture was stirred under nitrogen for at least 1 week at ambient temperature. After the reaction was complete (monitored by ^{1}H NMR), the excess phase-separated 1-bromoalkane was decanted. Then, the molten salt was washed with ethyl acetate and dried *in vacuo* at 50 °C for 24 h. The desired compound C$_{20}$MIM-Br was obtained as a white solid (96%). The identification was confirmed according to a previous report.[47] ^{1}H NMR (DMSO-d$_6$) δ 0.83 (s, 3H), 1.21 (t, 34H), 1.75 (t, 2H), 3.84 (s, 3H), 4.14 (d, 2H), 7.70 (s, 1H), 7.77 (s, 1H), 9.14 (s, 1H). ^{13}C NMR (DMSO-d$_6$) δ 13.84, 14.01, 22.03, 25.46, 28.35, 28.65, 28.80, 28.92, 28.94, 28.98, 29.00, 28.36, 31.24, 35.70, 48.68, 122.20, 123.52, 136.45.

Preparation of the sample mixtures. The samples were prepared by solution mixing in methanol. The ion salt (1 g) and methanol (10 mL) were mixed in a 20 mL flask and stirred for 30 min at room temperature to obtain a clear solution. Then, POSS-[COOH]$_8$ or Arm-COOH was added to the solution. The mixture was stirred for an additional 1 h, and the resulting clear solution was concentrated using a rotary evaporator. The homogeneous

mixture with POSS-[COOH]$_8$ was obtained as a white solid after drying *in vacuo*.

Differential scanning calorimetry. DSC thermograms were carried out using a SII DSC 6220 instrument by using approximately 10 mg of exactly weighed samples. The sample was placed on an aluminum open pan and cooled to -50 °C at a rate of 10 °C min^{-1} under a flow of nitrogen (30 mL min^{-1}) before being heated from –50 °C to 140 °C at the same rate. The melting temperatures (T_m) were determined as the onset of the second curves to eliminate heat history. Fusion enthalpy (ΔH_{fus}) was calculated from the areas of the endothermic peaks at the first cycle with the completely crystallized samples soaked in the liquid nitrogen before the measurements.

Thermogravimetric analysis. TGA was performed using an EXSTAR TG/DTA6220, Seiko Instrument, Inc., with a heating rate of 10 °C min^{-1} up to 500 °C under a flow of nitrogen (200 mL/min^{-1}). Residual water was removed by keeping the platinum pan at 110 °C for 1 h before the curve profiling. The decomposition temperatures (T_{5d}) were determined from the temperature with 5 % of weight loss.

Results and Discussion

The chemical structures of the fillers and ion salts used in this study are listed in Figure 1. Octa-substituted carboxy-POSS, POSS-[COOH]$_8$ and Arm-COOH as a comparison to evaluate the effect of POSS were synthesized according to the previous reports.[45,46] The samples were typically prepared as follows: A mixture of 1 g of ion salt in methanol (10 mL) was added to POSS-[COOH]$_8$ to give solutions with variable concentrations (1, 5, 10, and 20

wt %). After obtaining a clear solution, the mixture was concentrated by rotary evaporation at ambient temperature. The samples were stored in a glove box under an argon atmosphere to keep the water abundance below 1.5 wt % as determined by the Karl Fischer method. The samples containing Arm-COOH were prepared with the same manner as a comparison to evaluate the effects of POSS-[COOH]$_8$.
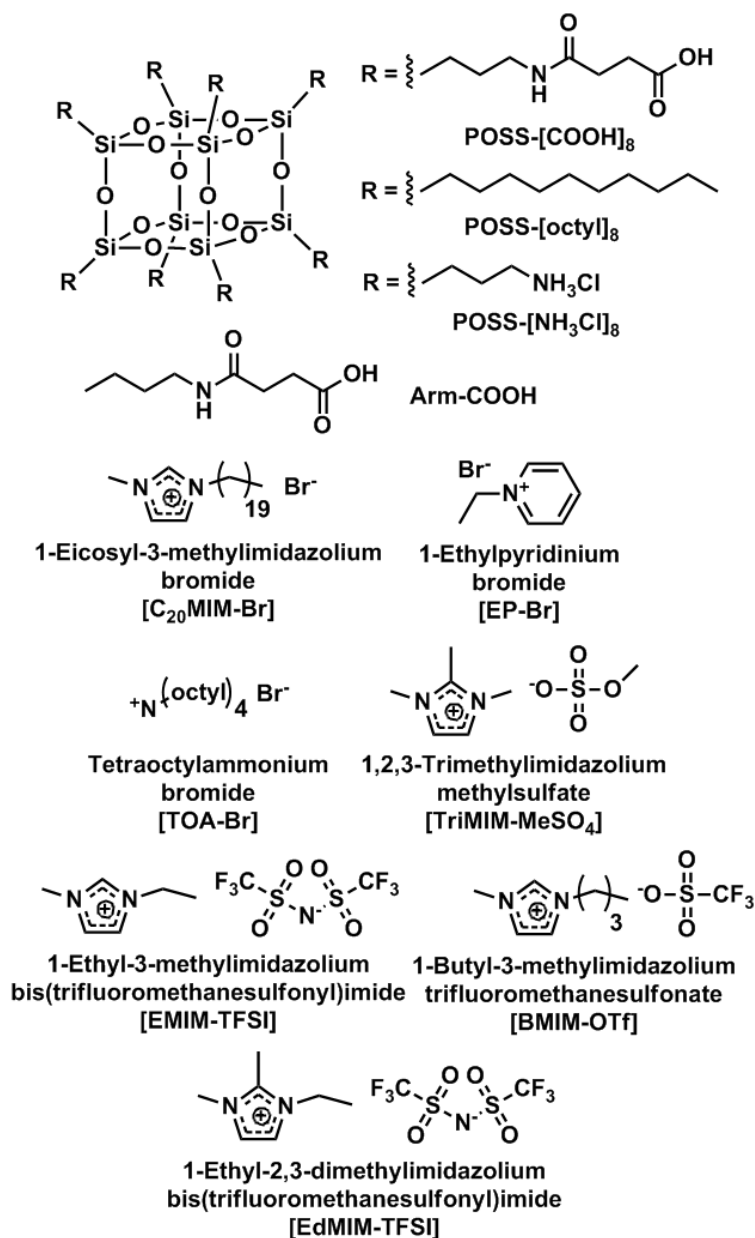
Figure 1. Chemical structures of the compounds used in this study.

DSC analyses were performed with the mixture samples (Figure 2). The T_m values were determined from the endothermic peaks observed at the second cycles (Table 1). By adding POSS-[COOH]$_8$ and Arm-COOH to the salts, the T_m values were lowered. The addition of 20 wt % POSS-[COOH]$_8$ dramatically decreased the T_m values of the salts by at least 14 °C. In particular, the Tm value of ethylpyridinium bromide, EP-Br, was lowered from 125 °C to 88 °C. It was demonstrated that POSS-[COOH]$_8$ can transform EP-Br into a definitional IL. Comparing the T_m values of Arm-COOH at the same wt % and mol %, the decrease in the T_m values was enhanced by increasing the concentration of POSS-[COOH]$_8$. These data clearly indicate that POSS is responsible for lowering the T_m values of ion salts.
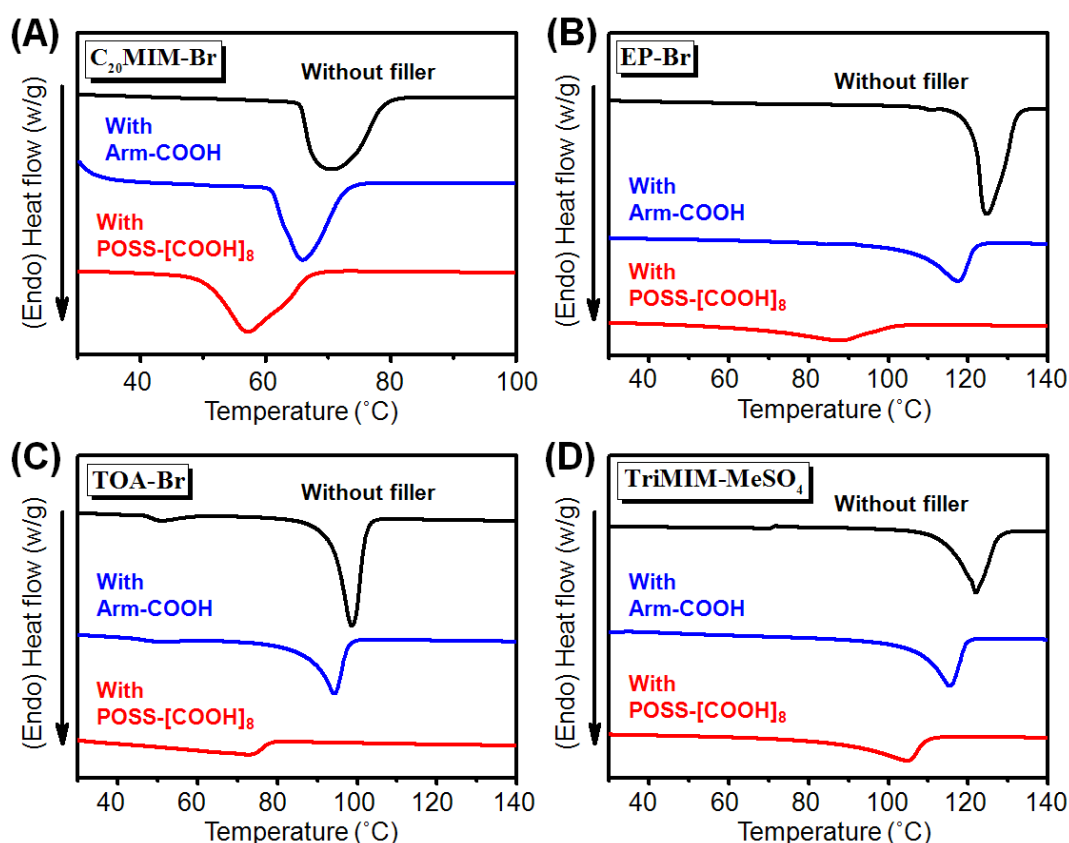
Figure 2. The representative DSC curves of the samples containing 20 wt % of the fillers in the second scan with a heating rate of 10 °C/min under nitrogen atmosphere.

Table 1. Melting temperatures, thermodynamic parameters, and decomposition temperatures with 5% of weight loss of the ion salts determined from the DSC and TGA curves[a]

Salt	wt %	POSS-[COOH]$_8$						Arm-COOH					
		mol %	T_m (°C)[a]	ΔT_m (°C)	T_{5d} (°C)[b]	H_{fus} (kJ/mol)[a]	S_{fus} (J/mol·K)[c]	mol %	T_m (°C)[a]	ΔT_m (°C)	T_{5d} (°C)[b]	H_{fus} (kJ/mol)[a]	S_{fus} (J/mol·K)[c]
	0	0	71	–	268	21.2	61	0	71	–	268	21.1	61
	1	0.26	69	−2	260	19.5	57	2.71	70	−1	257	20.2	59
C$_{20}$MIM-Br	5	1.31	67	−4	262	17.8	52	12.2	68	−3	257	18.0	53
	10	2.82	63	−8	264	17.3	51	23.4	67	−4	249	17.4	51
	20	6.20	57	−14	265	12.4	38	41.0	66	−5	231	16.3	48
	0	0	125	–	236	18.2	46	0	125	–	236	18.2	46
	1	0.11	122	−3	232	16.6	42	1.17	127	+2	233	18.0	45
EP-Br	5	0.56	117	−8	232	12.5	32	5.57	123	−2	233	15.4	39
	10	1.22	104	−21	233	9.3	25	11.5	120	−5	221	12.6	32
	20	2.73	88	−37	236	6.3	17	22.8	117	−8	221	11.3	29
	0	0	99	–	187	19.8	53	0	99	–	187	19.8	53
	1	0.32	97	−2	188	17.9	48	3.30	98	−1	188	18.6	50
TOA-Br	5	1.60	93	−6	192	14.4	39	14.6	98	−1	190	17.8	48
	10	3.45	85	−14	193	6.4	18	27.3	96	−3	194	15.1	41
	20	7.52	73	−26	195	4.4	13	46.1	94	−5	194	12.8	35
	0	0	122	–	n.d.[d]	18.9	48	0	122	–	n.d.[d]	18.9	48
	1	0.13	119	−3	n.d.[d]	17.4	44	1.37	121	−1	n.d.[d]	17.9	45
TriMIM-MeSO$_4$	5	0.66	117	−5	n.d.[d]	16.5	42	6.49	119	−3	n.d.[d]	17.1	44
	10	1.43	114	−8	n.d.[d]	14.0	36	13.3	118	−4	n.d.[d]	15.4	39
	20	3.20	104	−18	n.d.[d]	11.4	30	25.8	115	−7	n.d.[d]	14.2	37

[a]Obtained from the second heating curves in the DSC profiles.

[b]Determined from the temperatures with 5% of weight loss in the TGA curves.

[c]Calculated from the following relation: $\Delta S_{fus} = \Delta H_{fus}/T_m$.

[d]n.d.= not detectable.

To understand the mechanism of the lowering of the T_m values, the thermodynamic parameters (fusion enthalpy ΔH_{fus} and entropy ΔS_{fus}) in the melting process of the salts were evaluated from the areas of the endothermic peaks observed in the DSC profiles (Table 1). The mixtures with variable concentrations of POSS-[COOH]$_8$ showed lower ΔH_{fus} values than those of the mixtures containing Arm-COOH (Figure 3). In the previous reports on POSS-based ILs, the author observed similar tendencies for ΔH_{fus} and ΔS_{fus} to be lower than those of Arm-ILs when the T_m values of the POSS-ILs were small.[45,46] These results can be explained by the structural features of POSS. The rigid cubic structure of the POSS core could contribute to the isolation of the ion pairs which interact with the carboxyl groups of POSS. Thus, the interaction should be weakened and thus observed as a small ΔH_{fus} value.

Smaller values of ΔS_{fus} support this model. Isolation by POSS via the interaction with carboxyl groups induces a star-shaped distribution around the POSS core. In this state, the conformational variety should be reduced compared to that in the absence of POSS. Therefore, the salt mixtures containing POSS filler should show much smaller ΔS_{fus} values. Finally, the larger contribution of ΔH_{fus} should cause lowering of the T_m values.
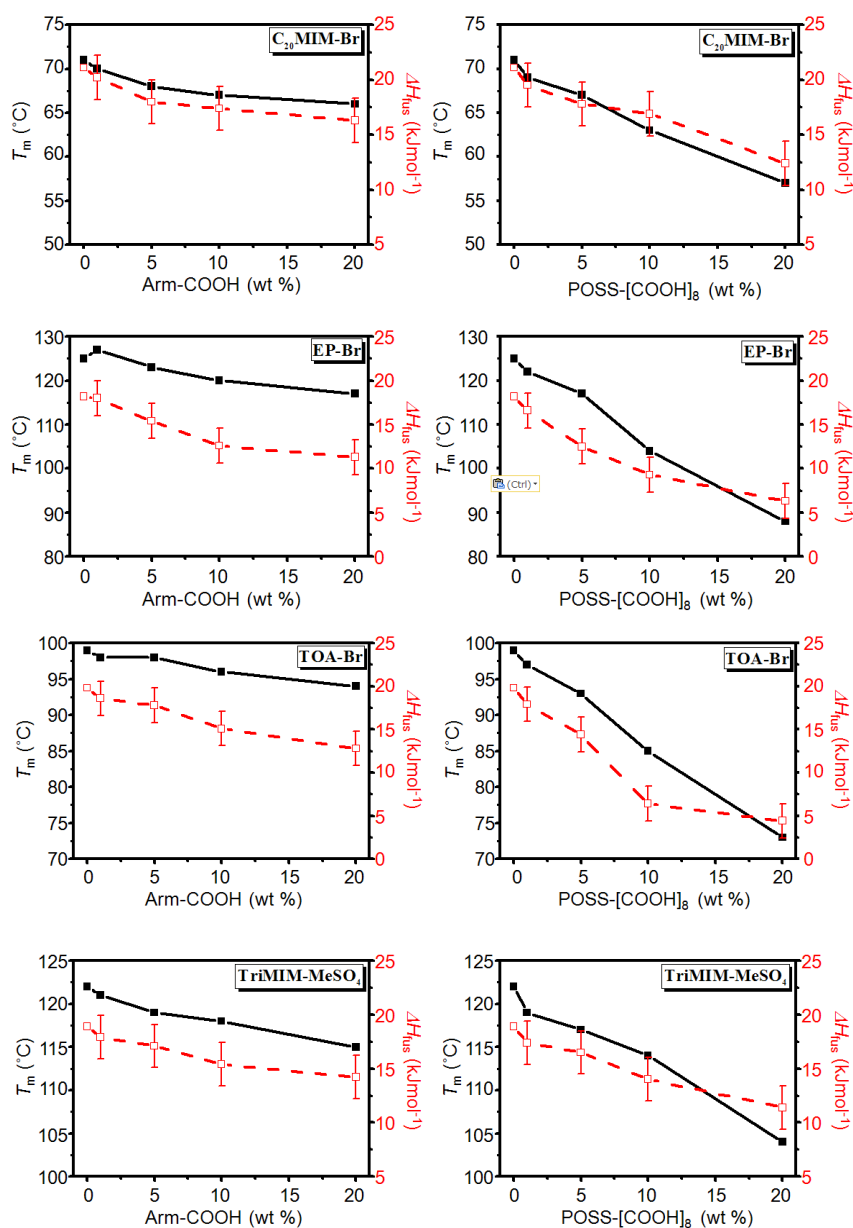

Figure 3. T_m (black solid dots) and ΔH_{fus} values (red clear dots) of the mixtures by adding the variable concentrations of the fillers.

The roles of the carboxyl groups were examined by replacing them with other functional groups. The author prepared samples using POSS derivatives such as POSS-[octyl]$_8$ and POSS-[NH$_3$Cl]$_8$ (Figure 1). The T_m values of the ILs remained almost constant or slightly decreased on addition of 20 wt % POSS-[octyl]$_8$ or POSS-[NH$_3$Cl]$_8$ (Figure 4 and Table 2). These results indicate two significant issues: Firstly, the existence of the silica cage has little effect on the melting process of the salt, and secondly the interaction between the POSS core and ion pairs could be dominated not by electrostatic interaction but by hydrogen bonding, since the positive charges in POSS-[NH$_3$Cl]$_8$ showed little effect on the T_m values.[48] These results suggest that the POSS effect on the enhancement of hydrogen-bond formation could also be of importance in the modulation of melting behaviors.

Table 2. Melting temperatures of the salts with various kinds of POSS derivatives

Salt	Filler (20 wt %)	T_m (°C)[a]	ΔT_m (°C)
C$_{20}$MIM-Br	None	71	–
	POSS-[octyl]$_8$	71	±0
	POSS-[NH$_3$Cl]$_8$	68	−3
EP-Br	None	125	–
	POSS-[octyl]$_8$	124	−1
	POSS-[NH$_3$Cl]$_8$	121	−3
TOA-Br	None	99	–
	POSS-[octyl]$_8$	98	−1
	POSS-[NH$_3$Cl]$_8$	95	−4
TriMIM-MeSO$_4$	None	122	–
	POSS-[octyl]$_8$	121	−1
	POSS-[NH$_3$Cl]$_8$	120	−2
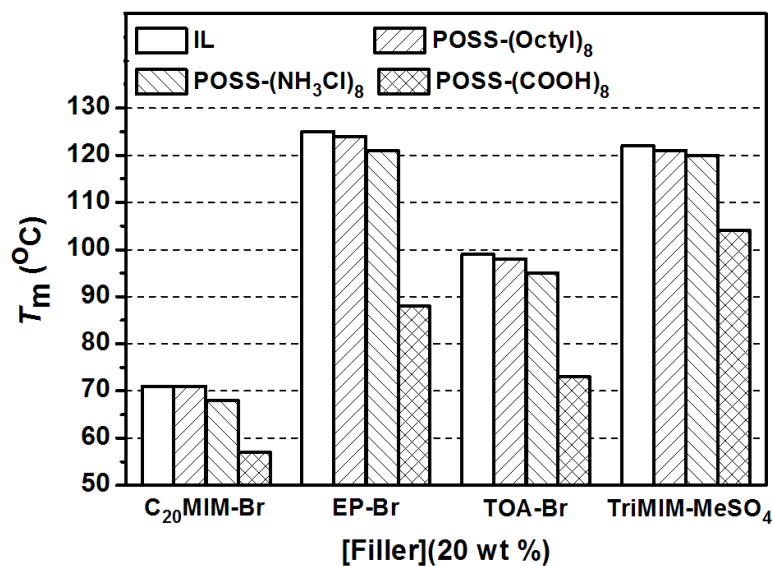
Figure 4. Comparison of the T_m values with various kinds of POSS fillers.

The feasibility of using the POSS filler with conventional ILs was examined (Table 3). The T_m values of the mixtures were determined from the DSC profiles (Figure 5). The same experiments were carried out with 1-ethyl-3-methylimidazolium bis(trifluoromethanesulfonyl) imide [EMIM-TFSI], 1-butyl-3-methylimidazolium trifluoromethanesulfonate [BMIM-OTf], and 1-ethyl-2,3-dimethylimidazolium bis(trifluoromethanesulfonyl)imide [EdMIM-TFSI], which intrinsically possess low T_m values of −14 °C, 17 °C, and 26 °C, respectively. Remarkably, the T_m values of BMIM-OTf and EdMIM-TFSI were lowered by adding POSS-[COOH]$_8$. These results suggest that the molecular interaction should be small in the ILs with lower T_m values. Therefore, the author presumed that the filler effects could be reduced, leading to the small changes in T_m values. In summary, these results indicate that POSS fillers can efficiently reduce the T_m values of salts.

Table 3 Melting and decomposition temperatures of the conventional ILs with the fillers

Salt	Filler (20 wt %)	T_m (°C)^a	ΔT_m (°C)	T_{5d} (°C)^b	ΔT_{5d} (°C)
EMIM-TFSI	None	−14	–	424	–
	Arm-COOH	−14	±0	237	−187
	POSS-[COOH]$_8$	−14	±0	408	−16
BMIM-OTf	None	17	–	404	–
	Arm-COOH	13,18	−4,+1	236	−168
	POSS-[COOH]$_8$	12,17	−5	398	−6
EdMIM-TFSI	None	26	–	445	–
	Arm-COOH	24	−2	233	−212
	POSS-[COOH]$_8$	22	−4	423	−22

^{a}Obtained from the second heating curves in the DSC profiles.
^{b}Determined from the temperatures with 5% of weight loss in the TGA curves.
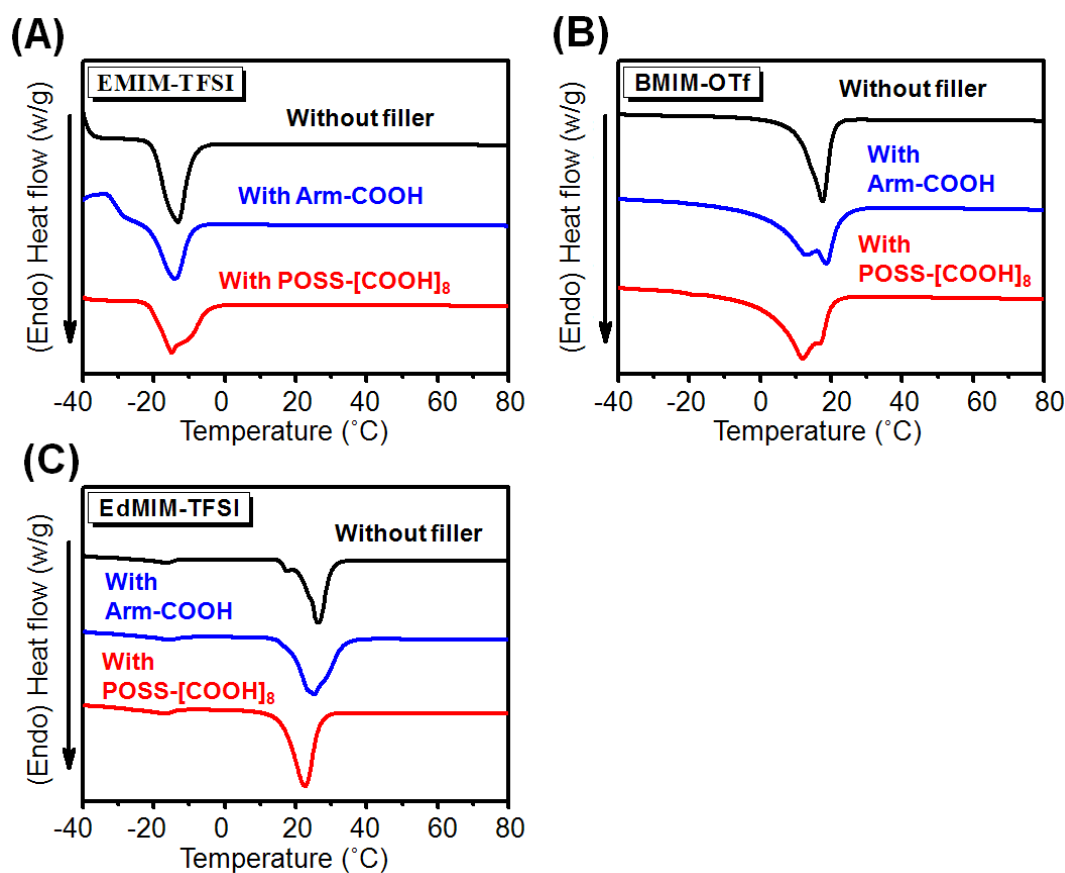
Figure 5. The representative DSC curves of the IL mixtures containing 20 wt % of the fillers in the second scan with a heating rate of 10 °C/min under nitrogen atmosphere.

The influence of the fillers on the thermal stability of the salts was investigated using TGA. Table 1 lists the decomposition temperature with 5% weight loss (T_{5d}) of the samples. The addition of Arm-COOH critically caused a reduction of the T_{5d} values of the salts. In contrast, POSS-[COOH]$_8$ induced a small decrease. In the case of tetraoctylammonium bromide (TOA-Br), the T_{5d} value increased. Because of the lower decomposition temperature of the carboxyl groups in the filler molecules than those of the salts, the POSS core can play a positive role in improving thermal stability. The highly symmetrical distribution of salt molecules induced by POSS could suppress molecular motion efficiently.

Conclusion

The author describes here the significant effect of POSS-[COOH]$_8$ as a molecular filler for ion salts on the lowering of T_m values. It is suggested that by the effective interaction of POSS with salt molecules via hydrogen bonds at the carboxyl groups, the structural features of the silica cube could be transduced. Finally, the large contribution of decreases of the fusion enthalpy in the melting can cause the lowering of T_m values. POSS fillers can be employed to improve the thermal stability of ILs. Furthermore, the author's concept and findings are versatile and not only apply to the development of new series of thermally-stable ILs but also to reinventing ion salts as ILs by decreasing their T_m value.

References

1. Tamada, M.; Watanabe, T.; Horie, K.; Ohno, H. *Chem. Commun.* **2007**, 4050.

2. Shim, Y.; Kim, H. J. *J. Phys. Chem. B* **2009**, *113*, 12964.

3. Zhang, Q.-G.; Wei, Y.; Sun, S.-S.; Wang, C.; Yang, M.; Liu, Q.-S.; Gao, Y.-A. *J. Chem. Eng. Data* **2012**, *57*, 2185.

4. Roy, D.; Maroncelli, M. *J. Phys. Chem. B* **2010**, *114*, 12629.

5. Lopes, J. N. A. C.; Pádua, A. A. H. *J. Phys. Chem. B* **2006**, *110*, 3330.

6. Heggen, B.; Zhao, W.; Leroy, F.; Dammers, A. J.; Müller-Plathe, F. *J. Phys. Chem. B* **2010**, *114*, 6954.

7. Paluch, M.; Haracz, S.; Grzybowski, A.; Mierzwa,; Pionteck, M. J.; Rivera-Calzada, A.; Leon, C. *J. Phys. Chem. Lett.* **2010**, *1*, 987.

8. Ferreira, A. R.; Freire, M. G.; Ribeiro, J. C.; Lopes, F. M.; Crespo, J. G.; Coutinho, J. A. P. *Ind. Eng. Chem. Res.* **2011**, *50*, 5279.

9. Ferreira, A. R. M.; Freire, G.; Ribeiro, J. C.; Lopes, F. M.; Crespo, J. G.; Coutinho, J. A. P. *Ind. Eng. Chem. Res.* **2012**, *51*, 3483.

10. Ogihara, W.; Kosukegawa, H.; Ohno, H. *Chem. Commun.* **2006**, 3637.

11. Banerjee, T.; Singh, M. K. Khanna, A. *Ind. Eng. Chem. Res.* **2006**, *45*, 3207.

12. Harrisson, S.; Mackenzie, S. R.; Haddleton, D. M. *Chem. Commun.* **2002**, 2850.

13. Parnham, E. R.; Morris, R. E. *J. Mater. Chem.* **2006**, *16,* 3682.

14. Goujon, N.; Wang, X.; Rajkowa, R.; Byrne, N. *Chem. Commun.* **2012**, *48*, 1278.

15. Barhdadi, R.; Courtinard, C.; Nédélec, J. Y.; Troupel, M. *Chem. Commun.* **2003**, 1434.

16. Dunn, M. H.; Cole, M. L.; Harper, J. B. *RSC Adv.* **2012**, *2*, 10160.

17. Liu, J.; Yang, X.; Cong, J.; Kloo, L.; Sun, L. *Phys. Chem. Chem. Phys.* **2012**, *14*, 11592.

18. Kim, T. Y.; Lee, H. W.; Stoller, M.; Dreyer, D. R.; Bielawski, C. W.; Ruoff, R. S.; Suh, K. S. *ACS Nano* **2011**, *5*, 436.

19. Nakamoto, H.; Watanabe, M. *Chem. Commun.* **2007**, 2539.

20. Yazaki, S.; Funahashi, M.; Kato, T. *J. Am. Chem. Soc.* **2008**, *130*, 13206.

21. Tian, H.; Gabrielsson, E.; Yu, Z.; Hagfeldt, A.; Kloo, L.; Sun, L. *Chem. Commun.* **2011**, *47*, 10124.

22. Yazaki, S.; Funahashi, M.; Kagimoto, J.; Ohno, H.; Kato, T. *J. Am. Chem. Soc.* **2010**, *132*, 7702.

23. Ke, C.; Li, J.; Li, X.; Shao Z.; Yi, B. *RSC Adv.* **2012**, *2*, 8953.

24. Widegren, J. A.; Magee, J. W. *J. Chem. Eng. Data* **2007**, *52*, 2331.

25. Ren, R.; Zuo, Y.; Zhou, Q.; Zhang, H.; Zhang, S. *J. Chem. Eng. Data* **2011**, *56*, 27.

26. Ogoshi, T.; Ueshima, N.; Yamagishi, T.; Toyota, Y.; Matsumi, N. *Chem. Commun.* **2012**, *48*, 3536.

27. Fraser, K. J.; Izgorodina, E. I.; Forsyth, M.; Scott, J. L.; MacFarlane, D. R. *Chem. Commun.* **2007**, 3817.

28. Tamada, M.; Watanabe, T.; Horie, K.; Ohno, H. *Chem. Commun.* **2007**, 4050.

29. Mizumo, T.; Fujita, R.; Ohno, H.; Ohshita, J. *Chem. Lett.* **2011**, *40*, 798.

30. Cha, J.-H.; Lee, W.; Lee, H. *J. Mater. Chem.* **2009**, *19*, 6542.

31. Kunze, M.; Montanino, M.; Appetecchi, G. B.; Jeong, S.; Schönhoff, M.; Winter, M.; Passerini, S. *J. Phys. Chem. A* **2010**, *114*, 1776.

32. MacFarlane, D. R.; Golding, J.; Forsyth, S.; Forsyth, M.; Deacon, G. B. *Chem. Commun.* **2001**, 1430.

33. Shirota, H.; Mandai, T.; Fukazawa H.; Kato, T. *J. Chem. Eng. Data* **2011**, *56*, 2453.

34. Van-Oanh, N.-T.; Houriez, C.; Rousseau, B. *Phys. Chem. Chem. Phys.* **2010**, *12*, 930.

35. Jiang, Y.-Y.; Wang, G.-N.; Zhou, Z.; Wu, Y.-T.; Geng, J.; Zhang, Z.-B. *Chem. Commun.* **2008**, 505.

36. Rodrı´guez, H.; Brennecke, J. F. *J. Chem. Eng. Data* **2006**, *51*, 2145.

37. Tanaka, K.; Adachi, S.; Chujo, Y. *J. Polym. Sci., Part A: Polym. Chem.* **2009**, *47*, 5690.

38. Tanaka, K.; Adachi, S.; Chujo, Y. *J. Polym. Sci., Part A: Polym. Chem.* **2010**, *48*, 5712.

39. Engel, P.; Mladenov, R.; Wulfhorst, H.; Jäger, G.; Spiess, A. C. *Green Chem.* **2010**, *12*, 1959.

40. Moniruzzaman, M.; Kamiya, N.; Goto, M. *Langmuir* **2009**, *25*, 977.

41. Brandt, A.; Ray, M. J.; To, T. Q.; Leak, D. J.; Murphy, R. J.; Welton, T. *Green Chem.* **2011**, *13*, 2489.

42. Xie, H.; Shen, H.; Gong, Z.; Wang, Q.; Zhao, Z. K.; Bai, F. *Green Chem.* **2012**, *14*, 1202.

43. Tanaka, K.; Chujo, Y. *Polym. J.* **2013**, *45*, 247.

44. Tanaka, K.; Chujo, Y. *J. Mater. Chem.* **2012**, *22*, 1733.

45. Tanaka, K.; Ishiguro, F.; Chujo, Y.; *Polym. J.* **2011**, *43*, 708.

46. Tanaka, K.; Ishiguro, F.; Chujo, Y. *J. Am. Chem. Soc.* **2010**, *132*, 17649.

47. Asuncion, M. Z.; Ronchi, M.; Abu-Seir, H.; Laine, R. M.; *C. R. Chim.* **2010**, *13*, 270.

48. Tanaka, K.; Murakami, M.; Jeon, J.-H.; Chujo, Y. *Org. Biomol. Chem.* **2012**, *10*, 90.

Chapter 3

Synthesis of Sulfonic Acid-Containing POSS and Its Filler Effects for Enhancing Thermal Stabilities and Lowering Melting Temperatures of Ionic Liquids

Chapter 3

Synthesis of Sulfonic Acid-Containing POSS and Its Filler Effects for Enhancing Thermal Stabilities and Lowering Melting Temperatures of Ionic Liquids

Abstract: This chapter demonstrates the design and synthesis of the efficient filler based on octa-substituted polyhedral oligomeric silsesquioxane (POSS) for simultaneously improving thermal stability and lowering melting temperature of ion salts. Accordingly, the sulfonic acid-presenting POSS showed the superior properties as a filler for improving thermal properties of ILs. Initially, the synthetic procedure for the sulfonic acid POSS is illustrated. The author found that the POSS filler has well dispersibility in the ion salts, providing the series of homogeneous mixtures with various types of ion salts or ILs. Next, it was indicated that the degradation temperatures of the ion salts were significantly elevated by adding the POSS filler. Moreover, the lowering effects on the melting temperatures were observed. Based on this effect, some of ionic salts were transformed to ILs by mixing the small amount of the POSS filler.
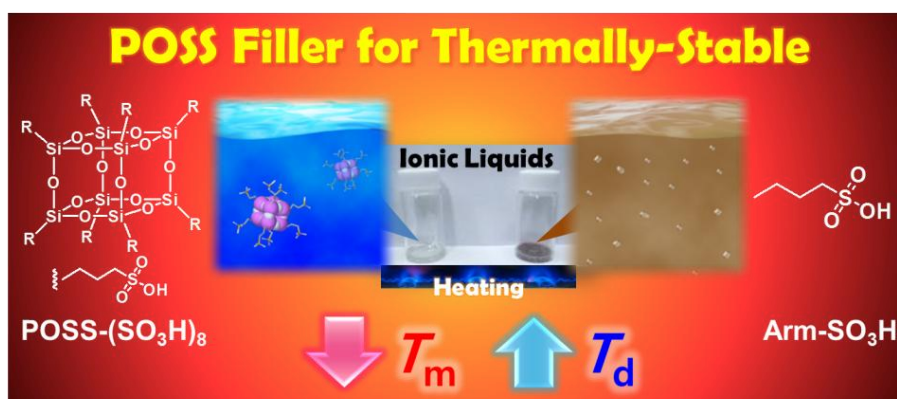
Introduction

Thermally-stable ionic liquids (ILs) have been required in a wide variety of research fields and industrial applications such as an electrolyte in lithium batteries[1–6] and high-temperature fuel cells[7–14] and a solvent in high temperature organic reactions[15–19]. To satisfy these demands, the series of the ion salts composed of organic compounds involving polymers were synthesized. On the other hand, it is still difficult in the invention of novel ILs to improve only the thermal stability without loss of other functions of ILs by altering chemical structures of the components because of the closed relationship between the thermal properties and the chemical structures. One of simple procedures to maintain the balance between the thermal stability and intrinsic functions could be the use of fillers which have been widely applied for the reinforcement of the polymeric materials.[20–23] If we can have the efficient fillers for improving the thermal stability of ILs and ion salts, we can expect to readily obtain the thermally-stable ILs with other characteristics. Therefore, it is of significance to develop the fillers which can reinforce the stability of ILs.

Recently, the author achieved the modulation of thermal properties of ion pairs using polyhedral oligomeric silsesquioxane (POSS).[24–26] The enhancement of thermal stability and lowering effects on the melting temperatures of ion pairs can be simultaneously obtained by tethering to the POSS core via covalent bonds.[24,25] As a result, the room-temperature ILs which are defined as the ionic salts with the melting temperature below 25 °C were produced based on POSS. Furthermore, the author has recently presented the molecular filler for lowering the melting temperatures of ionic salts by the POSS derivative.[26] By the hydrogen bond formation between the carboxylic acid in the POSS and the ionic salts, the crystallinity can be significantly reduced. Finally, the melting temperatures of the ionic salts can be greatly reduced. On the other hand, the thermal stabilities of most of the salts were spoiled by

adding the POSS filler. The next challenge is to develop the molecular filler for improving the thermal stability of ILs without increases of the melting temperatures.

This chapter is depicted on the molecular design for the efficient POSS filler for modulating thermal properties of conventional ILs and ionic compounds. The author designed the molecular filler based on POSS and synthesized the sulfonic acid-presenting POSS (POSS-$[SO_3H]_8$) in good yields. The well-dispersion ability of POSS-$[SO_3H]_8$ in various kinds of ionic compounds was observed. Finally, the author found that POSS-$[SO_3H]_8$ had significant effects for decreasing melting temperature and enhancing thermal stability of a wide variety of ionic compounds simultaneously. The author also confirmed from the calculation of thermodynamic parameters during the melting process that the rigid cubic and symmetric structure of POSS plays significant roles in the improvements of thermal properties.

Experimental Section

General. ^1H NMR and ^{13}C NMR spectra were measured with a JEOL EX–400 (400 MHz for ^1H and 10 MHz for ^{13}C) spectrometer. ^{29}Si NMR spectra were measured with a JEOL JNM-A400 (80 MHz) spectrometer. Coupling constants (*J* value) are reported in Hertz. The chemical shifts are expressed in ppm downfield from tetramethylsilane, using residual chloroform ($\delta = 7.24$ in ^1H NMR, $\delta = 77.0$ in ^{13}C NMR) or residual DMSO ($\delta = 2.49$ in ^1H NMR, $\delta = 39.5$ in ^{13}C NMR) as an internal standard. MASS spectra were obtained on a JEOL JMS–SX102A. Differential scanning calorimetry (DSC) thermograms were carried out on a SII DSC 6220 instrument by using *ca.* 10 mg of exactly weighed samples at heating rate of 10 °C/min. Thermogravimetric analysis (TGA) was performed on an EXSTAR TG/DTA 6220, Seiko Instrument, Inc., with the heating rate of 10 °C/min up to 500 °C under nitrogen

atmosphere. Residual methanol was removed by keeping in a vacuum oven at 100 °C for 1 h before the TGA measurements. Water abundances were evaluated with a Karl-Fischer Moisture Titrator MKC-501, Kyoto Electronics Manufacturing, Co., Ltd. (Kyoto, Japan). 1-Ethyl-3-methylimidazolium chloride [EMIM-Cl], 1-butyl-3-methylimidazolium bromide [BMIM-Br], 1-ethyl-2,3-dimethylimidazolium bis(trifluoromethanesulfonyl)imide [EdMIM-TFSI], 1-butyl-3-methylimidazolium trifluoromethanesulfonate [BMIM-OTf], 1-ethylpyridinium bromide [EP-Br] were purchased from TCI. 1-Butyl-3-methylimidazolium chloride [BMIM-Cl], 1-allyl-3-methylimidazolium chloride [AMIM-Cl], 1-ethyl-3-methylimidazolium bromide [EMIM-Br], tetrabutylammonium bromide [TBA-Br], and tetraoctylammonium bromide [TOA-Br] were purchased from WAKO. 1,2,3-Trimethylimidazolium methylsulfate [TriMIM-MeSO$_4$] and 1-benzyl-3-methylimidazolium hexafluorophosphate [BeMIM-HFPS] were purchased from SANTA CRUZ BIOTECHNOLOGY. 1-Ethyl-3-methylimidazolium bis(trifluoromethanesulfonyl)imide [EMIM-TFSI] and 1-butyl-3-methylimidazolium bis(trifluoromethanesulfonyl)imide [BMIM-TFSI] were purchased from Aldrich. All reagents were used as supplied without further purification. Synthesis of 1-eicosyl-3-methylimidazolium bromide[5] and octakis(3-chloropropyl)silsesquioxane[5] were carried out according to the previous papers.

Synthesis of sulfonic acid functionalized POSS, POSS-[SO$_3$H]$_8$. Octakis(3-chloropropyl)silsesquioxane[7] (1 g, 0.96 mmol) was suspended in 100 mL of an ethanol–water mixture solvent (1:3 v/v), and sodium sulfite (0.98 g, 7.7 mmol) was added with stirring. The reaction mixture was refluxed for 48 h under nitrogen. After cooling to the room temperature, unreacted POSS-[Cl]$_8$ was removed by filtration. The filtrate was concentrated by a rotary evaporator. The crude product was dissolved in conc. HCl (35 wt %), and the resulting solution was filtered and evaporated under the reduced pressure. The final product was

obtained in 47 % yield as a white solid. ^{1}H NMR (D$_2$O) δ 0.89 (br, 16H, SiCH$_2$), 1.89 (br, 16H, CH$_2$), 2.99 (br, 16H, CH$_2$SO$_3$H). ^{13}C NMR (D$_2$O) δ 7.6, 18.6, 55.55. ^{29}Si NMR (D$_2$O) δ −66.78.

Synthesis of Arm-SO$_3$H. Arm-SO$_3$H was prepared by the same protocol for POSS-[SO$_3$H]$_8$ from 1-chloropropane (0.84 mL, 9.6 mmol). The final product was obtained as a white solid in 83 % yield. ^{1}H NMR (D$_2$O) δ 0.98 (br, 16H, SiCH$_2$), 1.73 (br, 16H, CH$_2$), 2.88 (br, 16H, CH$_2$SO$_3$H). ^{13}C NMR (D$_2$O) δ 12.3, 16.8, 54.5.

Preparation of the samples. The samples were prepared by the solution method in methanol: The ionic compound (1 g) and methanol (20 mL) were mixed in a 50 mL flask and stirred for 30 min at room temperature to generate a clear solution. Then, POSS-[SO$_3$H]$_8$ or Arm-SO$_3$H dissolved in water (2 mL) was added into the solution. The mixture was additionally stirred for 1 h at room temperature, and the resulting clear solution was concentrated by a rotary evaporator. The homogeneous mixtures were obtained as a white solid after dried *in vacuo* and used for the analyses.

Differential scanning calorimetry, DSC. DSC thermograms were recorded on a SII DSC 6220 instrument by using approximately 10 mg of exactly weighed samples. The sample on the aluminum open pan was cooled to −50 °C at the rate of 10 °C/min under nitrogen flowing (30 mL/min) and then heated from −50 °C to 180 °C with the same rate. The melting temperatures (T_m) were determined as the onset of the second curves to eliminate heat history. Fusion enthalpy (ΔH_{fus}) was calculated from the areas of the endothermic peaks at the first cycle with the completely crystallized samples soaked in the liquid nitrogen before the measurements.

**Thermogravimetric analysis, TGA.** TGA was performed on an EXSTAR TG/DTA6220, Seiko Instrument, Inc., with the heating rate of 10 °C/min up to 700 °C under nitrogen flowing (200 mL/min). Residual water was removed by keeping on the platinum pan at 110 °C for 1 h before the curve profiling. The decomposition temperatures (T_{10d}) were determined from the temperature with 10% of weight loss.

Results and Discussion

In Chapter 2, the formation of hydrogen bonds between the carboxylic acid groups in the POSS filler and ion pairs is essential to express the lowering effect on the melting temperatures of the ion pairs.[26] Based on this fact, the author introduced the sulfonic acid groups into the POSS filler instead of the carboxylic acid groups to realize the stronger interaction between the end groups of POSS and the ionic matrices. The synthesis of POSS-$[SO_3H]_8$[29] and Arm-SO_3H as a comparison to evaluate the effect of the POSS core were synthesized using sulfonation of POSS-$[Cl]_8$[27,28] and 1-chloropropane by sodium sulfite according to Scheme 1, respectively. The chemical structures and thermal properties of conventional ionic compounds used in this study are listed in Figure 1 and Table 1. The preparation of the homogeneous samples containing the POSS filler and the ionic compounds was executed via the solution method: The mixtures of 1 g of the ion compounds in methanol (20 mL) was added to the POSS-$[SO_3H]_8$ in water (2 mL). After stirring until the precipitation completely disappeared, the resulting solution was concentrated *in vacuo*. The samples were stored in a glove box under an argon atmosphere to keep the water abundance below 1.5 wt % determined by the Karl Fischer method. The samples containing Arm-SO_3H was also prepared with the same procedure.

Scheme 1. Synthesis of the molecular fillers used in this study
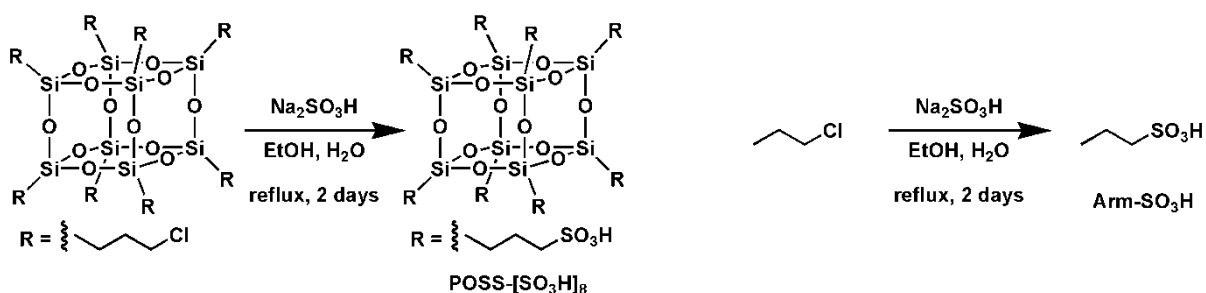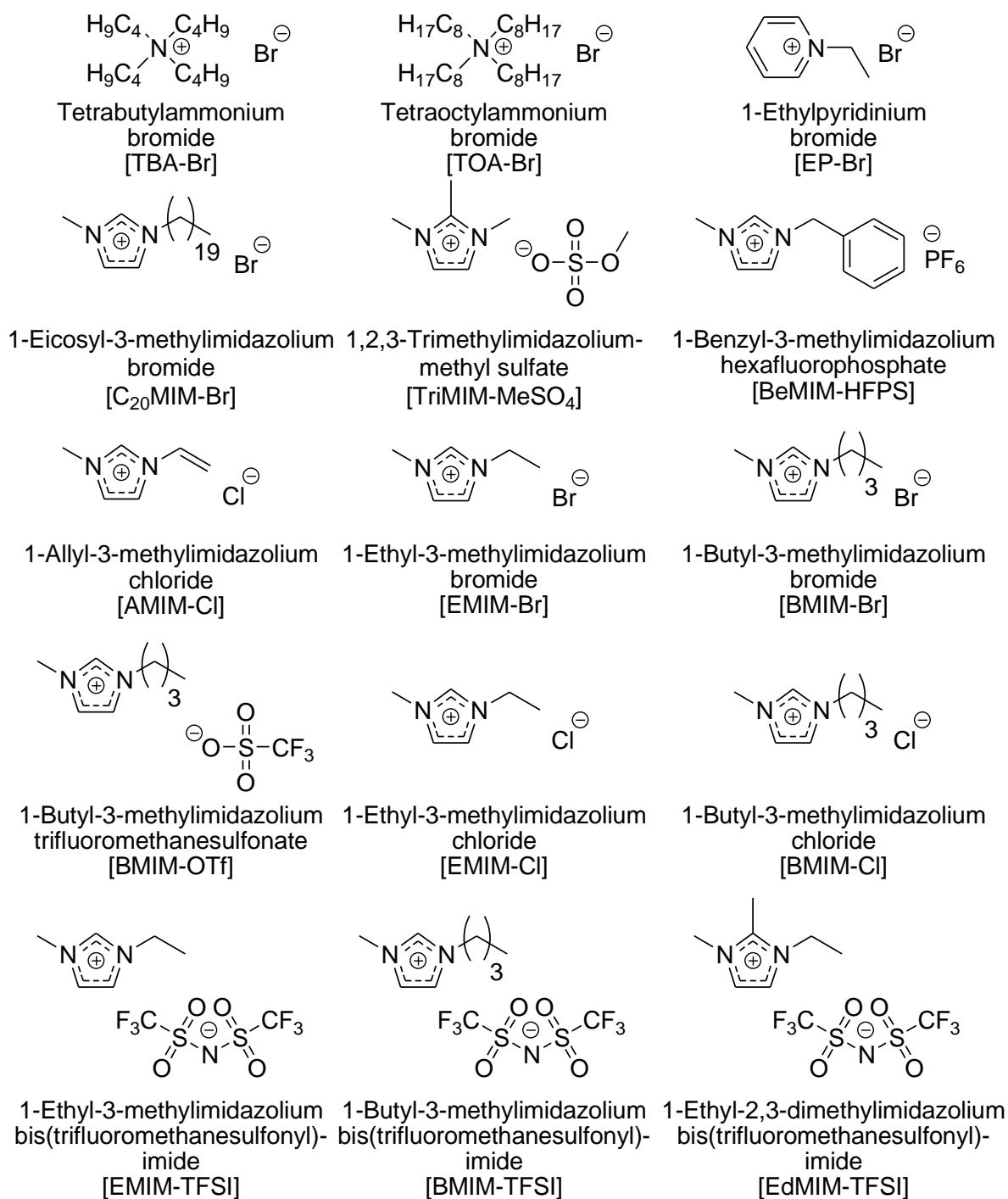
Figure 1. Chemical structures of the ion salts used in this study.

Table 1. Melting temperatures, thermodynamic parameters, and decomposition temperatures with 10% of weight loss of the conventional ion compounds with or without 20 wt % fillers

Salt	Filler	mol%	T_m (°C)[a]	ΔT_m (°C)	T_{10d} (°C)[b]	ΔT_{10d} (°C)	ΔH_{fus} (kJ/mol)[a]	ΔS_{fus} (J/mol·K)[c]
TriMIM-MeSO₄	–	0	122	–	n.d.[d]	–	18.9	48
	POSS	3.8	94	−28	n.d.[d]	–	11.9	32
	Arm	30.9	118	−4	n.d.[d]	–	16.3	42
BeMIM-HFPS	–	0	135	–	360	–	27.3	67
	POSS	5.4	111	−24	383	+23	18.4	48
	Arm	39.1	128	−7	342	−18	20.5	51
TBA-Br	–	0	92	–	199	–	30.9	79
	POSS	5.4	76	−16	228	+29	18.9	51
	Arm	39.4	93	+1	214	+15	26.7	71
TOA-Br	–	0	99	–	193	–	19.8	53
	POSS	8.9	76	−23	223	+30	9.3	27
	Arm	52.4	92	−7	207	+14	15.7	43
EP-Br	–	0	125	–	246	–	18.2	46
	POSS	3.2	88	−37	267	+13	11.7	32
	Arm	27.5	90	−35	235	−11	16.4	42
EMIM-Cl	–	0	79	-	276	–	25.7	73
	POSS	2.5	67	−12	283	+7	16.4	48
	Arm	22.8	68	−11	278	+2	18.1	52
BMIM-Cl	–	0	72	–	264	–	–	–
	POSS	3.0	n.d.[d]	–	284	+20	–	–
	Arm	26.0	n.d.[d]	–	256	−8	–	–
AMIM-Cl	–	0	n.d.[d]	–	246	–	–	–
	POSS	2.8	n.d.[d]	–	275	+29	–	–
	Arm	24.2	n.d.[d]	–	258	+12	–	–
EMIM-Br	–	0	80	–	296	–	11.7	33
	POSS	3.3	61	−19	299	+3	8.5	25
	Arm	27.8	75	−5	288	−8	10.7	31
BMIM-Br	–	0	77	–	278	–	18.1	52
	POSS	3.8	n.d.[d]	–	294	+16	–	–
	Arm	30.6	n.d.[d]	–	275	−3	–	–
C₂₀MIM-Br	–	0	70	–	280	–	21.2	61
	POSS	7.3	55	−15	289	+9	15.0	46
	Arm	47.2	65	–	277	−3	17.4	51
EMIM-TFSI	–	0	−14	–	424	–	22.4	86
	POSS	6.5	−23	−9	430	+14	16.9	68
	Arm	44.1	−18	−4	393	−31	19.0	76
BMIM-TFSI	–	0	−2	-	426	–	11.2	41
	POSS	7.0	−2	±0	428	+2	11.2	41
	Arm	45.8	−2	±0	389	−37	12.7	47
EdMIM-TFSI	–	0	26	–	445	–	15.0	50
	POSS	6.7	20	−6	434	−9	11.9	41
	Arm	44.9	24	−2	409	−36	14.1	47
BMIM-OTf	–	0	18	–	404	–	16.2	56
	POSS	4.9	10	−8	411	+7	14.9	53
	Arm	36.7	15	−3	343	−61	16.0	56

[a]Obtained from the second heating curves in the DSC profiles.

[b]Determined from the temperatures with 10% of weight loss in the TGA curves.

[c]Calculated from the following relation: $\Delta S_{fus} = \Delta H_{fus}/T_m$.

[d]n.d.= not detectable.

Initially, the author evaluated the effect of POSS filler on the melting temperature (T_m) of the ion salts, TriMIM-MeSO$_4$, BeMIM-HFPS, TBA-Br, TOA-Br, and EP-Br, which have relatively-high melting temperatures. The differences of T_ms before and after adding 20 wt % of POSS-[SO$_3$H]$_8$ or Arm-SO$_3$H are illustrated in Table 1. The T_m values were determined from the endothermic peaks observed at the second cycles from the DSC profiles (Figure 2). By adding POSS-[SO$_3$H]$_8$ and Arm-SO$_3$H to the ion salts, the T_m values were lowered. In particular, the samples with POSS-[SO$_3$H]$_8$ showed the lower T_m values than those with Arm-SO$_3$H. For example, the T_m value of TriMIM-MeSO$_4$ was lowered from 122 °C to 94 °C by POSS-[SO$_3$H]$_8$. On the other hand, Arm-SO$_3$H can reduce the Tm value to 118 °C. These data represent that POSS-[SO$_3$H]$_8$ can work as a filler for transforming TriMIM-MeSO$_4$ as a definitional IL. In the case of TBA-Br, the T_m values of the ion salts were hardly reduced by adding Arm-SO$_3$H even with excess amounts. These data clearly indicate that the POSS should be responsible for lowering T_m values of the ion salts. Especially, the molar percentages of the sulfonic acid groups in the POSS-[SO$_3$H]$_8$ mixtures are far smaller than those of Arm-SO$_3$H. These facts indicate that the existence of POSS should be responsible for lowering T_m values. The enhancement of the hydrogen bonding by the POSS core could increase the interaction to the ion pairs.[8] Significantly, according to the DSC profiles, the shapes of the endothermic peaks were subtly broadened in the presence of POSS-[SO$_3$H]$_8$. Furthermore, as representatively observed from the EP-Br sample, only the single peak can be obtained from the POSS-[SO$_3$H]$_8$-containing mixture although there are two peaks in the profile of the Arm-SO$_3$H-conting mixture. These results strongly suggest that the POSS filler should make strong interaction with the ion salts, and the crystallinity of the salts could be drastically reduced even in the presence of POSS-[SO$_3$H]$_8$.
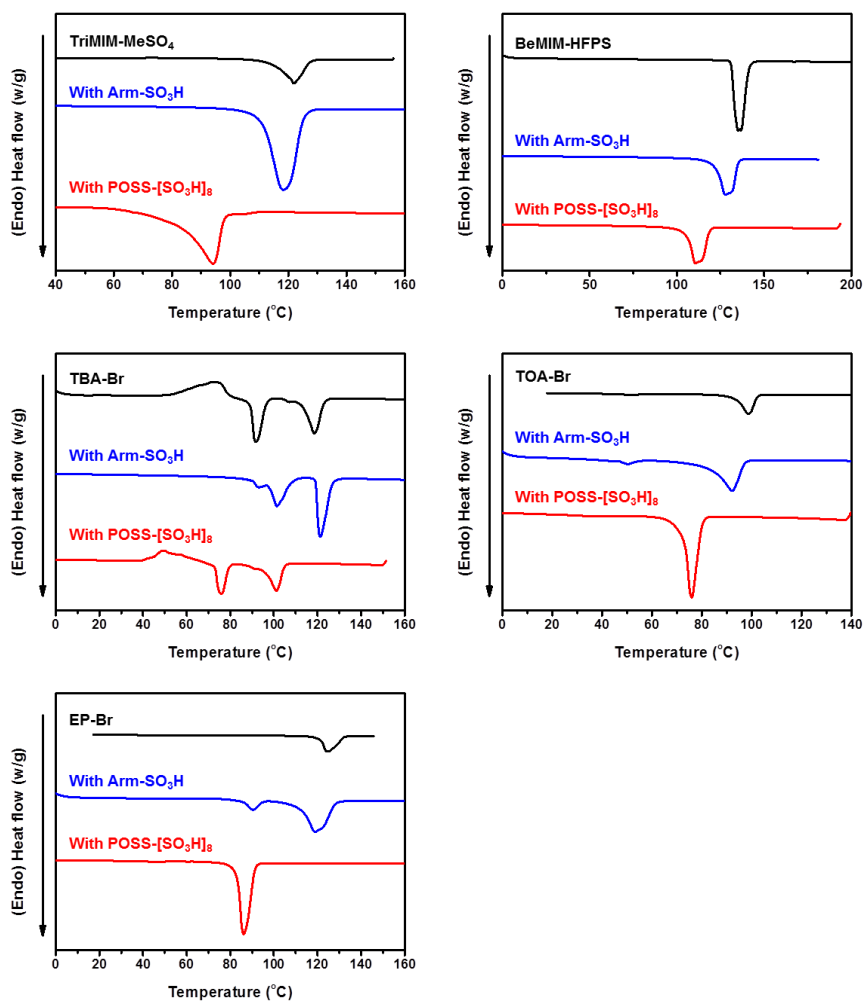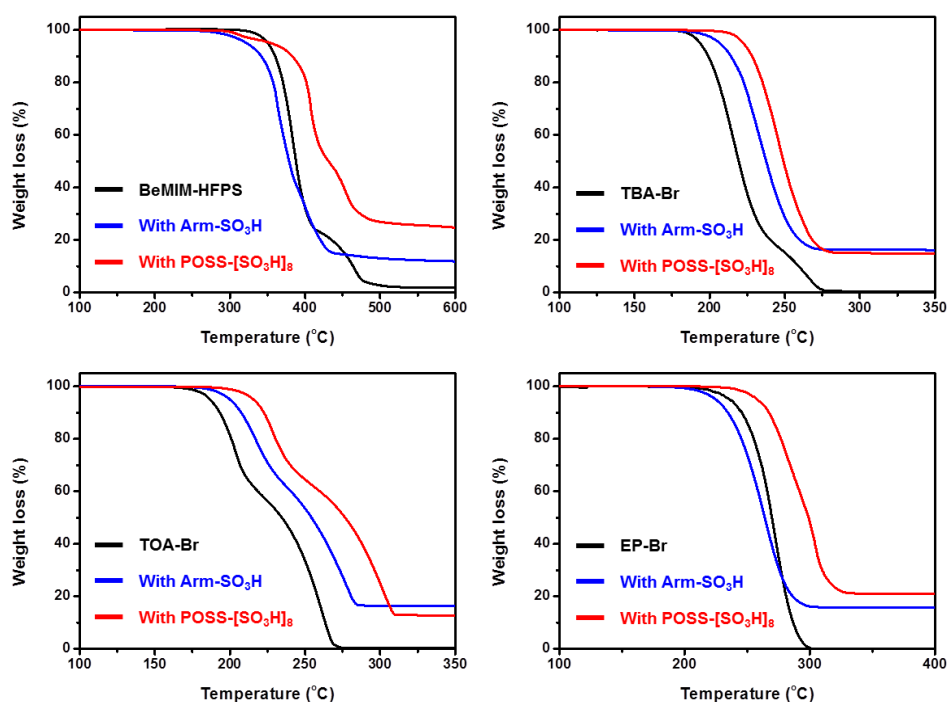
Figure 2. The representative DSC curves of the samples containing 20 wt % of the fillers in the second scan with a heating rate of 10 °C/min under nitrogen atmosphere.

The influence of the molecular fillers on the thermal stability was investigated by TGA (Figure 3). In Table 1, the degradation temperatures with 10% of weight loss (T_{10d}) are listed. The addition of the POSS-[SO$_3$H]$_8$ showed significant effect to enhancement of thermal stability of the salts. The salts containing POSS-[SO$_3$H]$_8$ showed higher T_{10d} values than those of Arm-SO$_3$H and the ion salts. In particular, the T_{10d} values of BeMIM-HFPS and EP-Br were increased by 23 °C and 13 °C, respectively. On the contrary, the addition of the Arm-SO$_3$H showed lower T_{10d} values than those of the ion salts. In the cases of TBA-Br and

TOA-Br, the POSS-[SO$_3$H]$_8$-containing samples showed higher T_{10d} values than those of the Arm-SO$_3$H-containing samples. These results indicate that thermal stability can be efficiently enhanced by adding POSS-[SO$_3$H]$_8$ as a filler. The rigid silica cage could suppress the molecular tumbling and prevent the degradation of the surrounding molecules. In other words, the POSS filler can affect the thermal properties of the ion salt molecules in the melting states. The strong interaction among the POSS filler and ion pairs could enable to transmitting the filler effect to the distant ion pairs from POSS. Moreover, it has been proposed that the ILs form the heterogeneous structures.[31,32] Thus, there is the possibility that the influence of the filler could be transmitted via the interaction among the IL molecules. The decomposition temperatures of POSS-[SO$_3$H]$_8$ and Arm-SO$_3$H with 5 % of weight loss are 433 °C and 234 °C, respectively. These data also support the POSS effect on the improvement of thermal stabilities of the ion salts
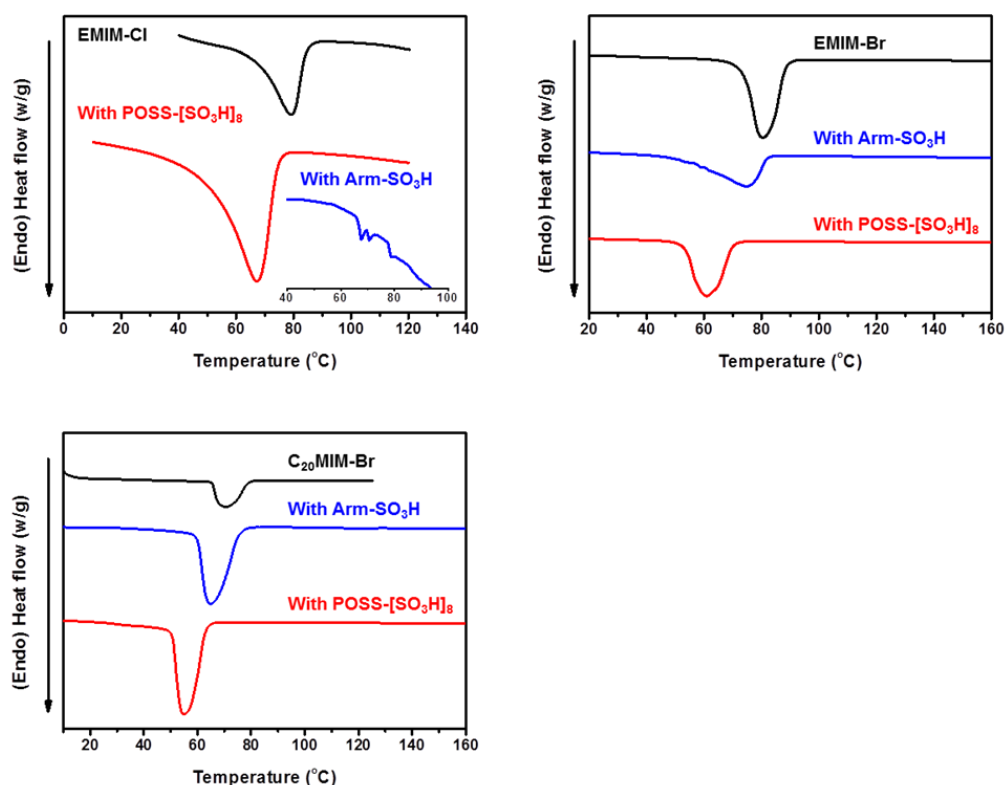

Figure 3. The representative TGA curves of the conventional ion salts containing 20wt % of the fillers with a heating rate of 10 °C/min under nitrogen atmosphere.

To prove the feasibility of the POSS filler to the ILs having lower melting temperatures, the author evaluated the thermal properties with the different sets of ILs including EMIM-Cl, BMIM-Cl, AMIM-Cl, EMIM-Br, BMIM-Br, and C_{20}MIM-Br, which intrinsically possess relatively lower T_m values than those of the previous ion salts (Figures 4 and 5). Furthermore, as the room-temperature ILs (RT-ILs) which are defined as the ion salts with the T_ms below 25 °C, EMIM-TFSI ($T_m = -14$ °C), BMIM-TFSI ($T_m = -2$ °C), EdMIM-TFSI ($T_m = 26$ °C), and BMIM-OTf ($T_m = 18$ °C) were selected. By adding POSS-[SO$_3$H]$_8$ to these ILs, the T_m values were significantly lowered. Surprisingly, the addition of POSS-[SO$_3$H]$_8$ to the RT-ILs can induce the decreases of the T_m values. For instance, the T_m values of EMIM-TFSI, EdMIM-TFSI, and BMIM-OTF were lowered by 9 °C, 6 °C, and 8 °C by adding POSS-[SO$_3$H]$_8$, respectively. These results clearly indicate that POSS-[SO$_3$H]$_8$ can be an efficient molecular filler for reducing the T_m values of the ILs.
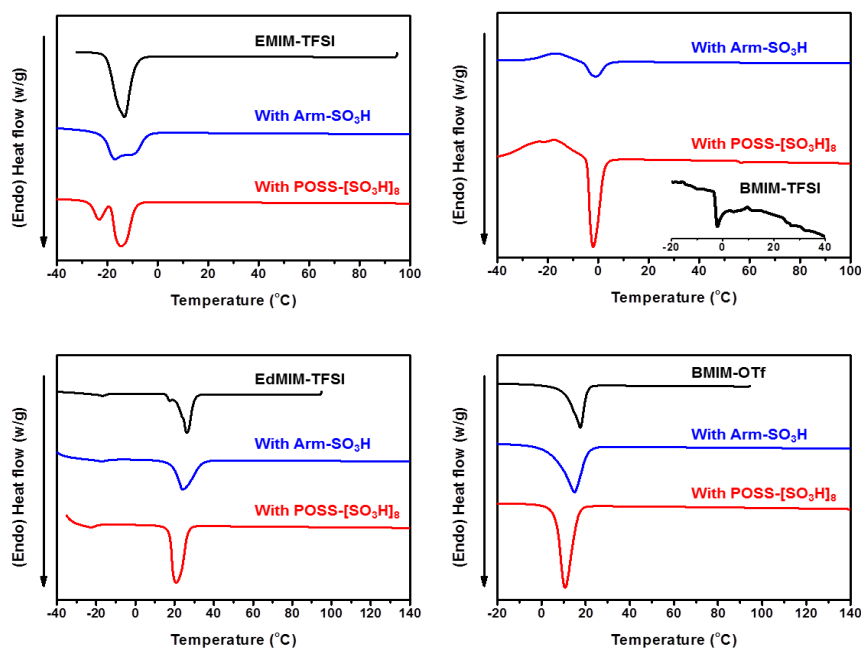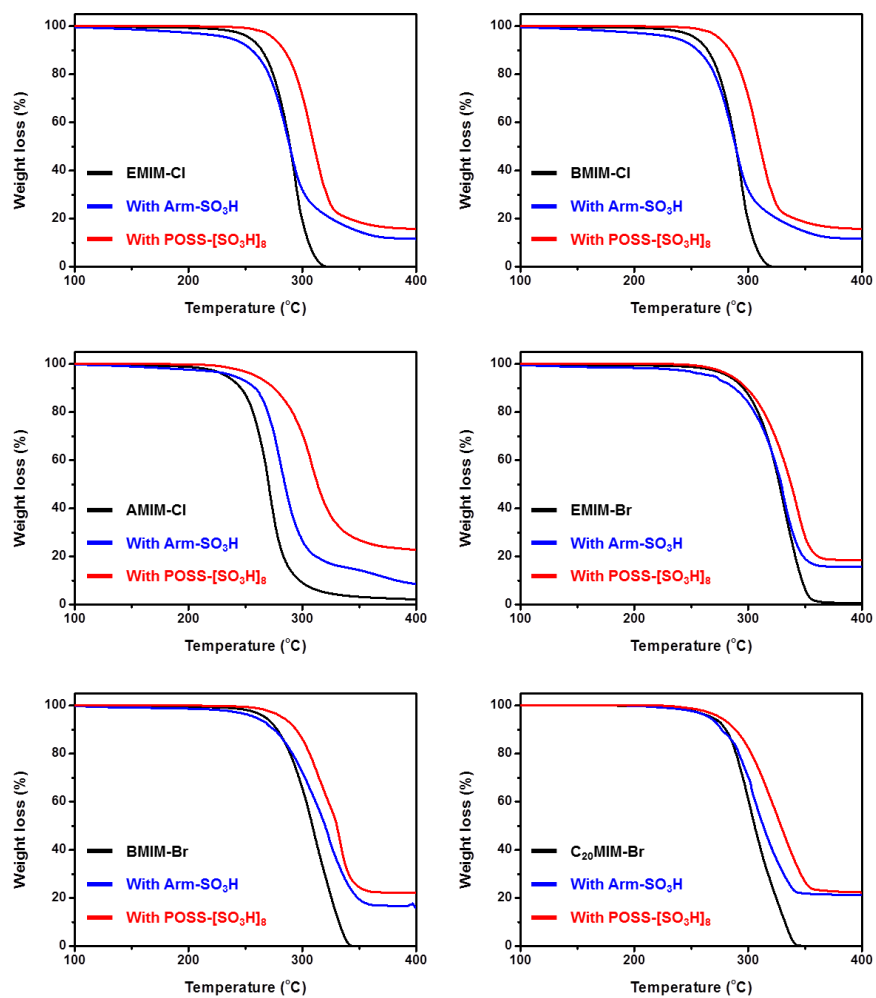

Figure 4. The representative DSC curves of the RT-ILs containing 20 wt % of the fillers in the second scan with a heating rate of 10 $^{\circ}$C/min under nitrogen atmosphere.

75

Figure 5. The representative DSC curves of the conventional ILs containing 20 wt % of the fillers in the second scan with a heating rate of 10 ^{o}C/min under nitrogen atmosphere.

Thermal stabilities of the ILs and the RT-ILs containing the fillers were examined (Figures 6 and 7). The addition of the POSS-[SO$_3$H]$_8$ to the ILs similarly induced the improvement of the thermal stabilities. The T_{10d} values of BMIM-Cl and BMIM-Br were enhanced by 20 °C and 16 °C, respectively. On the other hand, Arm-SO$_3$H critically caused the reduction of T_{10d} values of most ILs. From the samples with RT-ILs, higher T_{10d} values were observed over 400 °C in the presence of POSS-[SO$_3$H]$_8$ than those of pure RT-ILs. Some of the T_{10d} values of RT-ILs were highly decreased by adding Arm-SO$_3$H. These data prove the feasibility of the POSS filler for improving the thermal stability of ILs. From the series of measurements on the thermal properties, it can be summarized that the POSS filler can play positive roles in the modulation of the thermal properties of ion compounds.

Figure 6. The representative TGA curves of the conventional ILs containing 20 wt % of the fillers with a heating rate of 10 °C/min under nitrogen atmosphere.
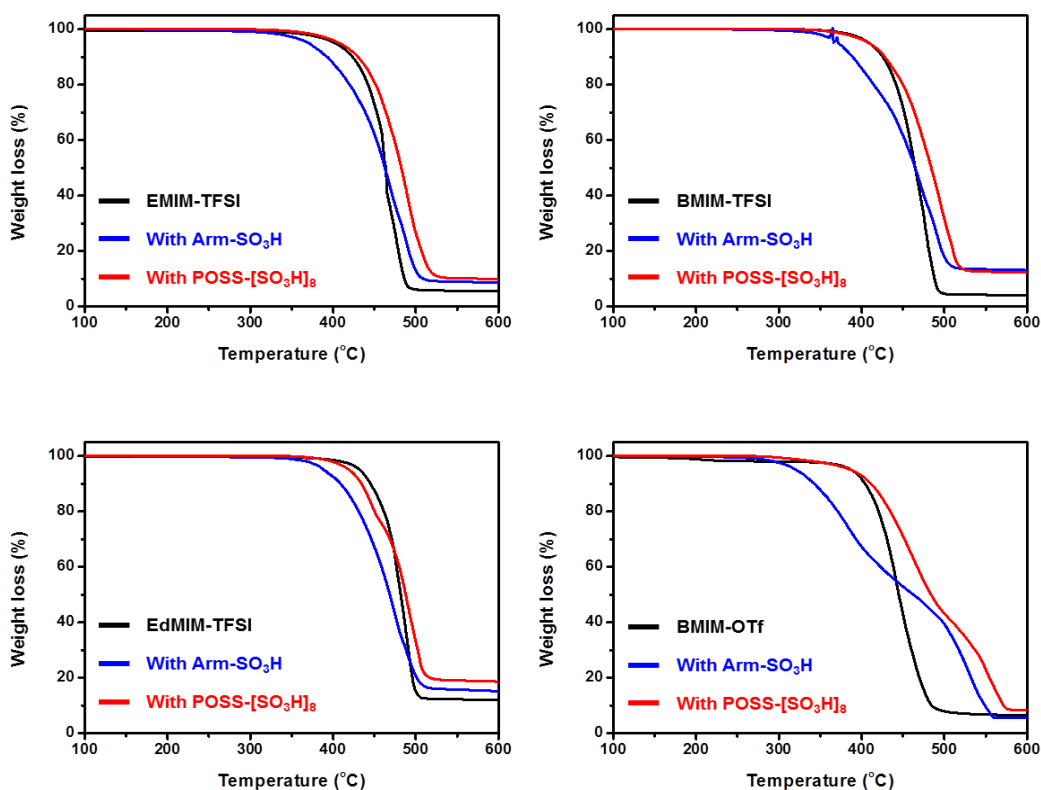
Figure 7. The representative TGA curves of the RT-ILs containing 20 wt % of the fillers with a heating rate of 10 °C/min under nitrogen atmosphere.

To obtain the information on the mechanism of the modulation of thermal properties by the POSS filler, the thermodynamic parameters (fusion enthalpy ΔH_{fus} and entropy ΔS_{fus}) in the melting process of the sample mixtures were evaluated from the areas of the endothermic peaks observed in the DSC profiles. The thermodynamic parameters were obtained with the samples containing 20 wt % of POSS-[SO$_3$H]$_8$. Accordingly, the smaller values of ΔH_{fus} and ΔS_{fus} were observed from the POSS filler-containing samples than those of the pure ionic

78

compounds and the mixtures containing Arm-SO$_3$H. These data represent that the interaction between ion pairs should be lowered in the crystals. In addition, the molecular symmetry should be maintained after the melting. These results can be explained by the similar mechanism proposed in the previous works[24-26,34]: The rigid cubic structures of the POSS core could disturb the interaction with the ion pairs as observed as small H_{fus} values. Thus, the T_m values could be reduced. In the liquid states, the ion pairs are captured and distributed around the POSS-core. In this state, the molecular shapes should form the sphere conformation, leading to the increase of the symmetry. Thus, because of decreases of ΔS_{fus}, the thermal stability to pyrolysis can be improved. Especially, since it is presumed that the sulfonic acid groups can form the strong interaction via hydrogen bonds with the ion pairs, the influence of POSS could be vividly observed in the samples.

Conclusion

To obtain the molecular filler for improving thermal stability and lowering melting temperatures of ILs, the author designed and synthesized POSS-[SO$_3$H]$_8$ which can make strong interaction with the sulfonic acid groups and the surrounding ion pairs via the robust hydrogen bonds. As a result, the author demonstrate that POSS-[SO$_3$H]$_8$ can work as an efficient molecular filler to show the desired properties. The data on the thermodynamic parameters suggest that the structural features of POSS such as rigid and highly-symmetric cube should affect the thermal properties by restricting the distribution of the surrounding ion pairs. The results described in this chapter can proof the validity of concept to use a molecular filler for modulating the properties of the ILs. Furthermore, the applicability of ILs could be expanded especially in high-temperature reactions by enhancing the thermal stability.

References

1. Zhou, Q.; Henderson, W. A.; Appetecchi, G. B.; Passerini, S. *J. Phys. Chem. C* **2010**, *114*, 6201.

2. Pringle, J. M.; Howlett, P. C.; MacFarlane, D. R.; Forsyth, M. *J. Mater. Chem*. **2010**, *20*, 2056.

3. Chakrapani, V.; Rusli, F.; Filler, M. A.; Kohl, R. A. *J. Phys. Chem. C* **2011**, *115*, 22048.

4. Zhou, Q.; Boyle, P. D.; Malpezzi, L.; Mele, A.; Shin, J. H.; Passerini, S.; Henderson, W. A. *Chem. Mater*. **2011**, *23*, 4331.

5. Weng, W.; Zhang, Z.; Lu, J.; Amine, K. *Chem. Commun*. **2011**, *47*, 11969.

6. Yoon, H.; Lane, G. H.; Shekibi, Y.; Howlett, P. C.; Forsyth, M.; Best, A. S.; MacFarlane, D. R. *Energy Environ. Sci*. **2013**, *6*, 979.

7. Bonhôte, P.; Dias, A. P.; Papageorgiou, N.; Kalyanasundaram, K.; Grätzel, M. *Inorg. Chem.* **1996**, *35*, 1168.

8. Buzzeo, M. C.; Evans, R. G.; Compton, R. G. *ChemPhysChem* **2004**, *5*, 1106.

9. Ito, K.; Nishina, N.; Ohno, H. *Electrochim. Acta* **2000**, *45*, 1295.

10. Wang, P.; Zakeeruddin, S. M.; Moser, J. E.; Humphry-Baker, R.; Grätzel, M. *J. Am. Chem. Soc.* **2004**, *126*, 7164.

11. Yoshizawa, M.; Ohno, H. *Electrochim. Acta* **2001**, *46*, 1723.

12. Washiro, S.; Yoshizawa, M.; Nakajima, H.; Ohno, H. *Polymer* **2004**, *45*, 1577.

13. Susan, M. A.; Kaneko, T.; Noda, A.; Watanabe, M. *J. Am. Chem. Soc.* **2005**, *127*, 4976.

14. Hayamizu, K.; Aihara, Y.; Nakagawa, H.; Nukuda, T.; Price, W. S. *J. Phys. Chem.*, *B* **2004**, *108*, 19527.

15. Rogers, R. D.; Seddon, K. R. *Science* **2003**, *302*, 792.

16. Wasserscheid, P.; Keim, W. *Angew. Chem., Int. Ed*. **2000**, *39*, 3772.

17. Welton, T. *Chem. Rev*. **1999**, *99*, 2071.

18. Ohno, H. *Bull. Chem. Soc. Jpn*. **2006**, *79*, 1665.

19. Buzzeo, M. C.; Evans, R. G.; Compton, R. G. *Chem. Phys. Chem*. **2004**, *5*, 1106.

20. Tanaka, K.; Chujo, Y. *J. Mater. Chem*. **2012**, *22*, 1733.

21. Tanaka, K.; Chujo, Y. *Polym. J.* **2013**, *45*, 247.

22. Tanaka, K.; Adachi, S.; Chujo, Y. *J. Polym. Sci. Part A: Polym. Chem*. **2009**, *47*, 5690.

23. Tanaka, K.; Adachi, S.; Chujo, Y. *J. Polym. Sci. Part A: Polym. Chem*. **2010**, *48*, 5712.

24. Tanaka, K. ; Ishiguro, F. ; Chujo, Y. *J. Am. Chem. Soc*. **2010**, *132*, 17649.

25. Tanaka, K. ; Ishiguro, F. ; Chujo, Y. *Polym. J*. **2011**, *43*, 708.

26. Jeon, J.-H.; Tanaka, K.; Chujo, Y. *RSC Adv*. **2013**, *3*, 2422.

27. Marciniec, B.; Butkiewicz, M.; Maciejewski, H.; Kubicki, M. *Organometallics* **2008**, *27*, 793.

28. Dutkiewicz, M.; Maciejewski, H.; Marciniec, B.; *Synthesis* **2009**, *12*, 2019.

29. Tanaka, K.; Murakami, M.; Jeon, J.-H.; Chujo, Y. *Org. Biomol. Chem*. **2012**, *10*, 90.

30. Pádua, A. A. H.; Gomes, M. F. C.; Canongia Lopes, J. N. A. *Acc. Chem. Res.* **2007**, *40*, 1087.

31. Canongia Lopes, J. N.; Price, S. L.; Pádua, A. A. H. *J. Phys. Chem. B* **2006**, *110*, 3330.

32. Asuncion, M. Z.; Ronchi, M.; Abu-Seir, H.; Laine, R. M. *C. R. Chimie* **2010**, *13*, 270.

Chapter 4

Rational Design of POSS Fillers for Simultaneous Improvements of Thermomechanical Properties and Lowering Refractive Indices of Polymer Films

Chapter 4

Rational Design of POSS Fillers for Simultaneous Improvements of Thermomechanical Properties and Lowering Refractive Indices of Polymer Films

Abstract: This chapter shows the design and synthesis of the polyhedral oligomeric silsesquioxane (POSS)-based dual functional molecular fillers for simultaneously lowering refractive indices and improving thermomechanical properties of conventional polymers. The author prepared the composite films with poly(methyl methacrylate) and polystyrene containing the series of the POSS derivatives with the single functional unit for interacting with polymer chains and hepta-cyclopentyl substituents for creating exclusive volumes around the POSS core. From the measurements of refractive indices of polymer composites, it was revealed that all POSS fillers can lower the refractive index of the films. In addition, thermal stabilities and mechanical properties were enhanced by adding POSS fillers.
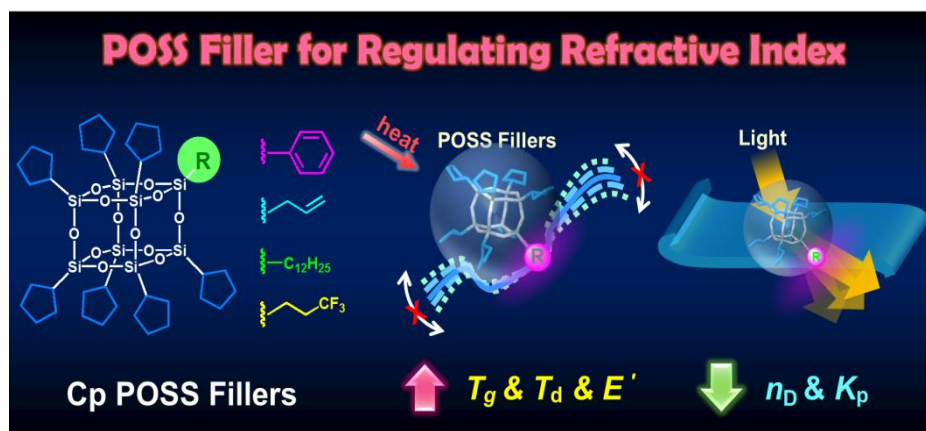
Introduction

Requirements of precise controls of optical properties in polymers have increased for improving the efficiency of conventional opto-electronic devices and generating advanced materials. For example, polymer films that have refractive index-gradients through the film contributes to improvements in luminescence efficiencies in electroluminescent devices by suppressing undesired reflection or scattering inevitably caused at the refraction gaps.[1] The use of molecular fillers is simple and feasible techniques for fabricating these functional-gradient materials because it is easy to control the local concentrations and modulate functions based on preprogrammed designs.[2,3] Thus, the development of effective molecular fillers should be potentially of great significance.

There are two categories of molecular fillers for the lowering refractive indices (RIs) of the materials; molecules with low dielectric constants such as perfluorinated compounds and large exclusion volumes as found with rigid caged compounds.[4–6] However, the introduction of these fillers into polymers often induces critical decreases in the thermal stabilities and mechanical properties of the polymer matrices. Because of poor compatibility of fluorine groups with polymer chains, phase separation can occur readily, leading to significant decreases in thermal durability. Although void spaces can efficiently reduce refractive indices, mechanical properties are also likely to be reduced. Thus, the maintenance of the balance between decreasing RIs while increasing thermomechanical properties is the critical requirement to the development of effective molecular fillers that lower RIs.

Polyoctahedral oligomeric silsesquioxanes (POSS) are well-known as molecular building blocks to construct functional materials as well as to improve the thermomechanical properties of polymers.[7–20] The rigid POSS structure can suppress the molecular motions of polymer chains, thereby enhancing the thermal and/or mechanical properties of the matrices. Particularly, the significant enhancement to the thermal stabilities of the polymers has been

observed by adding octa-substituted POSS derivative with vinyl and phenyl groups. In addition, it was implied that the symmetrical structure of the silica cube could contribute to reducing entropy differences in phase transitions.[21] Thereby, the molecular motion could be suppressed, resulting in the improvements of the thermal stabilities of POSS-containing composites. Furthermore, it has been reported that POSS is a suitable nanobuilding block for lowering refractive indices.[22,23] Recently, the significant effect of octa-substituted POSS derivatives with ethyl, vinyl, and cyclopentyl groups to lower RIs of the conventional polymer matrices (−0.0040, −0.0027, and −0.0010 with 1.5 mol % filler concentrations, respectively) was reported.[24] Because of the large exclusion volumes created around POSS cores, the RIs of polymer films decreased by adding these octa-substituted POSS derivatives. However, there is still a critical issue for simultaneously lowering a RI while enhancing the thermomechanical properties of the polymers by using designed molecular fillers.

In this chapter, the author explains the series of dual-functional POSS fillers for simultaneously increasing the thermomechanical properties and decreasing the refractive indices of polymer matrices. To solve the problem on the reduction of thermal stability induced by reducing packing density of the matrices for reducing refractive indices, the author designed the POSS fillers with two kinds of the substituents for enhancing the affinity of the POSS core to polymer chains and for creating exclusive volumes around filler molecules. The design concept, synthesis of the POSS fillers using incomplete cages of POSS and the results are described here.

Experimental Section

General. ^{1}H NMR spectra were measured with a JEOL EX–400 (400 MHz) spectrometer. Coupling constants (*J* value) are reported in Hertz. MASS spectra were obtained on a JEOL

JMS–SX102A. Scanning electron microscopy (SEM) images were performed using a JEOL JSM–5600 operated at an accelerating voltage of 15 kV. UV–vis absorption spectra were recorded with a SHIMADZU UV–3600UV–vis–NIR spectrophotometer. The refractive indices were determined with an Abbe refractometer DR–M4 (accuracy ±0.0002, ATAGO Co.,ltd., Tokyo, Japan) at 580 nm at 25 °C. Dynamic mechanical analysis (DMA) was performed on a SDM5600/DMS210, Seiko Instrument, Inc., with the heating rate of 2 °C / min at 1 Hz with 1 % strain under air. Differential scanning calorimetry (DSC) thermograms were carried out on a SII DSC 6220 instrument by using ~10 mg of exactly weighed samples at heating rate of 10 °C/min. The glass transition temperatures (T_g) were evaluated from the second monitoring curves after annealing at 100 °C for 10 min, followed by cooling to 30 °C. Thermogravimetric analysis (TGA) was performed on an EXSTAR TG/DTA 6220, Seiko Instrument, Inc., with the heating rate of 10 °C/min up to 500 °C under nitrogen atmosphere. Residual chloroform was removed by keeping in a vacuum oven at 100 °C for 1 h before the TGA measurements. The van der Waals volumes of POSS derivatives and the monomer unit of PMMA were calculated after the modeling using a semi-empirical AM1 method.

Materials. Trichlorocyclopentylsilane (Adrich), trichlorophenylsilane (Adrich), trichloro-dodecylsilane (Adrich), trichloro(3,3,3-trifluoropropyl)silane (Adrich), and allyltrichloro-silane (TCI) were purchased and used for the assays without further purification. PMMA (Mw = 350,000) and PS (Mw = 35,000) were purchased from Aldrich and used as received. Tetrahydrofuran (THF) and triethylamine (TEA) were distilled over sodium and calcium hydride, respectively.

Synthesis of silsesquioxane partial cage [(c-C$_5$H$_9$)$_7$Si$_7$O$_9$(OH)$_3$]. Incompletely condensed trisilanol (c-C$_5$H$_9$)$_7$Si$_7$O$_9$(OH)$_3$ was prepared in 29% yield by the hydrolytic condensation

reaction of trichlorocyclopentylsilane in reflux aqueous acetone, according to the procedure reported before.[25]

Synthesis of POSS fillers. The trisilanol (0.5 g, 0.6 mmol) and triethylamine (0.33 mL, 2.3 mmol) were cooled in an ice bath, and trichlorosilane (phenyl-, 93 μL, 0.6 mmol; allyl-, 84 μL, 0.6 mmol; dodecyl-, 0.17 mL, 0.6 mmol; trifluoropropyl-, 95 μL, 0.6 mmol) in THF was added slowly to the mixture. The resulting solution was stirred overnight at room temperature. After removing insoluble salts by filtration, the filtrate was concentrated to 5 mL and poured into excess acetonitrile. The white precipitate was collected by filtration and dried *in vacuo* to produce a white solid (Cp POSS-P, 71 %; Cp POSS-A, 70 %; Cp POSS-D, 67 %; Cp POSS-F, 60 %).

Cp POSS-P: ^{1}H NMR (CDCl$_3$, 400 MHz) δ 7.67 (m, 2 H), 7.36-7.42 (m, 3 H), 1.79 (m, 20 H), 1.56 (m, 36 H), 0.97 (m, 7 H); ^{13}C NMR (CDCl$_3$, 400 MHz) δ 139.8, 134.1, 129.7, 137.6, 26.7, 26.6, 26.5, 26.3, 26.2; ^{29}Si NMR (CDCl$_3$, 400 MHz) δ −66.09, −66.43; LRMS (NBA) [(M+H)$^+$] calcd. 977, found 977; HRMS (NBA) [(M+H)$^+$] calcd. 977.6554, found 976.2865.

Cp POSS-A: ^{1}H NMR (CDCl$_3$, 400 MHz) δ 5.76 (m, 1 H), 4.92 (m, 2 H), 1.79 (m, 20 H), 1.56 (m, 38 H), 0.97 (m, 7 H); ^{13}C NMR (CDCl$_3$, 400 MHz) δ 132.6, 114.6, 26.7, 26.6, 26.5, 26.3, 26.2, 19.7; ^{29}Si NMR (CDCl$_3$, 400 MHz) δ −66.47, −66.53; LRMS (NBA) [(M+H)$^+$] calcd. 941, found 941; HRMS (NBA) [(M+H)$^+$] calcd. 941.6233, found 940.2865.

Cp POSS-D: ^{1}H NMR (CDCl$_3$, 400 MHz) δ 1.79 (m, 20 H), 1.56 (m, 36 H), 1.39 (m, 4 H), 1.26 (m, 16 H), 0.97 (m, 7 H), 0.88 (t, 3 H), 0.59 (t, 2 H); ^{13}C NMR (CDCl$_3$, 400 MHz) δ 77.3, 76.6, 32.5, 26.7, 26.6, 26.5, 26.3, 26.2, 22.8, 22.7, 22.3, 14.1, 11.9; ^{29}Si NMR (CDCl$_3$, 400 MHz) δ −66.54, −66.69; LRMS (NBA) [(M+H)$^+$] calcd. 1069, found 1069; HRMS (NBA) [(M+H)$^+$] calcd. 1069.8784, found 1068.4430.

Cp POSS-F: ^{1}H NMR (CDCl$_3$, 400 MHz) δ 2.12 (t, 2 H), 1.79 (m, 20 H), 1.56 (m, 36 H), 0.97 (m, 7 H), 0.83 (t, 2 H); ^{13}C NMR (CDCl$_3$, 400 MHz) δ 130.1, 26.7, 26.6, 26.5, 26.3, 26.2, 24.1, 2.2; ^{29}Si NMR (CDCl$_3$, 400 MHz) δ −65.68, −65.93; LRMS (NBA) [(M+H)$^+$] calcd. 997, found 997; HRMS (NBA) [(M+H)$^+$] calcd. 997.6106, found 996.2739.

Preparation of polymer composites. The mixtures (20 mL) containing 1 g of polymers (PMMA or PS) and various amounts of POSS fillers in chloroform were stirred at room temperature for 3 h and then poured into the bottom of vessels (7 cm × 4.5 cm). After drying at room temperature for 2 days, the film samples were dried again in a vacuum oven at 60 °C for 2 h. The resulting films were used for the following measurements.

Determination of refractive indices of the polymer composites. According to the Lorentz–Lorenz equation, the refractive index (n) of the polymer (element 1) composites containing fillers (element 2) can be described using the molar fractions (α), molar refractions (R), and molar volumes (V).[26]

$$\frac{n^2 - 1}{n^2 + 2} = \alpha_1 \frac{n_1^2 - 1}{n_1^2 + 2} + \alpha_2 \frac{n_2^2 - 1}{n_2^2 + 2} = \alpha_1 \frac{R_1}{V_1} + \alpha_2 \frac{R_2}{V_2} \tag{1}$$

The degree of packing can be described by the molecular packing coefficient K_p that is defined as

$$K_p = \frac{V_{VDW}}{V_{int}} \tag{2}$$

where V_{int} and V_{VDE} are the intrinsic and van der Waals volumes of the molecules, respectively. Therefore, molecules that have significant abilities to lower the interactions between polymer chains would show a smaller K_p value. In addition, according to Vuks equation, equation 1 can be transformed to the equation 3.[27]

$$\frac{n^2-1}{n^2+2} = \alpha_1 \frac{n_1^2-1}{n_1^2+2} + \alpha_2 \frac{n_2^2-1}{n_2^2+2} = \alpha_1 \frac{K_{p1}R_1}{V_{VDW,1}} + \alpha_2 \frac{K_{p2}R_2}{V_{VDW,2}} \tag{3}$$

In the case of amorphous polymers, the K_p values (K_{p1}) were determined to be 0.68.[28] Therefore, the author can simply calculates K_{p2} values by measuring the refractive indices of the composite (n) using equation 3.
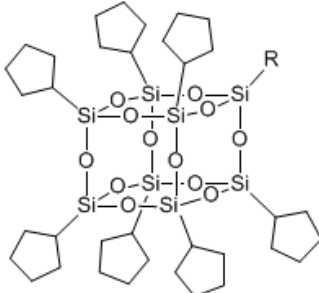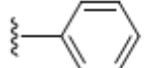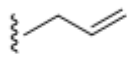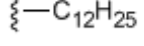
Results and Discussion

The author designed the POSS fillers with two kinds of substituents at the vertices of the silica cube. In the previous report, it was found that cyclopentyl groups can create large exclusive volumes around filler molecules, lowering the RIs of the matrices.[24] Thus, the author introduced the seven cyclopentyl groups in the POSS fillers. To reinforce the thermomechanical properties of the polymeric materials, the introduction of the functional units to enhance intermolecular interactions among polymer chains or symmetries of the chemical structure of the components to reduce the transition entropy is the typical manner.[24] However, the former strategy negatively affected to the lowering of RIs. Thus, the author sought to apply symmetric POSS for the reinforcement of polymers.[29,30] In other words, the author envisioned a scenario that by interacting POSS fillers only with a single polymer chain, molecular motions should be suppressed. Then, thermal and mechanical properties could be

improved. According to the previous report, phenyl- and vinyl-POSS showed large enhancements to the thermal stability of PS.[20] Long alkyl chains-substituted POSS can improve the thermal stability of PMMA. Based on these results, the author selected the phenyl-, allyl-, dodecyl-, and trifluoropropyl groups to obtain high affinity to the polymer chains.

The chemical structures and thermal decomposition temperatures with 20 wt % weight loss (T_{d20}) of the POSS fillers used in this study as a filler are listed in Table 1. These POSS derivatives are composed of heptacyclopentyl groups for lowering refractive indices and one functional unit for improving the durability of the polymers using poly(methyl methacylate) (PMMA) and polystyrene (PS). The composites containing POSS fillers were prepared by blending POSS fillers and polymers in solution. The mixtures of polymers (1.0 g) in chloroform (20 mL) were added to the POSS fillers with various concentrations (from 0.5 to 2 mol % to the monomer unit of the polymers) and stirred until the mixtures turned clear. Then, the resulting mixtures were poured into the polypropylene vessels (7 cm × 4.5 cm), and the sample films for measurements were obtained after drying in a vacuum oven at 60 °C for 2 h.

Table 1. Chemical structures and decomposition temperatures with 20 wt% weight loss of POSS fillers used in this study

Framework	Description	Chemical structure (R)	T_{d20} (°C)[a]
	Cp POSS-P		391
	Cp POSS-A		376
	Cp POSS-D	$-C_{12}H_{25}$	375
	Cp POSS-F	CF_3	380

[a]Determined from TGA.

Initially, the author investigated the surface morphologies of the composite films using scanning electron microscopy (SEM). Significant phase separation or aggregation of POSS fillers were hardly observed in the PMMA composites (Figures 1). These results suggest that homogeneous dispersions of the POSS fillers were realized in PMMA.

In contrast, inhomogeneity, implying the aggregation or phase separation was observed in the PS film. In the PS composites containing 0.5 mol % of POSS fillers, aggregated masses of POSS fillers were hardly observed on the surface morphologies as seen in Figure 1. They become easily visible in PS composites containing 1.0 mol % of POSS fillers. However, the sizes of these inhomogeneities in PS composites were below 100 nm except for the sample containing Cp POSS-F. Therefore, the author concludes that sufficient transparency for measuring refractivity with good reproducibility occurs at less than 1 mol % concentrations of the POSS fillers. Most samples showed turbidity with the 1.5 mol % POSS fillers, and the transparency of the composite films decreased drastically. The phase separation of POSS fillers was significant in most of the composite films containing 2 mol % POSS fillers. The processability of the film and reproducibility for the refraction measurements were reduced. Thus, the author discusses the filler effects with data sets obtained from samples containing POSS fillers (0.5 and 1.0 mol %).

PMMA Composites

PS Composites

0.5 mol %	1.0 mol %	0.5 mol %	1.0 mol %
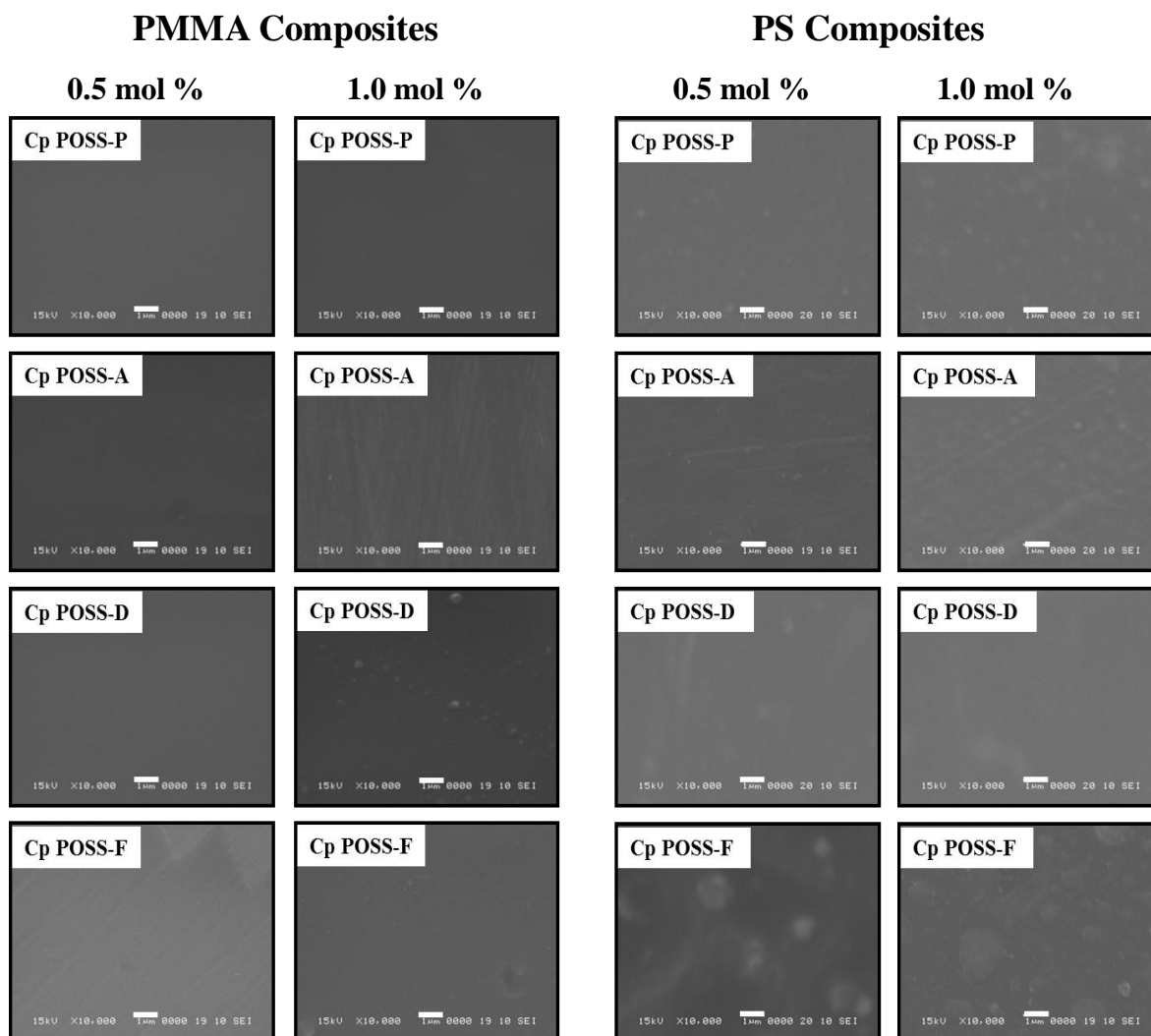
Figure 1. SEM images of PMMA and PS composites containing POSS fillers (0.5 and 1.0 mol %). Scale bars represent 1 μm.

RIs of the composite films with variable concentrations of POSS fillers were measured using an Abbe refractometer. The averages of the values at five distinct points in the composite films are shown in Table 2. The RIs of polymer films with POSS fillers were lower than that of pure polymers. Moreover, the RIs of the polymers decreased corresponding with increases in POSS filler concentrations (Figure 2). From these results, as expected, the POSS fillers described here have the ability to lower refractive indices of polymer films. The mechanism of the lowering of refractivity can be explained by the findings in the previous

93

report.[24] The cyclopentyl groups on POSS can effectively create the exclusion volumes. Consequently, the reduction of the packing of the polymer chains likely occurs, resulting in the lowering refractivity. According to the recent reports, the degree of decreases in RIs by the present POSS fillers is large enough for the application to the optical fibers.[31,32] Thus, the author's concept for the design of molecular fillers could be applicable in the practical materials.
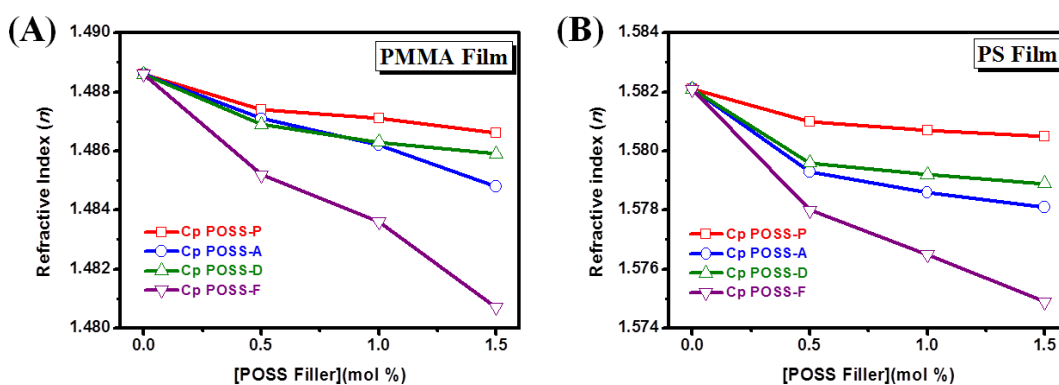
Figure 2. Refractive indices (n) of the (A) PMMA and (PS) composites containing various concentrations of POSS fillers.

Table 2. Differences of refractive indices (Δn) induced by adding variable concentrations of POSS fillers and representative molecular packing coefficients (K_{p2}) of POSS fillers[a]

	PMMA				PS			
	0.5 mol%	1.0 mol%	1.5 mol%		0.5 mol%	1.0 mol%	1.5 mol%	
Filler	Δn^{b}	Δn^{b}	Δn^{b}	$K_{p2}{}^{c}$	Δn^{d}	Δn^{d}	Δn^{d}	$K_{p2}{}^{c}$
Cp POSS-P	−0.0012	−0.0015	−0.0020	0.442	−0.0011	−0.0014	−0.0016	0.557
Cp POSS-A	−0.0015	−0.0024	−0.0038	0.361	−0.0028	−0.0035	−0.0040	0.364
Cp POSS-D	−0.0017	−0.0023	−0.0027	0.375	−0.0025	−0.0029	−0.0032	0.429
Cp POSS-F	−0.0034	−0.0050	−0.0079	0.201	−0.0040	−0.0055	−0.0072	0.279

[a]Measured at 25 °C with an Abbe refractometer. The values were calculated from the averages measured at five distinct points in the composite films.
[b]Caculated from the subtraction from the refractive index of the PMMA films (1.4886).
[c]Caculated from the refractive indices of composite films containing 1.0 mol % of POSS fillers.
[d]Caculated from the subtraction from the refractive index of the PS films (1.5821).

The degree of the packing of polymer chains and filler molecules can be estimated by the packing coefficients, K_{p1} and K_{p2}, respectively according to the equations shown in the experimental sections. The author has obtained the K_{p1} value as 0.677 with the pure polymer films corresponded to other reports (*ca.* 0.68).[24] From these data, the author can claims that air bubbles or the residual solvents inside the polymer films did not influence the refractive indices in the author's experiments. To evaluate the degree of packing of the POSS fillers, the author determined the K_{p2} values according to equation 3 (Table 2). It was found that all POSS fillers used in this experiment showed lower values than that of K_{p1}. These results indicate that the POSS filler should reduce the packing of polymer chains in the materials. Therefore, polymer composites with POSS fillers showed the lower refractive indices than those of the polymer films in the absence of POSS.

Next, the thermal properties of the composites were examined. Table 3 shows the results of DSC for polymer composites containing POSS fillers. The values were determined from the second heating curves to eliminate the heat history in the samples. The glass transition temperatures (T_g) of composites gradually shifted to higher temperatures by increasing the POSS fillers concentrations. These results were attributed to a reduction in the segmental mobility of polymer chains in the composites. Even though the packing of the polymer chains should be reduced by adding POSS fillers, the POSS fillers were responsible for the suppression of molecular motions. In particular, the substituent effect at the single group on POSS on the T_g values was obtained. This fact suggests that the interaction between the single substituent on POSS and polymer chains should play a crucial role in changing the thermal properties.

Table 3. The results of DSC with polymer composites containing POSS fillers[a]

| Filler	PMMA				PS			
	0.5 mol%	0.5 mol%	1.0 mol%	1.0 mol%	0.5 mol%	0.5 mol%	1.0 mol%	1.0 mol%
	T_g (°C)	ΔT_g (°C)	T_g (°C)	ΔT_g (°C)	T_g (°C)	ΔT_g (°C)	T_g (°C)	ΔT_g (°C)
none	72	–	72	–	80	–	80	–
Cp POSS-P	75	+3	87	+15	81	+1	82	+2
Cp POSS-A	74	+2	84	+12	83	+3	84	+4
Cp POSS-D	75	+3	78	+6	82	+2	84	+4
Cp POSS-F	76	+4	78	+6	83	+3	82,93	+2,+13

[a]Determined from the second heating curves.

Thermal stabilities of polymer composites containing POSS fillers were examined by TGA. Figure 3 shows the TGA curves of composites containing POSS fillers (0.5 and 1.0 mol %), and Table 4 summarizes the T_{d20} using the polymer composites containing POSS fillers. Since the significant thermal degradation was observed in the composites around the temperature with 20% weight loss assigned as the main chain scissions, the thermal stabilizing effects by POSS fillers were discussed by comparing the T_{d20} values of the composites. Residual chloroform was removed by keeping in a vacuum oven at 100 °C for 1 h before the measurements. Thermal reinforcement of PMMA composites by loading POSS fillers were observed as shown in Figure 3A and 3C. The dodecyl group of Cp POSS-D shows the enhancement to the thermal stability of PMMA. The T_{d20} value of PMMA composite containing 1.0 mol % of Cp POSS-D increased by 27 °C.

Table 4. The decomposition temperatures with 20 wt % mass loss of polymer composites containing POSS fillers[a]

Filler	PMMA				PS			
	0.5 mol%	0.5 mol%	1.0 mol%	1.0 mol%	0.5 mol%	0.5 mol%	1.0 mol%	1.0 mol%
	T_{d20} (°C)	ΔT_{d20} (°C)	T_{d20} (°C)	ΔT_{d20} (°C)	T_{d20} (°C)	ΔT_{d20} (°C)	T_{d20} (°C)	ΔT_{d20} (°C)
none	263	–	263	–	390	–	390	–
Cp POSS-P	283	+20	297	+34	394	+4	397	+7
Cp POSS-A	284	+21	303	+40	394	+4	397	+7
Cp POSS-D	282	+19	290	+27	392	+2	394	+4
Cp POSS-F	268	+5	282	+19	392	+2	392	+2

[a]Determined from TGA curves.
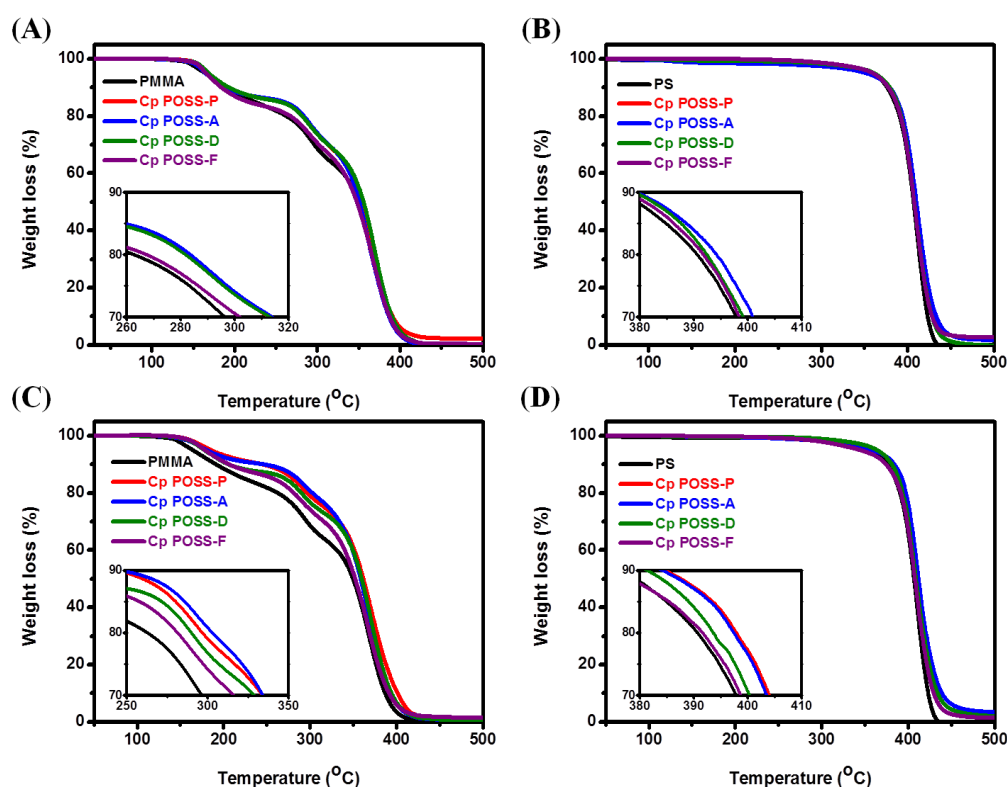
Figure 3. TGA thermograms of PMMA (0.5 mol % (A) and 1.0 mol % (C)) and PS (0.5 mol % (B) and 1.0 mol % (D)) composites containing POSS fillers with a heating rate of 10 °C/min under nitrogen atmosphere.

Similar tendency was observed in PS composites. Pure PS exhibits a T_{d20} at 390 °C. The T_{d20} value of PS increases by 4 °C by adding the Cp POSS-D. In addition, the thermal stability of polymer composites was gradually enhanced corresponding with increases in concentration of Cp POSS-D. Moreover, the T_{d20} values of the polymer composites containing 1.0 mol % Cp POSS-A significantly improved the thermal stability of PMMA: +40 °C and same for PS: +7 °C. Furthermore, the addition of 2.0 mol % Cp POSS-A greatly induced to the improvements of the thermal stability of PMMA (+51 °C) and PS (+10 °C). These effects were also observed in composites containing Cp POSS-P. The T_{d20} value of the PMMA composite containing 1.0 mol % Cp POSS-P increased dramatically by 34 °C. The

PMMA composite containing 2.0 mol % Cp POSS-P showed higher T_{d20} value at 318 °C. It is likely that a longer alkyl chain and an unsaturated group could interact with the polymer chains because of the strong hydrophobic interaction and tangle formation.

The mechanical properties of the polymer composites containing POSS fillers were evaluated by DMA (temperature scan at 1 Hz). Representative sets of DMA curves using the composites containing 0.5 and 1.0 mol % of POSS fillers are shown in Figure 4. The mechanical properties of the polymer composites containing POSS fillers are listed in Table 5. The POSS fillers improved the storage modulus (E') with the resulting highest increase seen on adding Cp POSS-D even at 1.0 mol %. The E' value of composite was dramatically enhanced by five-fold. In addition, the E' value with 1.0 mol % Cp POSS-P increased by 67%. The E' value of the PMMA composite containing 1.0 mol % Cp POSS-A was 1.8-times larger than that of pure PMMA film. In the PS composites, similar effects were also observed. The E' values of PS composites were improved by adding POSS fillers. These results suggest that the one functional group as longer alkyl chain or unsaturated groups of POSS fillers could make an interaction with the polymer chains. As a result, POSS fillers should suppress the motion of polymer chains. From these data involving DSC, TGA and DMA, it is summarized that the POSS fillers used in this study have significant abilities to simultaneously improve thermomechanical properties and lower the refractive indices of polymers.

Table 5. The results of DMA with polymer composites containing POSS fillers[a]

Filler	PMMA						PS					
	0.5 mol%			1.0 mol%			0.5 mol%			1.0 mol%		
	E' (GPa)[a]	$\Delta E'$ (GPa)[a]	tan (°C)	E' (GPa)[a]	$\Delta E'$ (GPa)[a]	tan (°C)	E' (GPa)[a]	$\Delta E'$ (GPa)[a]	tan (°C)	E' (GPa)[a]	$\Delta E'$ (GPa)[a]	tan (°C)
none	560	–	70	560	–	70	870	–	89	870	–	89
Cp POSS-P	770	+210	73	880	+320	74	1380	+510	95	1360	+490	93
Cp POSS-A	1160	+600	74	1460	+900	75	1060	+190	94	910	+40	95
Cp POSS-D	2590	+2030	76	2870	+2310	78	1100	+230	92	1270	+400	96
Cp POSS-F	1050	+490	74	1060	+500	75	1040	+170	82	630	−240	80

[a] The values represented at 25 °C, and the errors are within 5%.
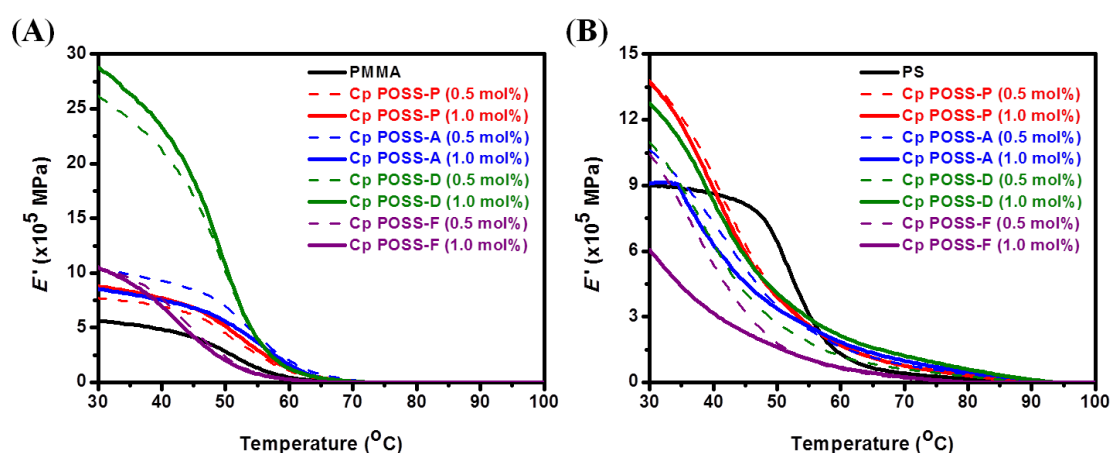
Figure 4. Dynamic mechanical curves (depicting E') of (A) PMMA and (B) PS composites containing POSS fillers (0.5 and 1.0 mol %).

Conclusion

The author describes here the molecular design for the dual-functionalized fillers based on POSS. According to the results with octa-substituted POSS fillers, the series of the heptacyclopentyl- and the single heterogeneous substituent-containing POSS were designed and synthesized. It was observed that the modified POSS can have the ability to enhance thermomechanical properties of conventional polymers with large exclusion volumes around filler molecules. This effect can be explained by the structural feature of POSS: The highly

symmetrical structure of the silica cube should reduce entropy changes during the transition involving pyrolysis, resulting in the large enhancement of thermomechanical properties of polymer matrices. The author's findings and the design concept are applicable not only for obtaining robust optical materials but also for producing highly-effective thermomechanical nanofillers based on polymer composites.

References

1. Mont, F. W.; Kim, J. K.; Schubert, M. F.; Schubert, E. F.; Siegel, R. W. *J. Appl. Phys.* **2008**, *103*, 083120.

2. Liu, J.-H.; Yang, P.-C.; Chiu, Y.-H. *J. Polym. Sci. A: Polym. Chem*. **2006**, *44*, 5933.

3. Lee, S.; Jeong, Y.-C.; Lee, J.; Park, J.-K. *Opt. Lett.* **2009**, *34*, 3095.

4. Choi, S.-S.; Lee, H. S.; Kim, E. K.; Baek, K.-Y.; Choi, D.-H.; Hwang, S. S. *Mol. Cryst. Liq. Cryst.* **2010**, *520*, 231.

5. Ro, H. W.; Kim, K. J.; Theato, P.; Gidley, D. W.; Yoon, D. Y. *Macromolecules* **2005**, *38*, 1031.

6. Hedrick, J. L.; Miller, R. D.; Hawker, C. J.; Carter, K. R.; Volksen, W.; Yoon, D. Y.; Trollsås, M. *Adv. Mater.* **1998**, *10*, 1049.

7. Su, H.-W.; Chen, W.-C. *Mater. Chem. Phys.* **2009**, *114*, 736.

8. Hong-Ji, C.; Meng, F. *Macromolecules* **2007**, *40*, 2079.

9. Jeon, J.-H.; Tanaka, K.; Chujo, Y. *RSC Adv.* **2013**, *3*, 2422.

10. Blanco, I.; Bottino, F. A. *Polym. Compos.* **2013**, *34*, 225.

11. Mitsuishi, M.; Zhao, F.; Kim, Y.; Watanabe, A.; Miyashita, T. *Chem. Mater.* **2008**, *20*, 4310.

12. Araki, H.; Naka, K. *Polym. J.* **2012**, *44*, 353.

13. Araki, H.; Naka, K. *J. Polym. Sci. Part A: Polym. Chem.* **2012**, *50*, 4170.

14. Wu, S.; Hayakawa, T.; Kikuchi, R.; Grunzinger, S. J.; Kakimoto, M. *Macromolecules* **2007**, *40*, 5698.

15. Hosaka, N.; Torikai, N.; Otsuka, H.; Takahara, A. *Langmuir* **2007**, *23*, 902.

16. Gunji, T.; Sakai, Y.; Arimitsu, K.; Abe, Y. *J. Polym. Sci., Part A: Polym. Chem.* **2007**, *45*, 3273.

17. Takamura, N.; Gunji, T.; Hatano, H.; Abe, Y. *J. Polym. Sci., Part A: Polym. Chem.* **1999**, *37*, 1017.

18. Laine, R. M. *J. Mater. Chem.* **2005**, *15*, 3725.

19. Laine, R. M.; Sulaiman, S.; Brick, C.; Roll, M.; Tamaki, R.; Asuncion, M. Z.; Neurock, M.; Filhol, J.-S.; Lee, C. -Y.; Zhang, J.; Goodson, T., III; Ronchi, M.; Pizzotti, M.; Rand, S. C.; Li, Y. *J. Am. Chem. Soc.* **2010**, *132*, 3708.

20. Tanaka, K.; Adachi, S.; Chujo, Y. *J. Polym. Sci. Part A: Polym. Chem.* **2009**, *47*, 5690.

21. Asuncion, M. Z.; Ronchi, M.; Abu-Seir, H.; Laine, R.M. *C. R. Chimie* **2010**, *13*, 270.

22. Yang, C.-C.; Chen, W.-C.; Chen, L.-M.; Wang, C.-J. *Proc. Natl. Sci. Counc. ROC(A)* **2001**, *25*, 339.

23. Hao, N.; Böhning, M.; Schönhals, A. *Macromolecules* **2007**, *40*, 9672.

24. Tanaka, K.; Adachi, S.; Chujo, Y. *J. Polym. Sci. Part A: Polym. Chem.* **2010**, *48*, 5712.

25. Fehr, F. J.; Budzichowski, T. A.; Blanski, R. L.; Weller, K. J.; Ziller, J. W. *Organometallics* **1991**, *10*, 2526.

26. Groh, W.; Zimmermann, A. *Macromolecules* **1991**, *24*, 6660.

27. Vuks, M. F. *Opt. Spectrosc.* **1964**, *68*, 441.

28. Tanio, N.; Irie, M. *Jpn. J. Appl. Phys., Part I* **1997**, *36*, 743.

29. Tanaka, K.; Ishiguro, F.; Chujo, Y. *Polym. J.* **2011**, *43*, 708.

30. Tanaka, K.; Ishiguro, F.; Chujo, Y. *J. Am. Chem. Soc.* **2010**, *132*, 17649.

31. Evert, A.; James, A.; Hawkins, T.; Foy, P.; Stolen, R.; Dragic, P.; Dong, L.; Rice, R.; Ballato, J. *Opt. Express* **2012**, *20*, 17393.

32. Hutsel, M. R.; Gaylord, T. K. *Appl. Opt.* **2012**, *51*, 5442.

Chapter 5

Enhancement of Optical Properties of Dyes for Bioprobes

# by Freezing Effect of Molecular Motion

Using POSS-core Dendrimer

Chapter 5

Enhancement of Optical Properties of Dyes for Bioprobes

by Freezing Effect of Molecular Motion Using POSS-core Dendrimer

Abstract: This chapter demonstrates that the POSS-core dendrimer induced various kinds of favorable properties of trisvinylpyridinium triphenylamine (TP3PY) as a bioprobe. By using the amphiphilicity of the POSS-core, the complexes of TP3PY with G2 POSS-core dendrimer were prepared, and the series of properties were investigated for the application as a bioprobe. Initially, it was shown that the adsorption of TP3PY onto the vessels was highly prohibited by the complex formation with the dendrimers. The solution states of the dendrimer complexes were maintained at least for 7 days. Moreover, it was found that the improvement of quantum yields and the elongation of fluorescent lifetimes were observed by the complexation with the dendrimers. Similar photochemical properties were obtained in a glassy state of 2-methyltetrahydrofuran at −196 ˚C. The molecular rotations occurring at the excited state could be restricted by the complex formation with dendrimers.
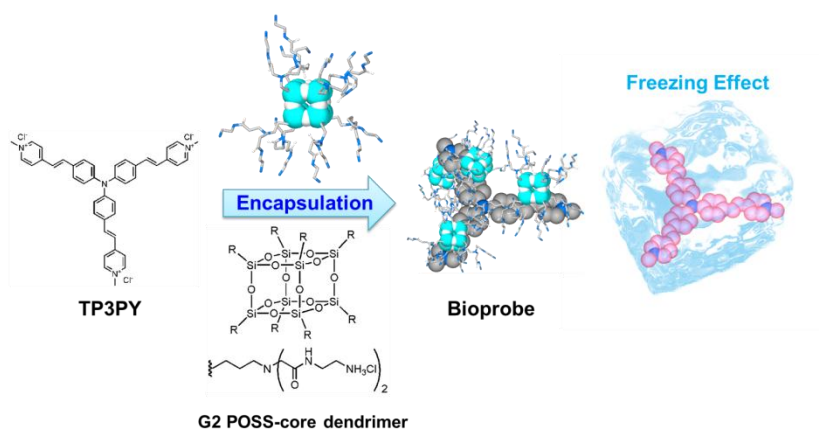
Introduction

The optical materials which show the strong emission in deep red or near-infrared regions are strongly required in bioimaging.[1] Since the vital body shows higher tolerance and lower self-emission, the background noise and the autofluorescence of the samples can be suppressed and the optical detection is applicable for the detection at deep spots inside vital bodies.[2] The series of electron-withdrawing group-conjugated triphenylamine derivatives are known as the fluorophore with the strong emission in the deep red region.[3] Moreover, the branched donor-acceptor skeleton shows non-linear optical properties, resulting in the large applicability for multi-photon excitation.[3] However, the poor water-solubility and the strong adsorption ability limit to the conventional usages as a bioprobe.

Dyes located at the interfaces or in the solid matrices often show the attractive optical properties for bioprobes. For example, the lipophilic molecules can be readily adsorbed onto the silica materials composed of the low dielectric Si–O–Si bonds via strong hydrophobic interaction. Thus, in the dye-loaded glass materials, the rigid silica frameworks can inhibit the aggregation by isolating each molecule and maintain the well-dispersion state of the dyes in the matrices, resulting in the suppression of the self-quenching.[4] Consequently, the enhancement of the emission quantum yields or the elongation of fluorescence life times was observed.[4] These phenomena are applicable to improve the signal to noise ratio in the images in the optical methods using the dye as a marker for bioimaging. Okamoto and coworkers presented that the molecular rotations of the dimethylaminopyrene-tethered DNA base at the excited sate were regulated by the duplex formation of DNA.[5] Multi-color emission was observed from the aqueous solutions containing the modified DNA oligomer at the ambient temperature. These phenomena improved the accuracy on the detection by correlating the one emission signal from another one at a different wavelength. Such characteristics are promised to be a key for developing advanced optical probes. However, there are problems to apply

these characteristics to develop a bioimaging probe. It is difficult to realize these properties with the dye-loaded materials under biological conditions and particularly maintain the well-dispersion states of the dye/matrix complexes without loss of the induced properties. Furthermore, the size-distribution of the complexes inhibits the precise controls of the locations of the complexes *in vivo*. In order to produce the sophisticated probes, these problems should be solved.

Polyoctahedral oligomeric silsesquioxanes (POSS, Figure 1) have been used as building blocks not only for functional nanomaterials but also for biomaterials.[6] The typical POSS molecule possesses a cubic rigid structure represented by the formula $R_8Si_8O_{12}$, where the central inorganic core (Si_8O_{12}) is functionalized with organic moieties (R) at the eight vertices. POSS can be regarded as a kind of glass materials. Therefore, the luminescence of the POSS core was hardly observed.[7] On the other hand, the modified POSS with the chromophores showed attractive characteristics.[8] Moreover, POSS had a low dielectric constant due to the closed silica structure.[9] Thereby, the water-soluble POSS-core dendrimers showed the amphiphilicity and the entrapping ability of various kinds of guest molecules.[10,11] Compared to the same generation of the polyamidoamine dendrimer, it was found that a larger amount of guest molecules were encapsulated with high affinity.[10] Next the author's interests have directed to regulate the molecular rotation of the dyes by encapsulating into the POSS-core dendrimers similarly used as the bulk silica materials[11].

In this chapter, the author shows that the POSS-core dendrimer can induce various kinds of favorable properties of trisvinylpyridinium triphenylamine (TP3PY, Figure 1)[3a] as a bioprobe. The author encapsulated TP3PY into G2 POSS-core dendrimer and evaluated the properties for applying the dendrimer complexes. The undesired adsorption of TP3PY onto the vessels was highly prohibited by encapsulation. In addition, the improvement of quantum yields and the elongation of fluorescent lifetimes were observed by encapsulating into the dendrimers.

Similar photochemical properties were realized in the frozen glassy matrix of 2-methyltetrahydrofuran at −196 ˚C. This is, to the best of the author's knowledge, to show the dendrimer can show the freezing effect on the molecular rotation of the encapsulated molecule and accomplish to express the favorable optical properties under biocompatible circumstances.
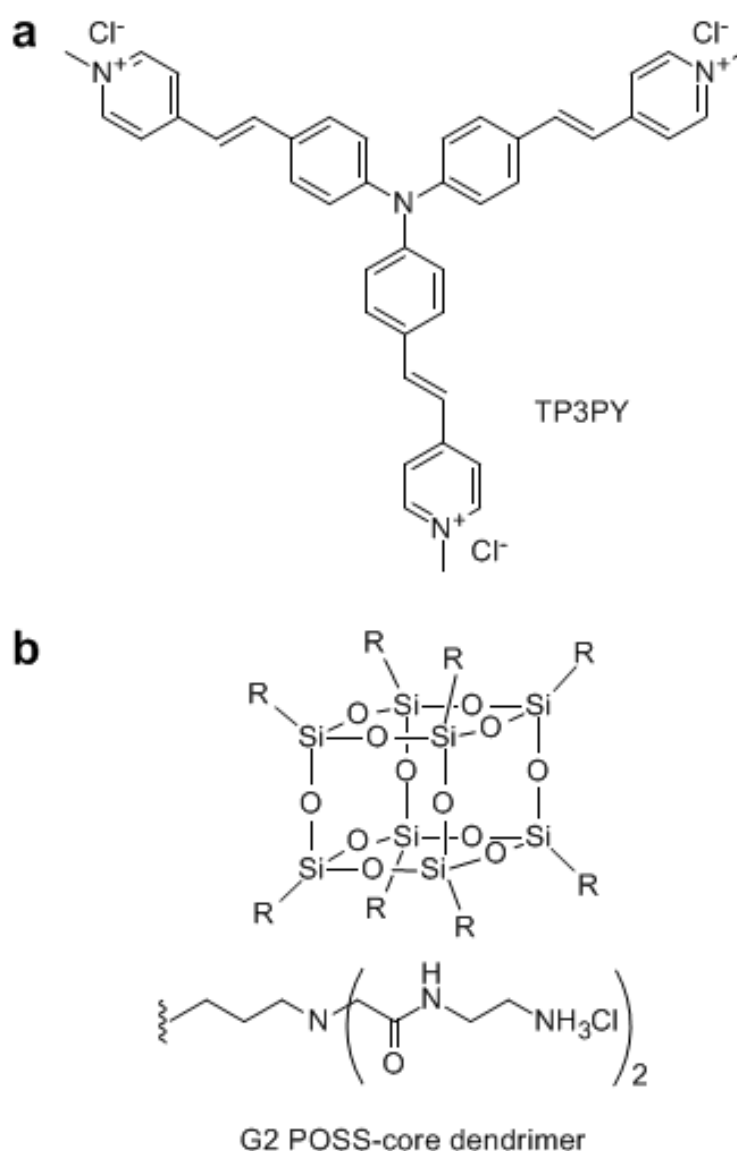
Figure 1. Chemical structures of the dye and the dendrimer used in this study.

Experimental Section

General. ^{1}H NMR and ^{13}C NMR spectra were measured with a JEOL EX-400 (400 MHz for ^{1}H and 100 MHz for ^{13}C) spectrometer. ^{29}Si NMR spectra were measured with a JEOL JNM-A400 (80 MHz) spectrometer. Coupling constants (*J* value) are reported in hertz. The chemical shifts are expressed in ppm downfield from tetramethylsilane, using residual chloroform ($\delta = 7.24$ in ^{1}H NMR, $\delta = 77.0$ in ^{13}C NMR) as an internal standard. The UV–vis absorption spectra were obtained on a SHIMADZU UV-3600 spectrometer. Emission spectra of the samples were monitored by a Perkin Elmer LS50B fluorometer using a 1 cm path length cell. The excitation bandwidth was 0.1 nm. The emission bandwidth was 0.1 nm. Fluorescence lifetime analysis was carried out on a HORIBA FluoreCube spectrofluorometer system; excitation at 375 nm was carried out using a UV diode laser (NanoLED-375L). Masses of dendrimers were determined with an ESI mass spectroscopy or a MALDI-TOF mass spectroscopy (acceleration voltage 21 kV, negative mode) with DHB (2,5-dihydroxybenzoic acid) as a matrix. TP3PY was synthesized according to the previous report.[3a]

Octaammonium POSS, 1. (3-Aminopropyl)triethoxysilane (100 mL, 0.427 mol) and conc. hydrochloric acid (35–37%, 135 mL) in methanol (800 mL) produced POSS **1** as a white precipitate after 5 days at room temperature. The product was obtained after filtration, washing with cold methanol, and drying. The compound **1** was spectroscopically pure in 30% yield (18.8 g). ^{1}H NMR (DMSO-d_6) δ 8.23 (s, 24H), 2.76 (t, 16H), 1.71 (m, 16H), 0.72 (t, 16H). ^{13}C NMR (DMSO-d_6) δ 40.53, 20.13, and 7.96. ^{29}SiNMR (DMSO-d_6) δ −66.4 (s). MALDI–TOF [(M+H)$^+$] calcd. 880.41, found 879.42.

G2 POSS-core dendrimer, 3. To a suspension of POSS **1** (1 g, 0.852 mmol) and diisopropylamine (15 mL, 86.1 mmol) in DMF (50 mL) ethyl bromoacetate (9.5 mL, 86.1 mmol) was added, and the reaction mixture was stirred at 60 °C for 16 h. The resulting mixture was concentrated *in vacuo*, and extracted with ethyl acetate. The organic phase was washed with brine and dried over $MgSO_4$. The crude product **2** of ethyl ester (1.07 g) as a yellow oil was obtained after evaporation. Then, the ethyl ester was dissolved in 200 mL of ethylenediamine, and incubated at 60 °C for 24 h. The reaction mixture was concentrated *in vacuo*, and washed with diethyl ether. The white solid **3** (1.30 g, 0.523 mmol, 61%) was precipitated in methanol (100 mL) by adding 35–37% HCl (10 mL); ^{1}H NMR (D_2O, 400 MHz) δ 4.18 (br, 32H), 3.53 (brs, 32H), 3.33 (brs, 16H), 3.14 (brs, 32H), 1.75 (brs, 16H), 0.68 (brs, 16H): ^{13}C NMR (D_2O, 100 MHz) δ 166.7, 59.4, 56.1, 38.9, 36.5, 18.1, 9.9: ^{29}Si NMR (D_2O, 80 MHz) δ −67.4: MALDI–TOF [(M+H)$^+$] calcd. 2484.41, found 2484.97.

Complexation with the dendrimers. General procedure for the complexation of TP3PY by the dendrimers is described here. The stock solutions of TP3PY (×10) in methanol and G2 POSS-core dendrimer (×10) in water were mixed at room temperature, and then the 500 μL of the samples were prepared by adding the solvents.

Evaluation of the amount of the retained ligand into the G2 POSS-core dendrimer. The sample solutions were stored under ambient conditions and filtered through Nanosep 3K centrifugal devices (Pall Life Sciences) by centrifugation (2000 *g*, 30 min, 25 °C). The concentration of TP3PY was determined from the light absorption of the filtrates. The amounts of retention were evaluated by comparing to the absorptions of the filtrates.

Fluorescence measurements of the complexes. The fluorescence emission of TP3PY (10 μM) under excitation at 474 nm was monitored at 25 °C using 1 cm path length cell. The excitation bandwidth was 1 nm. The emission bandwidth was 1 nm. The quantum yields were determined as an absolute value with an integral sphere.

Lippert–Mataga plots. The Lippert equation:

$$\nu_{fl} = \nu_{ab} - \frac{2\Delta f}{hca^3} \left(\mu_E - \mu_G \right)^2 + \text{const.} \qquad (1)$$

where h equals Planck's Constant, c equals the velocity of light in a vacuum, a is the Onsager cavity radius, n and ε the refractive index and the dielectric constant of the solvent, ν_{fl} and ν_{ab} the fluorescence and absorption wavelength (expressed in cm^{-1} units), μ_E and μ_G the dipole moment (expressed in Debye units) in the excited and the ground state, respectively,

$$\Delta f = \frac{\varepsilon - 1}{2\varepsilon + 1} - \frac{n^2 - 1}{4n^2 + 2} \qquad (2)$$

While the slope is

$$\text{Slope} = -\frac{2\Delta f}{hca^3} \left(\mu_E - \mu_G \right)^2 \qquad (3)$$

Based on the calculation performed above it can be concluded that for the single excited state of TP3PY has a larger dipole moment than the ground state.

Results and Discussion

TP3PY and G2 POSS-core dendrimer were synthesized according to the previous reports.[3a,12] The solution samples were prepared by adding the stocked solution of TP3PY in methanol into that of G2 POSS-core dendrimer in water and adjusting the desired concentration with the solvents. To monitor the dispersibility of the complexes in PBS, the samples in the quartz vessels were stored at 25 °C in the dark, and then further treatments were carried out. The fluorescence spectra were obtained with the excitation light at 474 nm. The quantum yields of fluorescence emission from TP3PY (Φ) were determined as an absolute value with an integrating sphere.

To confirm the encapsulation of TP3PY into the dendrimer and to evaluate the essential stoichiometry of G2 POSS-core dendrimer for solubilizing TP3PY in PBS, the author compared the absorption of the supernatants obtained from the solutions containing TP3PY with various concentrations of G2 POSS-core dendrimer after the storage under ambient conditions (Figure 2).[13] If the solution state is maintained, the concentration of the dissolved TP3PY should be less affected. Based on this idea, the absorption changes of the supernatants were investigated after 3 days. The solutions containing 10 μM TP3PY in PBS with various concentrations of G2 POSS-core dendrimer were prepared, and the centrifugation was treated with the solutions after 3 days. The supernatant of the pure TP3PY provided significant lower absorption with the peak at 474 nm after 3 days. In contrast, the degree of the decrease of the absorption from the supernatant reduced corresponding to the increase of the concentration of

G2 POSS-core dendrimer. It was found that the decreases of the absorption were completely suppressed in the presence of 10 equivalents. From the dynamic light scattering experiments, the significant values were less obtained over the detectable region (2 nm ~). These facts suggest that 10 equivalents of G2-POSS core dendrimer are necessary to maintain the solution state of TP3PY. The branched and larger size of TP3PY than that of the POSS-core dendrimer might require an excess amount of the dendrimer for the stabilization of the solution state. The author added the 10-fold concentration of G2 POSS-core dendrimer for following experiments to maintain the well-dispersion. The emission intensities of TP3PY were enhanced even after 3 days incubation by the encapsulation. The photochemistry of TP3PY in the dendrimers will be mentioned as below.
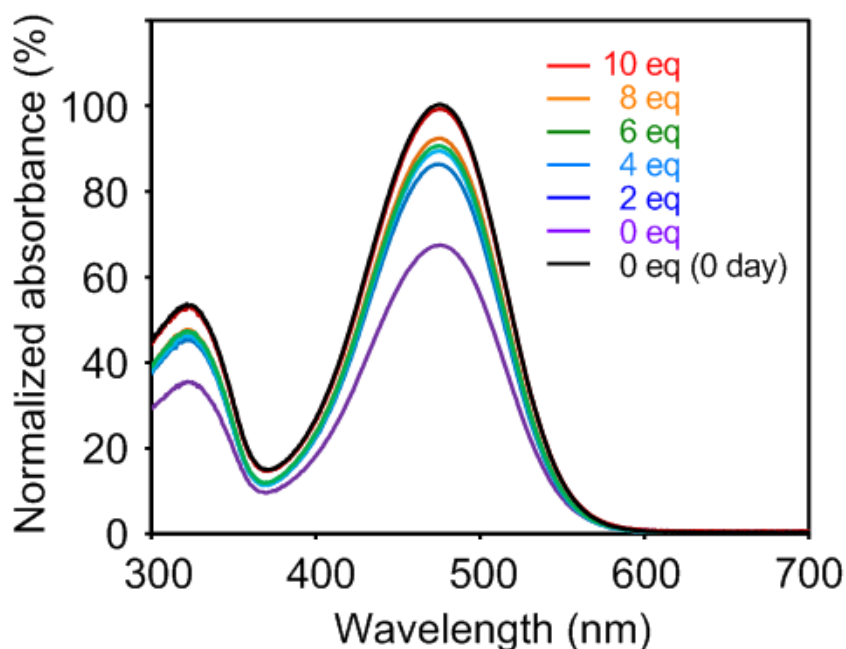
Figure 2. The absorption changes of TP3PY in the filtrates with various ratios of G2 POSS-core dendrimer to TP3PY. The samples in PBS were stored at 25 °C for 3 days in darkness and passed through the size-exclusive filter.

The complex stability of G2 POSS-core dendrimer with TP3PY was examined. The solutions containing 10 μM TP3PY in PBS with or without 100 μM G2 POSS-core dendrimer were put into the quartz cells, and the time-courses of the absorption changes from the solutions were monitored (Figure 3). In the absence of G2 POSS-core dendrimer, the absorption decreased, and the magnitude of the absorption decreased by 50 % after 7 days. In addition, the quartz cell was obviously stained. These results indicate that TP3PY should be adsorbed onto the wall of the vessels. On the other hand, the significant decrease was hardly observed in the presence of G2 POSS-core dendrimer even after 7 days. The absorption was maintained at 94 %. Moreover, the quartz cell seemed to be kept clean after the experiments. These results clearly indicate that G2 POSS-core dendrimer has the superior ability to improve the stability of the dye against undesired aggregation or adsorption in PBS by encapsulating.
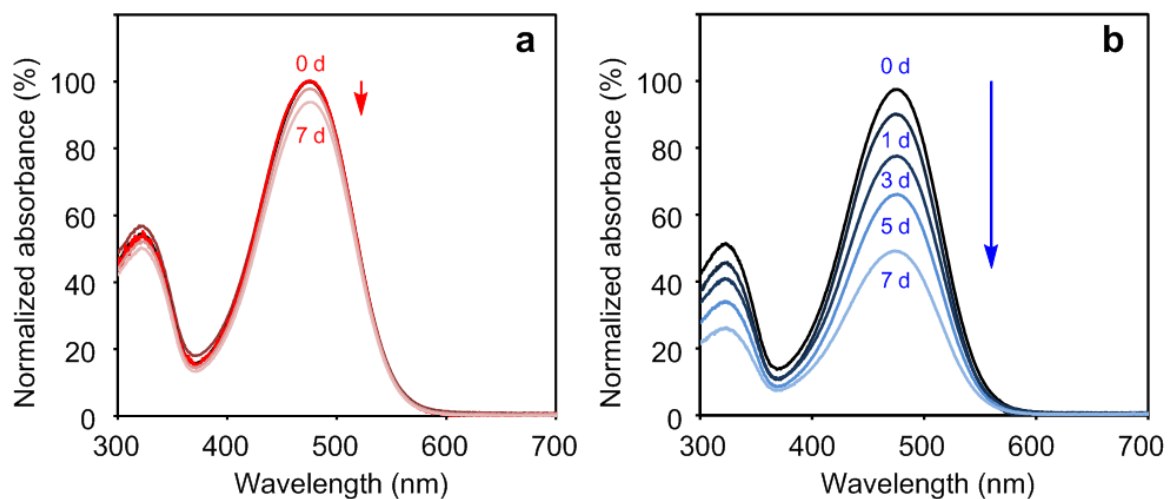
Figure 3. Time-courses of the absorption changes of TP3PY in the filtrates in the presence (a) or absence (b) of G2 POSS-core dendrimer (10 eq.). The samples in PBS were stored at 25 °C in darkness and passed through the size-exclusive filter.

The emission properties of TP3PY in the presence or absence of G2 POSS-core dendrimer were investigated in various solvents (Figure 4). Significant enhancements of quantum yields were observed by the encapsulation in each solvent (Table 1). The quantum yield of the emission of TP3PY was enhanced 6-folds by encapsulating into the dendrimers in THF due to the increase of the magnitude of emission intensity. In water and acetonitrile, new emission bands were observed. From these data, it is proposed that G2 POSS-core dendrimer plays a significant role in the improvements of the emission intensity of TP3PY. As shown in Table 1, the peak position of TP3PY was strongly affected by the solvent polarity. Nevertheless, the peak positions of the emission were slightly shifted before and after the complexation. These data suggest that the polarity changes caused by the complex formation should be hardly responsible for the enhancement of the optical properties.

Table 1. Optical properties of TP3PY[a]

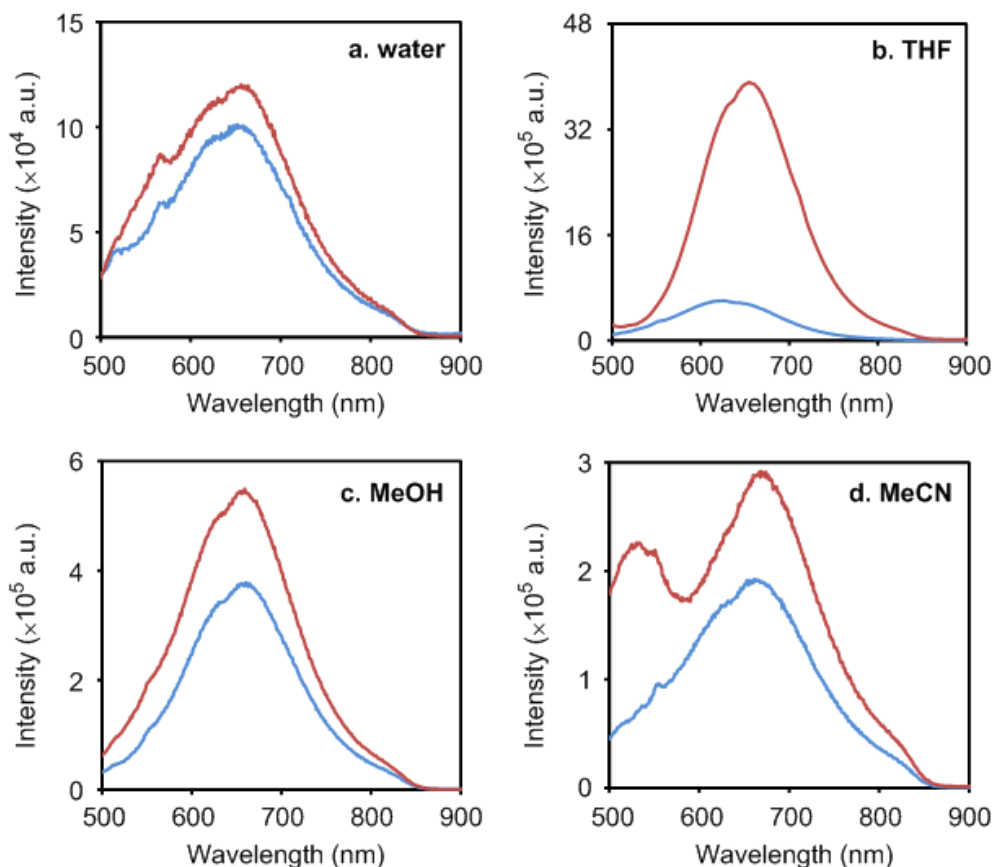|	TP3PY			Dendrimer complex[b]		
	λ_{em} [nm][c]	$\Delta\lambda$ [nm][d]	Φ^{e} [$\times 10^{-2}$]	λ_{em} [nm][c]	$\Delta\lambda$ [nm][d]	Φ^{e} [$\times 10^{-2}$]
THF	621	147	0.658	634	160	4.02
MeCN	648	174	0.320	649	175	0.390
MeOH	646	172	0.566	646	172	0.687
Water	648	174	0.267	655	181	0.343

[a]10 μM solutions.
[b]In the presence of 100 μM G2 POSS-core dendrimer.
[c]Excitation wavelength was at 474 nm.
[d]Stokes shifts.
[e]Determined as a relative value.

Figure 4. Emission spectra of TP3PY in the presence (red line) or absence (blue line) of G2 POSS-core dendrimer (10 eq.) at 25 °C in various kinds of solvents with the excitation light at 474 nm. The stock solutions of TP3PY (×10) and G2 POSS-core dendrimer (×10) were mixed at room temperature, and then 500 μL of the samples were prepared by adding the solvents. The measurements were executed within 10 min.

To clarify the mechanism of the enhancement to the quantum yields by encapsulating into the POSS-core dendrimer, the series of analyses were executed. According to the solvatochromic shift of the emission from TP3PY, the Lippert–Mataga plot (Figure 5) is prepared.[14] The linear relationship between the solvent polarity and the Stokes shift was obtained. This fact indicates that the emission band with the peak at 650 nm of TP3PY is assigned as the induced charge transfer band. In addition, the transition dipole moment ($\Delta\mu$)
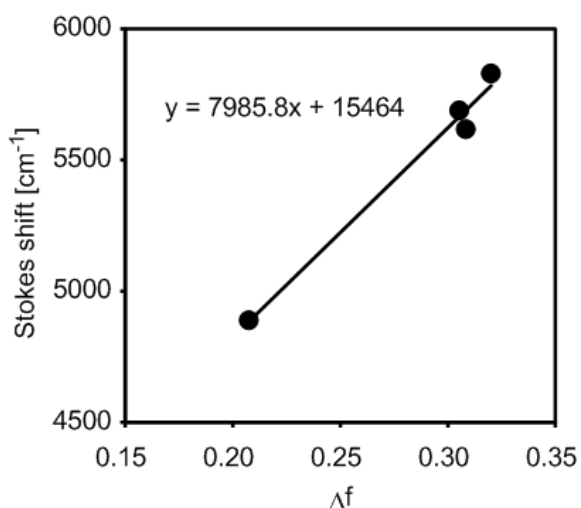
Figure 5. Lippert–Mataga plots of the Stokes shifts of TP3PY vs the solvent function Δf defined in eq. 2 for a series of various solvents.

was calculated as 11.80 D from the slope of the fitting line. The relatively larger $\Delta\mu$ value proposes that the emission of TP3PY at 650 nm is assigned as a twisted-intramolecular charge transfer (TICT) band.[5,14] The new emission peak at 550 nm assigned as the localized excitation (LE) band was observed at −196 °C in 2-methyltetrahydrofuran, resulting in the dual-emission (Figure 6). These data also support the assumption that the emission of TP3PY is originated from the TICT band. From the data, it can be claimed that the POSS-core dendrimer has the significant effect to suppress the motions of the encapsulated molecules. The author measured the fluorescence life times of TP3PY (Figure 7). Interestingly, it was revealed that the new emission with the peak at 550 nm had a long life time. It is suggested that the emission from the LE band appeared after the encapsulation. The twisting at the excited state was inhibited by encapsulating into the POSS-core dendrimers at room temperature. These results clearly indicate that the non-irradiation decay caused by the molecular tumbling should be significantly suppressed by encapsulating into the POSS-core dendrimer, and therefore, the emission of TP3PY could be enhanced. Moreover, the optical

probes having the longer life times were feasible for improving the signal to noise ratio by delaying the detection time for subtracting the self-emission. The encapsulation by the POSS-core dendrimer can be applied for this purpose.
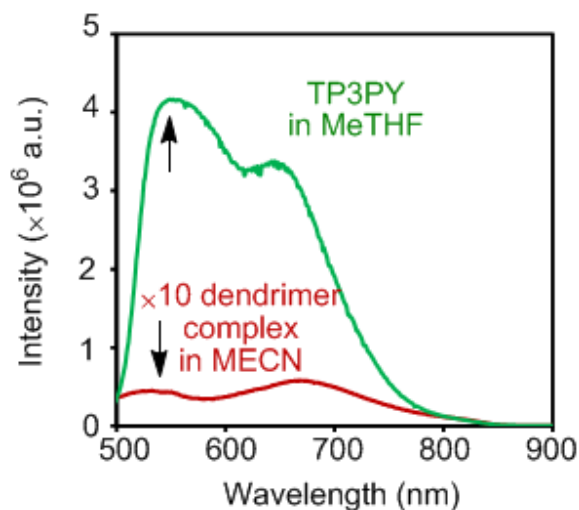
Figure 6. Emission spectra of TP3PY at −196 °C in 2-methyltetrahydrofuran with the excitation light at 474 nm.
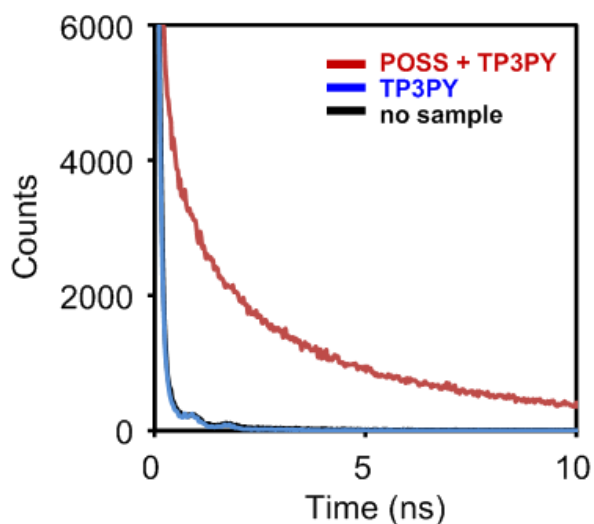
Figure 7. Fluorescence decay curves of TP3PY in PBS. All measurements were monitored at 25 °C with the excitation light at 375 nm.

Conclusion

The author describes that the POSS-core dendrimer enhanced various kinds of the properties of TP3PY for applying a bioprobe. Initially, the TP3PY complexes with G2 POSS-core dendrimer showed superior dispersibility in the buffer. The undesired adsorption of TP3PY onto the vessels was effectively suppressed. In addition, the improvement of quantum yields and elongation of fluorescent lifetime were observed from the dendrimer/dye complexes. It was proposed that the molecular rotation of TP3PY at the excited state could be suppressed in the complexes with the POSS-core dendrimer. Consequently, the emission band which is detected at low temperature can be observed at room temperature from the dendrimer/dye complexes. These results represent that the POSS-core dendrimers can create the special spots where the molecular motion of the entrapped molecules should significantly decrease in water.

References

1. (a) Weissleder, R.; Ntziachristos, V. *Nat. Med.* **2003**, *9*, 123–128; (b) R. Weissleder, *Nat. Biotechnol.* **2001**, *19*, 316; (c) Frangioni, J. V. *Curr. Opin. Chem. Biol.* **2003**, *7*, 626.

2. (a) Kiyose, K.; Kojima, H.; Nagano, T. *Chem. Asian J.* **2008**, *3*, 506; (b) Koide, Y.; Urano, Y.; Hanaoka, K.; Terai, T.; Nagano, T. *ACS Chem. Biol.* **2011**, *6*, 600; (c) Kiyose, K.; Aizawa, S.; Sasaki, E.; Kojima, H.; Hanaoka, K.; Terai, T.; Urano, Y.; Nagano, T. *Chem. Eur. J.* **2009**, *15*, 9191.

3. (a) Allain, C.; Schmidt, F.; Lartia, R.; Bordeau, G.; Fiorini-Debuisschert, C.; Charra, F.; Tauc, P.; Teulade-Fichou, M.-P. *ChemBioChem* **2007**, *8*, 424; (b) Lartia, R.; Allain, C.;

Bordeau, G.; Schmidt, F.; Fiorini-Debuisschert, C.; Charra, F.; Tauc, P.; Teulade-Fichou, M.-P. *J. Org. Chem.* **2008**, *73*, 1732; (c) Fiorini-Debuisschert, C.; Berline, I.; Metgé, G.; Charra, F.; Mihaly, M.; Allain, C.; Bordeau, G.; Teulade-Fichou, M.-P. *Nonlin. Opt. and Quantum Optics* **2009**, *38*, 271.

4. Kajiwara, Y.; Nagai, A.; Chujo, Y. *J. Mater. Chem.* **2010**, *20*, 2985.

5. Okamoto, A.; Tainaka, K.; Nishiza, K.; Saito, I. *J. Am. Chem. Soc.* **2005**, *127*, 13128.

6. (a) Laine, R. M. *J. Mater. Chem.* **2005**, *15*, 3725. (b) Cordes, D. B.; Lickiss, P. D.; Rataboul, F. *Chem. Rev.* **2010**, *110*, 2081. (c) Liu, H.; Kondo, S.; Takeda, N.; Unno, M. *J. Am. Chem. Soc.* **2008**, *130*, 10074. (d) Mitsuishi, M.; Zhao, F.; Kim, Y.; Watanabe, A.; Miyashita, T. *Chem. Mater.* **2008**, *20*, 4310. (e) Wu, S.; Hayakawa, T.; Kikuchi, R.; Grunzinger, S. J.; Kakimoto, M. *Macromolecules* **2007**, *40*, 5698. (f) Hosaka, N.; Torikai, N.; Otsuka, H.; Takahara, A. *Langmuir* **2007**, *23*, 902; (g) Wu, J.; Mather, P. T. *J. Macromol. Sci., Part C: Polym. Rev.* **2009**, *49*, 25; (h) Cordes, D. B.; Lickiss, P. D.; Rataboul, F. *Chem. Rev.* **2010**, *110*, 2081; (i) Li, G.; Wang, L.; Ni, H.; Pttman Jr., C. U. *J. Inorg. Organomet. Polym.* **2001**, *11*, 123; (j) Pakjamsai, C.; Kawakami, Y. *Des. Monomers Polym.* **2005**, *8*, 423.

7. (a) He, C.; Xiao, Y.; Huang, J.; Lin, T.; Mya, K. Y.; Zhang, X. *J. Am. Chem. Soc.* **2004**, *126*, 7792; (b) Azinović, D.; Cai, J.; Eggs, C.; König, H.; Marsmann, H. C.; Vepřek, S. *J. Lumin.* **2002**, *97*, 40.

8. (a) Lo, M. Y.; Ueno, K.; Tanabe, H.; Sellinger, A. *Chem. Rec.* **2006**, *6*, 157; (b) Lo, M. Y.; Zhen, C.; Lauters, M.; Jabbour, G. E.; Sellinger, A. *J. Am. Chem. Soc.* **2007**, *129*, 5808;

9. (a) Yang, C.-C.; Chen, W.-C.; Chen, L.-M.; Wang, C.-J. *Proc. Natl. Sci. Counc. ROC(A)* **2001**, *25*, 339; (b) Hao, N.; Böhning, M.; Schönhals, A. *Macromolecules* **2007**, *40*, 9672.

10. (a) Tanaka, K.; Inafuku, K.; Naka, K.; Chujo, Y. *Org. Biomol. Chem.* **2008**, *6*, 3899; (b) Tanaka, K.; Inafuku, K.; Adachi, S.; Chujo, Y. *Macromolecules* **2009**, *42*, 3489; (c) Tanaka, K.; Inafuku, K.; Chujo, Y. *Chem. Commun.* **2010**, *46*, 4378; (d) Tanaka, K.; Inafuku, K.; Chujo, Y. *Bioorg. Med. Chem.* **2008**, *16*, 10029.

11. (a) Tanaka, K.; Adachi, S.; Chujo, Y. *J. Polym. Sci. Part A: Polym. Chem.* **2009**, *47*, 5690; (b) Tanaka, K.; Ishiguro, F.; Chujo, Y. *J. Am. Chem. Soc.* **2010**, *132*, 17649; (c) Tanaka, K.; Ishiguro, F.; Chujo, Y. *Polym. J.* **2011**, *43*, 708; (d) Tanaka, K.; Adachi, S.; Chujo, Y. *J. Polym. Sci. Part A: Polym. Chem.* **2010**, *48*, 5712.

12. Tanaka, K.; Kitamura, N.; Naka, K.; Morita, M.; Inubushi, T.; Chujo, M.; Nagao, M.; Chujo, Y. *Polym. J.* **2009**, *41*, 287.

13. Tanaka, K.; Ohashi, W.; Kitamura, N.; Chujo, Y. *Bull. Chem. Soc. Jpn* **2011**, *84*, 612.

14. Valeur, B. *Molecular Fluorescence*; Wiley-VCH: Weinheim, Germany, 2002.

Chapter 6

Enhancement of Affinity in Molecular Recognition via Hydrogen Bonds by POSS-Core Dendrimer and Its Application for Selective Complex Formation between Guanosine Triphosphate and 1,8-Naphthyridine Derivatives

Chapter 6

Enhancement of Affinity in Molecular Recognition via Hydrogen Bonds by POSS-Core Dendrimer and Its Application for Selective Complex Formation between Guanosine Triphosphate and 1,8-Naphthyridine Derivatives

Abstract: This chapter shows that the polyhedral oligomeric silsesquioxane (POSS) core in the dendrimer can enhance the affinity of the molecular recognition via hydrogen bonds between 1,8-naphthyridine and guanosine nucleotides. The complexation of the naphthyridine ligands with the series of guanosine nucleotides was investigated, and it is shown that the POSS core should play a significant role in the stabilization of the complexes via hydrogen bonds. Finally, this chapter demonstrates that the 1,8-naphthyridine ligand can selectively recognize guanosine triphosphate by assisting with the POSS-core dendrimer.
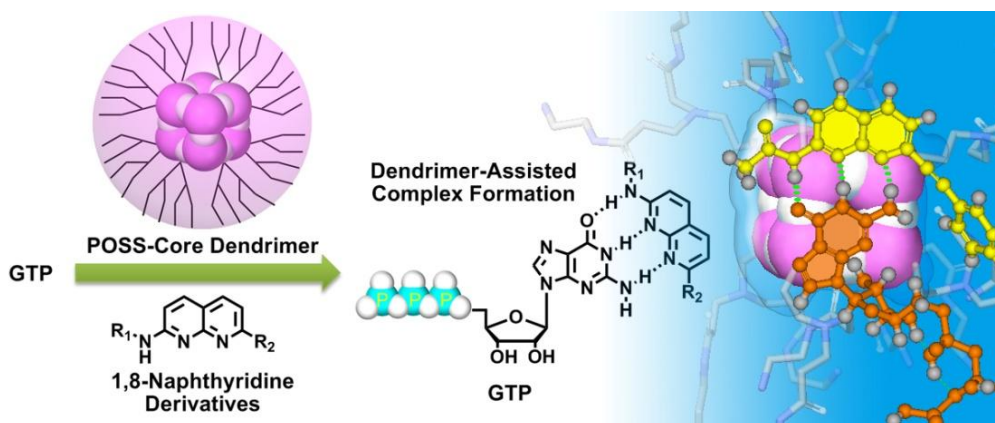
Introduction

Hydrogen-bond-mediated molecular recognition in water is a topic with high relevance to biological systems. To realize the stable complexation between the receptor and the target, the elaboration for maintaining the binding affinity should be necessary to compensate the inhibition of the bond formation by hydration.[1] One of familiar examples can be seen in the RNA polymerases. In the active pocket, the recognition with the nucleoside triphosphates based on the hydrogen-bond patterns can be accomplished along the template sequences with high fidelity in the gene transcription.[2] In contrast, the complexation with the complementary nucleosides can be hardly observed in water without enzymes.

The 1,8-naphthyridine derivatives can work as a receptor with guanosine nucleotides.[3] Nakatani and coworkers have presented the series of the 1,8-naphthyridine derivatives for the highly-sensitive recognition of the nucleobases.[4] Cooperative interaction plays a significant role in the enhancement of the affinity, leading to the specific recognition to the guanine-involving mismatch sites in DNA.[5] Cywinski and coworkers have reported the cyclic GMP (cGMP)-selective recognition using the modified polymer particles with the naphthyridine derivatives.[6] The cooperativity between the zeta potential of the particles and the recognition property of the naphthyridine receptor can show the molecular recognition ability for cGMP with high specificity.

Hydrophilic polymeric materials, which can retain the guest molecules, are a versatile platform as a biosensor or a vessel for drug delivery system.[7] In particular, because of the uniform structures, the characteristics of the dendrimers can be readily modulated by the size tuning and the peripheral modification.[8] These advantages of the dendrimers are feasible for site- and time-selective delivery. Chujo and coworkers have recently reported the retention ability of water-soluble dendrimers composed of polyhedral oligomeric silsesquioxane (POSS).[9] In the polar solvents, the POSS-core dendrimers could form the globular

conformation even in the lower generation and create the distinct hydrophobic space around the POSS core.[10,11] Consequently, the larger amounts of the hydrophobic guest molecules can be sustained inside the dendrimers than those of the same generation of the polyamidoamine (PAMAM) dendrimer which has similar dendrons.[10] The author's next interests have directed to realize the selective capturing for the biomolecules using the hydrophobic distinct spaces inside the POSS-core dendrimers.

In this chapter, the author describes the influence on the binding affinity with the naphthyridine ligand and guanosine derivatives by the POSS-core dendrimer. The binding constants were evaluated from the fluorescence quenching by adding the series of guanosine nucleotides. In addition, from the investigation of the recognition mechanism with the PAMAM dendrimer and various kinds of naphthyridine derivatives, it was suggested that the POSS core should offer the hydrophobic space where the strength of the hydrogen bonds should be enhanced. This is the first example, not only for using the amphiphilicity of the dendrimer to enhance the molecular recognition via hydrogen bonding in aqueous phase but also for capturing the biomolecules by the dendrimer.

Experimental Section

General. ^{1}H NMR and ^{13}C NMR spectra were measured with a JEOL EX–400 (400 MHz for ^{1}H and 100 MHz for ^{13}C) spectrometer. ^{29}Si NMR spectra were measured with a JEOL JNM–A400 (80 MHz) spectrometer. Coupling constants (J value) are reported in Hertz. The chemical shifts are expressed in ppm downfield from tetramethylsilane, using residual dimethyl sulfoxide ($\delta = 2.50$ in ^{1}H NMR, $\delta = 39.5$ in ^{13}C NMR) as an internal standard. Emission from the samples was monitored using a Perkin Elmer LS50B at 25 °C using 1 cm path length cell. MASS spectra were obtained on a JEOL JMS–SX102A. The G2 PAMAM

dendrimer was purchased from Aldrich as a methanol solution and directly used for the analyses.

The compound 4. The reaction mixture containing 9.07 g of malic acid (67.6 mmol) and 6.67 g of 2,6-diaminopyridine (61.1 mmol) was slowly added to 40 mL of 95 % H_2SO_4 at 0 °C. After stirring at 110 °C for 3 h, the solution was neutralized with NH_4OH, and the product was yielded as a precipitate. The compound **4** was separated by the filtration as a white powder (9.05 g, 92 %). ^1H NMR (DMSO− d_6) δ 11.85 (br, 2H), 7.64 (d, 1H, J = 9.6 Hz), 7.63 (d, 1H, J = 9.2 Hz), 6.32 (d, 1H, J = 9.2 Hz), 6.01 (d, 1H, J = 8.9 Hz). LRMS (NBA) $[(M+H)^+]$ calcd. 162, found 162.

The compound 5. The hydroxyl compound **4** (1.0 g, 6.21 mmol) was refluxed with 50 mL of $POCl_3$ for 4 h. After cooling, the reaction solution was neutralized with NH_4OH, and extracted with chloroform. Evaporation of the chloroform extract gave the crude product which was recrystallized from toluene giving 370 mg of the pure product **5** as a yellow powder (33 %). ^1H NMR (DMSO− d_6) δ 7.86 (d, 1H, J = 8.0 Hz), 7.82 (d, 1H, J = 8.8 Hz), 7.17 (d, 1H, J = 8.0 Hz), 6.75 (d, 1H, J = 6.8 Hz), 5.33 (bs, 2H). LRMS (NBA) $[(M+H)^+]$ calcd. 180, found 180.

The compound 2. In a 25-mL round-bottom flask, 100 mg of 2-amino-7-chloro-1,8-naphthyridine (**5**) (0.557 mmol), 10 mg of $PdCl_2(PPh_3)_2$ (cat.) and 3 mg of CuI (cat.) were stirred in 5 mL of dry THF under argon. To the solution, 0.6 mL of triethylamine was slowly added through a syringe. The mixture was stirred at room temperature for 30 min and then 0.1 mL of ethynylbenzene (0.980 mmol) was added. The reaction was stirred at room temperature overnight. Upon removal of the volatiles under reduced pressure, the residue was

dissolved in dichloromethane, passed through a plug of celite and then washed with ethyl acetate. The product was dried under vacuum. Column chromatography in silica gel with an increasing gradient of methanol in chloroform (chloroform/methanol from 20 : 1 to 10 : 1) yielded 41 mg of pure compound **2** (30 %) as a white powder. ^{1}H NMR (CDCl$_3$) δ 7.92 (d, 1H, J = 8.0 Hz), 7.85 (d, 1H, J = 8.8 Hz), 7.62 (m, 2H), 7.41 (d, 1H, J = 8.4 Hz), 7.37 (m, 3H), 6.77 (d, 1H, J = 8.8 Hz) , 5.05 (br,1H). ^{13}C NMR (CDCl$_3$) δ 159.97, 155.80, 145.35, 137.59, 136.26, 132.18, 129.07, 128.34, 122.13, 121.68, 116.77, 133.70, 90.57, 89.32. LRMS (NBA) [(M+H)$^+$] calcd. 246, found 246: LRMS (NBA) [(M+H)$^+$] calcd. 246.1031, found 246.1021.

The compound 1. In a 25-mL round-bottom flask, 30 mg of **2** (0.122 mmol) and 5 mL of acetic anhydride were stirred in 10 mL of chloroform at room temperature for 3 h. After evaporation, the compound **1** (28 mg, 80 %) was purified as a white powder from column chromatography in silica gel with ethyl acetate. ^{1}H NMR (CDCl$_3$) δ 9.04 (br,1H), 8.55 (d, 1H, J = 8.8 Hz), 8.18 (d, 1H, J = 8,8 Hz), 8.11 (d, 1H, J = 8,4 Hz), 7.65 (m, 2H), 7.60 (d, 1H, J = 8.4 Hz), 7.41 (m, 3H), 2.31 (s, 3H). ^{13}C NMR (CDCl$_3$) δ 170.27, 154.74, 154.64, 146.78, 138.94, 136.58, 132.27, 129.42, 128.47, 124.02, 121.90, 119.70, 115.97, 91.39, 89.13, 25.08. LRMS (NBA) [(M+H)$^+$] calcd. 288, found 288: LRMS (NBA) [(M+H)$^+$] calcd. 288.1137, found 288.1125

The compound 6. 2,6-Diaminopyridine (10 g, 91.7 mmol), 13 g of 3-ketobutanal dimethyl acetal, and 100 mL of 85% H$_3$PO$_4$ were stirred at 90 °C for 3 h. The reaction was quenched by neutralizing, and the crude product was obtained from the extraction with chloroform and washed by water five times. Column chromatography in silica gel with the mixture solvent (chloroform : methanol = 10 : 1) afforded 13.1 g of **6** as a white powder (90 %). ^{1}H NMR

(CDCl$_3$) δ 7.83(d,1H, J = 7.2 Hz), 7.81 (d, 1H, J = 8.8 Hz), 7.07(d, 1H, J = 8.0 Hz), 6.69 (d, 1H, J = 8.8 Hz), 4.93 (br, 2H), 2.69 (s, 3H). LRMS (NBA) [(M+H)$^+$] calcd. 160, found 160.

The compound 3. In a 25-mL round-bottom flask, 100 mg of **6** (0.628 mmol) and 5 mL of acetic anhydride were stirred in 10 mL of chloroform at room temperature for 3 h. After evaporation, the compound **3** (107 mg, 85 %) was purified as a white powder from column chromatography in silica gel with ethyl acetate. ^{1}H NMR (CDCl$_3$) δ 8.55 (br,1H), 8.46 (d, 1H, J = 7.2 Hz), 8.15 (d, 1H, J = 7.2 Hz), 8.02 (d, 1H, J = 8.0 Hz), 7.29 (d, 1H, J = 5.2 Hz), 2.76 (s, 3H), 2.28 (s, 3H). LRMS (NBA) [(M+H)$^+$] calcd. 202, found 202. LRMS (NBA) [(M+H)$^+$] calcd. 202.0980, found 202.0972.

Octaammonium POSS 7. (3-Aminopropyl)triethoxysilane (100 mL, 0.427 mol) and conc. hydrochloric acid (35–37 %, 135 mL) in methanol (800 mL) produced **7** as a white precipitate after 5 days at room temperature. The product was obtained after filtration, washing with cold methanol, and drying. The compound **7** was spectroscopically pure in 30 % yield (18.8 g). ^{1}H NMR (DMSO-d_6) δ 8.23 (s, 24H), 2.76 (t, 16H), 1.71 (m, 16H), 0.72 (t, 16H). ^{13}C NMR (DMSO-d_6) δ 40.53, 20.13, and 7.96. ^{29}SiNMR (DMSO-d_6) δ −66.4 (s). MALDI–TOF [(M+H)$^+$] calcd. 880.41, found 879.42.

Methyl ester-terminated POSS-core dendrimer 8. Amberlite IRA-400 ion-exchange resin (100 g) was prepared by successive washing with water (4 × 150 mL), 1 M NaOH (3 × 150 mL), water (6 × 150 mL), and MeOH (6 × 150 mL), which was the elution solvent; the resin was suspended in eluent and chilled (−10 °C, 2 h) before use. A half of the resin beads were loaded onto a column (3.5 cm outside diameter), and the other half was used to dissolve a suspension of neutralized **7** (5.0 g, 4.27 mmol) in the minimum amount of eluent below 0 °C.

Elution across the column produced a MeOH solution of neutralized **7**. Immediately, methyl acrylate (100 mL, 1.11 mol) was added via syringe to a solution of neutralized **7**, and the resulting mixture was heated for 48 h at 80 °C. The reaction solution was concentrated *in vacuo*, and extracted with ethyl acetate. The organic phase was washed with brine, dried over MgSO$_4$. The product **8** (6.10 g, 2.60 mmol, 63 %) as a colorless oil was obtained after evaporation: ^{1}H NMR (CD$_3$OD) δ 3.62 (s, 24 H), 2.18 (s, 16 H), 1.40 (m, 16 H), 0.96 (s, 48 H), 0.57 (m, 16 H). ^{13}C NMR(CD$_3$OD) δ 174.48, 57.24, 52.17, 50.39, 33.13, 21.39, 10.19. ^{29}Si NMR (CD$_3$OD) δ −66.2. MALDI–TOF [(M+H)$^+$] calcd. 1811.08, found 1812.01.

G2 POSS-core dendrimer 9. The solution containing **8** (6.1 g, 2.60 mmol) with an excess of ethylenediamine (100 mL, 1.48 mol) was stirred for 4 days at 4 °C. After removing ethylenediamine, washing with diethyl ether, and dialyzing in water, the G2 POSS-core dendrimer **9** was obtained in 92 % yield (6.3 g, 2.39 mmol) as a white powder. ^{1}H NMR (CDCl$_3$) δ 3.23 (t, 32 H), 2.72 (t, 32 H), 2.66 (t, 32 H), 2.43 (t, 16 H), 2.39 (t, 32 H), 1.46 (m, 16 H), 0.54 (t, 16 H). ^{13}C NMR (CDCl$_3$) δ 171.97, 80.03, 49.19, 33.67, 28.18, 28.06, 21.12, 10.57. ^{29}Si NMR (CDCl$_3$) δ −66.2 (s). MALDI–TOF [(M+H)$^+$] calcd. 2722.86, found 2722.18.

Complexation with the dendrimers. General procedure for the entrapping by the dendrimers is described here. Samples containing the guest molecules and each dendrimer were sonicated for 30 sec, and allowed to equilibrate in darkness overnight.

Evaluation of the amount of the encapsulated ligand into the G2 POSS-core dendrimer. The sample solutions were stored under ambient conditions for 2 days and filtered through Nanosep 3K centrifugal devices (Pall Life Sciences) by centrifugation (2000g, 30 min, 25 °C). The concentration of the ligand **1** was determined from the fluorescence emission of the

filtrates. The encapsulation was evaluated by comparing to the intensities of the filtrates at 0 day (I_0) and 2 days (I_{2d}). The results are shown in Figure 2.

Fluorescence measurements of the complexes. The fluorescence emission of the ligand solution (10 μM) in the presence and absence of the dendrimers (100 μM, pH = 5.0) with or without guanosine derivatives under excitation at 330 nm was monitored using a Perkin Elmer LS50B at 25 °C using 1 cm path length cell. The excitation bandwidth was 1 nm. The emission bandwidth was 1 nm. The quantum yields were determined as an absolute value with an integral sphere.

Stern–Volmer plots. The data were analyzed in terms of the Stern–Volmer equation:

$$\frac{I_0}{I} = 1 + K_{SV}[Q]$$

The emission intensity was plotted according to a Stern–Volmer equation, reporting I_0/I versus the concentrations of guanosine derivatives [Q], where I_0 is the intensity in the absence of quencher and I is the intensity in the presence of a quencher. K_{SV} is the Stern–Volmer quenching constant. A plot of I_0/I versus [Q] yields an intercept of one and a slope equal to K_{SV}.

Binding constants calculation. If the non-emissive complex formation between the naphthyridine ligand and guanosine nucleotides occurs, the binding constant (K_A) can be calculated with the number of the binding molecules (*n*) from the following equation:

$$\log\frac{I_0 - I}{I} = \log K_A + n\log[Q]$$

Results and Discussion

The author designed the ligand **1** as shown in Figure 1. The author expected that the POSS core can provide hydrophobic spaces inside dendrimer, leading to the enhancement of the hydrogen bonding. The 1,8-naphthyridine moiety can make a complex with the guanine skeleton via hydrogen bonds.[3] In particular, as applied for fluorescence sensors for guanosine nucleotides in the previous works[3], the fluorescence emission can be quenched via electron transferring through the hydrogen bonds.[6] In other words, the decrease of the emission represents the complex formation of the naphthyridine ligand with guanosine nucleotides. Thereby, the binding constants can be evaluated with the Stern–Volmer equation in the case of the non-emissive complex model according to equation 2.[14] These optical properties of the naphthyridine can make possible to quantitatively assess the stability of the complexes of the naphthyridine moiety with guanosine nucleotides. The benzene ring is expected to play a role in the adsorption of the ligand at the surface of the POSS core via the hydrophobic interaction to be recruited into the internal space of the POSS-core dendrimers. The terminal amino groups are expected to recruit the guanosine nucleotides by the electrostatic interaction with the phosphate groups.
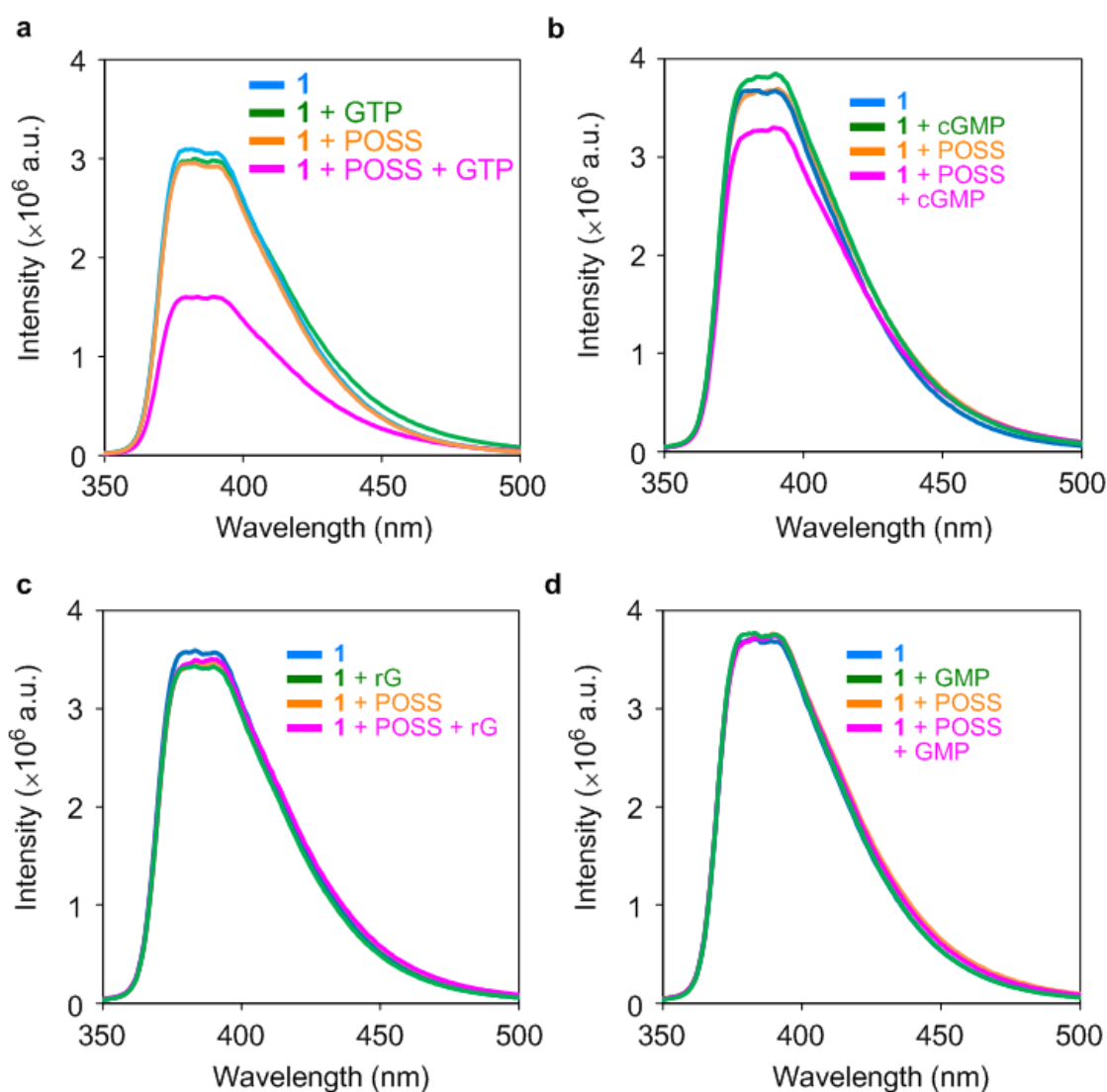

G2 POSS-core dendrimer

$R_1 = R_2 = H: rG$
$R_1, R_2 = -PO_2H-: cGMP$
$R_1 = PO_3H, R_2 = H: GMP$
$R_1 = P_3O_9H_4, R_2 = H: GTP$

1
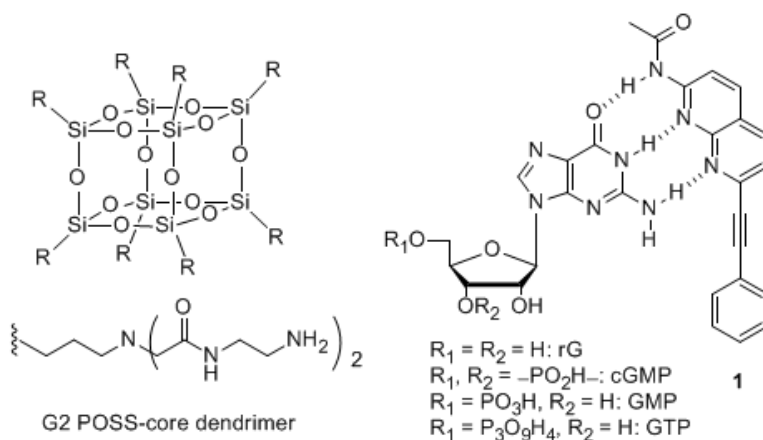
Figure 1. Chemical structures of G2 POSS-core dendrimer and the complexes of the ligand 1 and the guanosine nucleotides used in this study.

Initially, 1-amino-7-chloronaphthyridine was prepared according to the previous reports.[12] The ligand **1** was obtained via Sonogashira–Hagihara cross coupling reaction, following the acetylation at the amino group of the 7 position. The second generation of the POSS-core dendrimer (G2 POSS-core dendrimer) was prepared according to the literatures.[9,15] The complexation of the G2 POSS-core dendrimer with the naphthyridine ligand was performed by mixing. To confirm the retention into the dendrimer, the author investigated the fluorescence emission of the filtrate passed through the size-exclusive filter.[11] If the naphthyridine ligand forms aggregation or adsorbs onto the wall of vessels, the filtrate shows significant low emission intensity. On the other hand, if the naphthyridine ligand can be retained into the dendrimers, the adsorption should be inhibited. Thereby, the fluorescence can be observed from the filtrates. In addition, the emission intensity of the filtrate can represent the amount of the retention. The author prepared the solution with various concentrations of the G2 POSS-core dendrimer and investigated the intensity changes of the filtrate after 2 days from the ligand **1** (Figure 2). The filtrate in the absence of the G2 POSS-core dendrimer provided subtle emission from the ligand **1**. In contrast, fluorescence emission from the filtrate was mostly maintained in the presence of the G2 POSS-core dendrimer. These results suggest that 10 μM of the ligand **1** should be retained into the dendrimer (100 μM). Moreover, it was found that the naphthyridine ligand retained into the G2 POSS-core dendrimer can maintain the good dispersion state without non-specific aggregation or adsorption to the wall of the vessels at least for two days. This is enough length for doing further experiments.
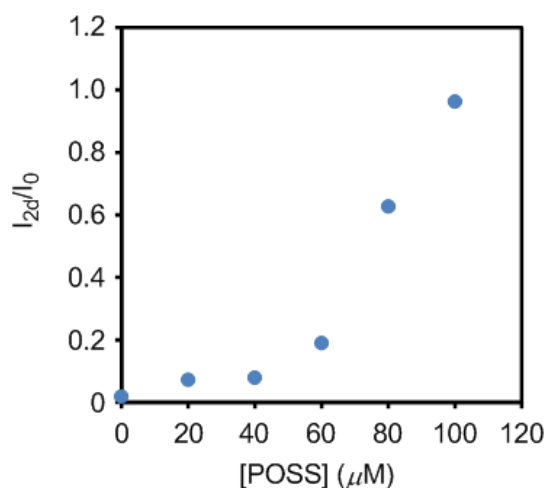
Figure 2. Emission changes of the filtrates after 2 days. The solutions containing 10 μM **1** and variable concentrations of the G2 POSS-core dendrimer were stored under ambient conditions for 2 days and then passed through the size-exclusive filter membrane by centrifugation. Emission spectra were obtained with the excitation light at 330 nm at 25 °C.

The author investigated the changes of fluorescence intensity from the ligand **1** by adding the series of the guanosine nucleotides. The emission spectra were obtained from the aqueous solutions containing 10 μM ligand **1** and 100 μM G2 POSS-core dendrimer with an excitation light at 330 nm (Figure 3). The strong fluorescence emission with the peak around 380 nm was observed from the ligand **1** in the aqueous solution. The addition of guanosine triphosphate (GTP) caused the significant quenching of the emission from the ligand **1** (Figure 3a). The complex formation with GTP was suggested. In the presence of cGMP, the emission was also quenched (Figure 3b). Corresponding to the results reported by Cywinski *et al.*, the complex formation via hydrogen bonds should occur between the ligand **1** and cGMP.[6] Slight influences on the emission intensity were observed by adding rG and GMP to the solution. These results suggest that the interaction particularly between GTP and the ligand **1** can be enhanced by the G2 POSS-core dendrimer.

Figure 3. Emission changes of 10 μM **1** in the presence and absence of 100 μM G2 POSS-core dendrimers by adding 100 μM guanosine nucleotides in water at 25 $^{\circ}$C. Excitation wavelength was 330 nm.

To evaluate the role of the POSS-core, the author performed fluorescence measurements with the same procedure using the G2 PAMAM dendrimer which possesses the ethylene-diamine core instead of POSS. By adding guanosine nucleotides including GTP, the emissions from the ligand **1** were less affected (Figure 4a). These results clearly indicate that the POSS core should take responsible for enhancing the complex formation between the

133

ligand **1** and GTP. The hydrophobic space around the POSS core could reduce the hydration of the naphthyridine ligand, resulting into the enhancement of the affinity of the complex via hydrogen bonds. Moreover, the fluorescence measurements were also carried out with adenosine triphosphate (ATP), and it was found that the emission was hardly changed (Figure 4b). This result suggests that the triphosphate group should less influence on the emission property of the naphthyridine derivatives.
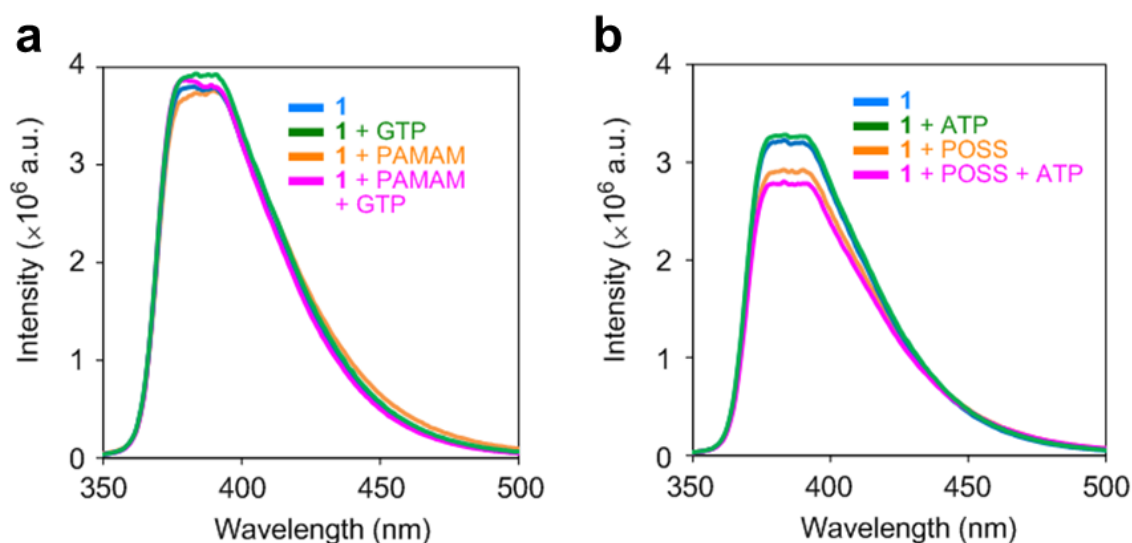
Figure 4. Emission changes of 10 μM **1** in the presence and absence of (a) 100 μM G2 PAMAM dendrimers by adding 100 μM GTP and (b) 100 μM G2 POSS-core dendrimers by adding 100 μM ATP in water at 25 °C. Excitation wavelength was 330 nm.

The author prepared the Stern–Volmer plots with guanosine nucleotides as a quencher (Figure 5A, Table 1). Based on the formation of a non-emissive complex model, the binding constants were calculated (Figure 5B). All plots obtained from the titration of GTP and cGMP were fitted on the line, and the binding constants can be determined. It was found that POSS can enhance the binding affinity with GTP approximately 10-times larger than that

with cGMP. These results suggest that the ligand **1** can selectively recognize GTP in the G2 POSS-core dendrimer.
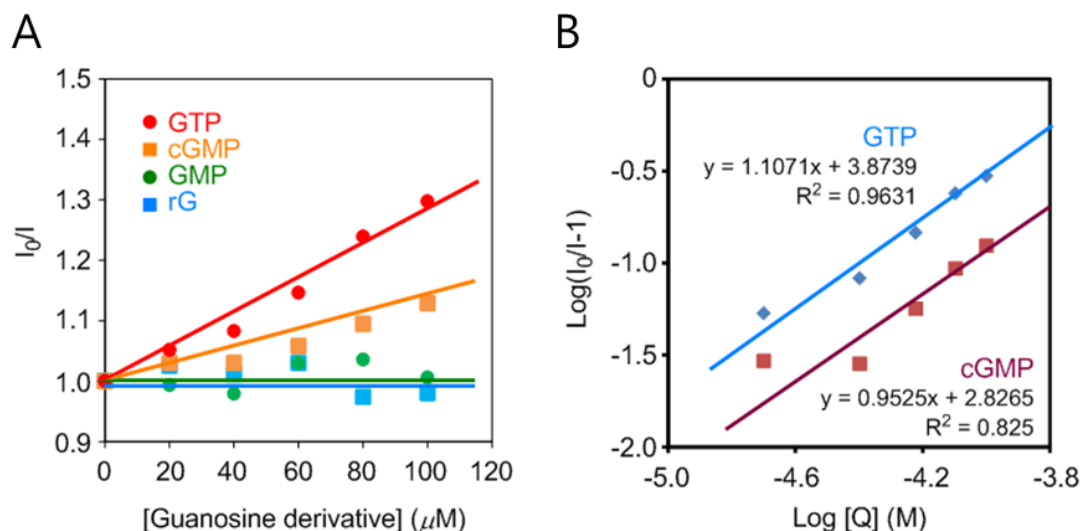
Figure 5. (A) Stern–Volmer plots with the solution containing 10 μM **1** by adding various kinds of guanosine derivatives. (B) The plots for determining the binding constants between the ligand **1** and guanosine nucleotides according to the above equation. The slopes represent the number of the binding guanosine nucleotides. The y-intercepts represent the logK_A values. The lines are prepared with the least-square method. R^2 is determination coefficient.

Table 1. Optical properties and the binding constants of the ligand **1**[a]

Nucleotides[b]	Φ[c]	K_{SV} [$\times 10^3$ mol L^{-1}][d]	n[e]	K_A [M^{-1}][e]
none	0.39	n.d.[f]	n.d.[f]	n.d.[f]
rG	0.39	n.d.[f]	n.d.[f]	n.d.[f]
GMP	0.39	n.d.[f]	n.d.[f]	n.d.[f]
cGMP	0.34	1.14	0.95	670
GTP	0.30	2.83	1.10	7500

[a]Procedures and conditions are described in the Experimental.

[b]100 μM solutions.

[c]Determined as an absolute value.

[d]Quenching constants were determined with the slopes of the fitting line in the Stern-Volmer plots.

[e]Calculated according to the reference 12.

[f]n.d. = not determined because of too weak interaction.

In order to investigate the influences of the substituents at the naphthyridine ligand on the recognition, the emission spectra were measured with various kinds of the naphthyridine derivatives[12] listed in Figure 6. The retention of these derivatives into the G2 POSS-core dendrimer with the same manner as above, and emission changes were examined. Significant quenches were hardly observed by adding guanosine nucleotides to the series of the naphthyridine ligands. These results mean that all substituents at the ligand **1** are necessary to maintain the recognition ability. The hydrogen bonds and the hydrophobic interaction to the surface of the POSS core might cooperatively contribute to the selective recognition of the ligand **1** with GTP in the G2 POSS-core dendrimer.
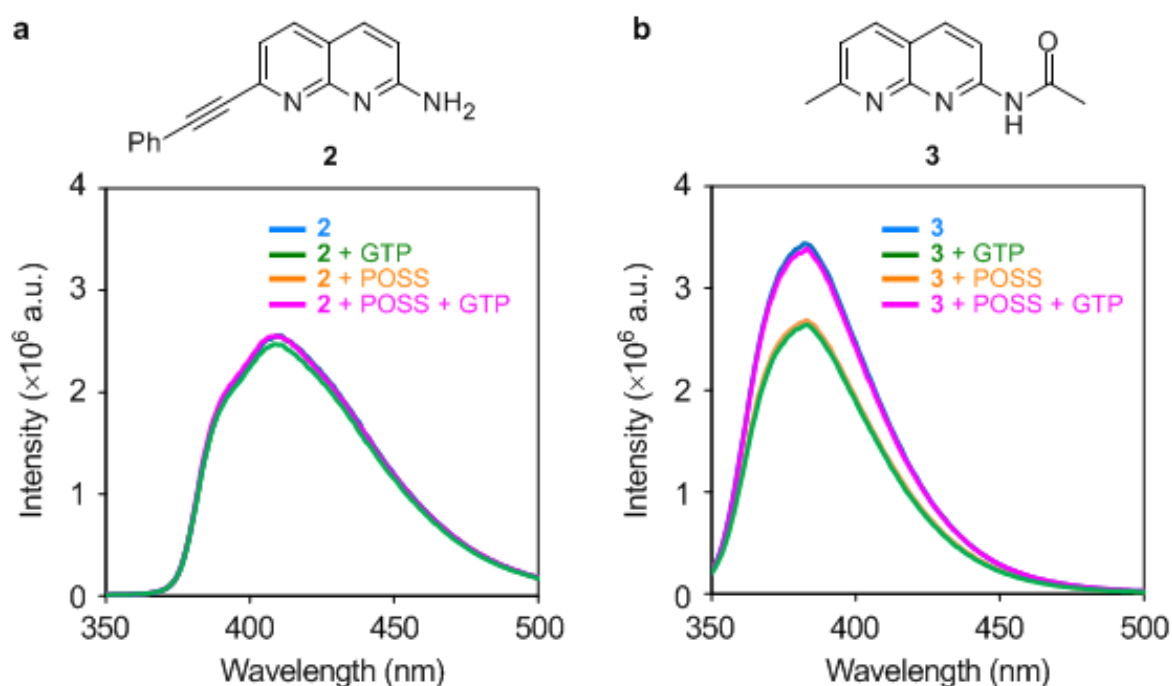

Figure 6. Chemical structures and emission changes of 10 μM (a) **2** and (b) **3** in the presence and absence of 100 μM G2 POSS-core dendrimers by adding 100 μM GTP in water at 25 °C. Excitation wavelength was 330 nm.

To elaborate the influence of the charge at the surface of the dendrimer, the emission intensity of the complex was compared in various pH solutions (Figure 7). Under alkaline condition, the degree of fluorescence quench was reduced, while the quenching ability can be maintained under acidic condition. These results indicate that the terminal-ammonium groups should contribute to recruiting GTP via electrostatic interaction. Under the extremely acidic condition in 0.1 N hydrochloric acid, the fluorescence emission was largely suppressed (Figure 8, $\Phi = 0.13$), and the new peak appeared at the longer wavelength region. Therefore, the protonation of the naphthyridine moiety induced by the triphosphate moiety of GTP should be hardly responsible for the quenching. From the series of data, the recognition model for guanosine nucleotides by the dendrimer complex can be proposed. The naphthyridine ligand and G2 POSS-core dendrimer form the stable complex in which guanosine nucleotides can come and go out. GTP should be retained in the complex for relatively-longer time because of the cooperative interaction via the hydrogen bonds with the naphthyridine ligand and the stronger electrostatic attraction. Thus, selective capturing for GTP by the dendrimer complex could be observed.
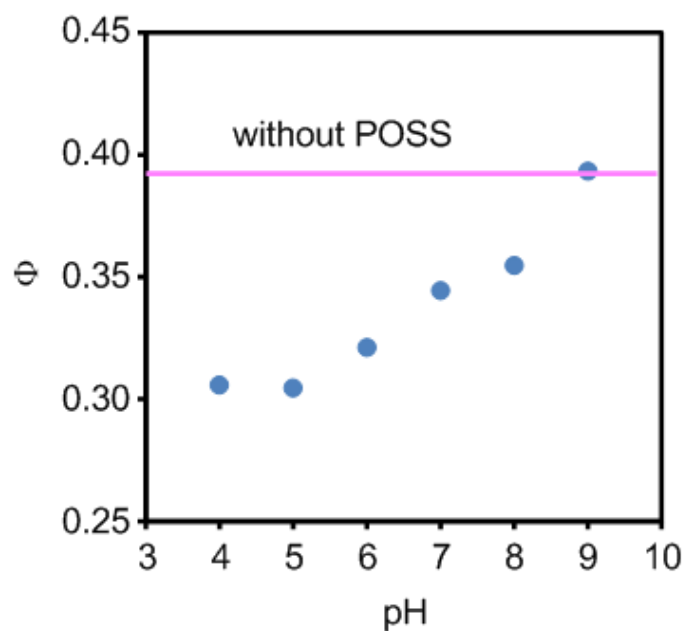
Figure 7. The influence of pH on the quantum yields of the emission from the solutions containing 10 μM **1**, 100 μM G2 POSS-core dendrimer, and 100 μM GTP in 50 mM sodium phosphate buffer at 25 °C. Excitation wavelength was 330 nm.
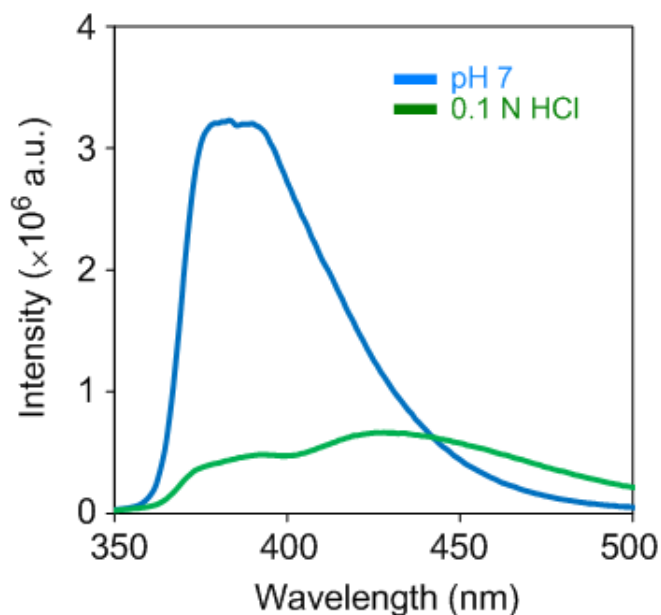
Figure 8. Emission spectra of the solutions containing 10 μM **1** in 50 mM sodium phosphate buffer (pH = 7.0) and 0.1 N HCl at at 25 °C. Excitation wavelength was 330 nm.

Conclusion

The author presents that the binding affinity of the naphthyridine ligand with GTP can be enhanced by the POSS-core dendrimer. Although the affinity is lower than those of the aptamers[16] as previously reported, this system is applicable in a wide pH range and salt concentration. These data indicate that the dendrimer complex with the naphthyridine ligand can selectively recognize and capture GTP. Furthermore, in this system, the POSS-core dendrimer and the ligand molecules make interaction only via the non-covalent bonds. Therefore, it can be expected that the target guest molecules can be tuned by replacing the ligand units. This might be applicable not only for developing the new tools for biosensing but also for modulating the concentrations of the targets in the cells.

References

1. Sawada, T.; Yoshizawa, M.; Sato, S.; Fujita, M. *Nat. Chem*. **2009**, *1*, 53.

2. Westover, K. D.; Bushnell, D. A.; Kornberg, R. D. *Cell* **2004**, *119*, 481.

3. (a) Liao, J. H.; Chen, C. T.; Chou, H. C.; Cheng, C. C.; Chou, P. T.; Fang, J. M.; Slanina, Z.; Chow, T. J. *Org. Lett*. **2002**, *4*, 3107; (b) Fang, J. M.; Selvi, S.; Liao, J. H.; Slanina, Z.; Chen, C. T.; Chou, P. T. *J. Am. Chem. Soc*. **2004**, *126*, 3559; (c) Xu, Z.; Morita, K.; Sato,Y.; Dai, Q.; Nishizawa, S.; Teramae, N. *Chem. Commun*. **2009**, 6445; (d) Sato, Y.; Nishizawa, S.; Yoshimoto, K.; Seino, T.; Ichizawa, T.; Morita, K.; Teramae, N. *Nucleic Acids Res*. **2009**, *37*, 1411.

4. Nakatani, K.; Hagihara, S.; Goto, Y.; Kobori, A.; Hagihara, M.; Hayashi, G.; Kyo, M.; Nomura, M.; Mishima, M.; Kojima, C. *Nat. Chem. Biol.* **2005**, *1*, 39.

5. (a) Nakatani, K.; Sando, S.; Saito, I. *Nat. Biotechnol.* **2001**, *19*, 51; (b) Nakatani, K.; Sando, S.; Kumasawa, H.; Kikuchi, J.; Saito, I. *J. Am. Chem. Soc.* **2001**, *123*, 12650; (c) Peng, T.; Dohno, C.; Nakatani, K. *Angew. Chem. Int. Ed.* **2006**, *45*, 5623.

6. Cywinski, P. J.; Moro, A. J.; Ritschel, T.; Hildebrandt, N.; Löhmannsröben, H. G. *Anal. Bioanal. Chem.* **2011**, *399*, 1215.

7. (a) Matsumoto, S.; Yamaguchi, S.; Ueno, S.; Komatsu, H.; Ikeda, M.; Ishizuka, K.; Iko, Y.; Tabata, K. V.; Aoki, H.; Ito, S.; Noji, H.; Hamachi,I. *Chem. –Eur. J.* **2008**, *14*, 3977; (b) Matsumoto, S.; Yamaguchi, S.; Wada, A.; Matsui, T.; Ikeda, M.; Hamachi, I. *Chem. Commun.* **2008**, 1545; (c) Komatsu, H.; Matsumoto, S.; Tamaru, S.; Kaneko, K.; Ikeda, M.; Hamachi, I. *J. Am. Chem. Soc.* **2009**, *131*, 5580; (d) Boekhoven, J.; Brizard, A. M.; Kowlgi, K. N. K.; Koper, G. J. M.; Eelkema, R.; van Esch, J. H. *Angew. Chem. Int. Ed.* **2010**, *49*, 4825.

8. (a) Morimoto, N.; Ogino, N.; Narita, T.; Akiyoshi, K. *J. Biotechnol.* **2009**, *140*, 246; (b) Morimoto, A.; Qiu, X.-P.; Winnik, F. M.; Akiyoshi, K. *Macromolecules* **2008**, *41*, 5985; (c) Morimoto, N.; Ohki, T.; Kurita, K.; Akiyoshi, K. *Macromol. Rapid Commun.* **2008**, *29*, 672.

9. (a) Jaffrés, P.-A.; Morris, R. E. *J. Chem. Soc., Dalton Trans.* **1998**, 2767; (b) Feher, F. J.; Wyndham, K. D. *Chem. Commun.* **1998**, 323; (c) Feher, F. J.; Wyndham, K. D.; Soulivong, D.; Nguyen, F. *J. Chem. Soc., Dalton Trans.* **1999**, 1491; (d) Zhang, X.; Haxton, K. J.; Ropartz, L.; Cole-Hamilton, D. J.; Morris, R. E. *J. Chem. Soc., Dalton Trans.* **2001**, 3261.

10. (a) Tanaka, K.; Inafuku, K.; Naka, K.; Chujo, Y. *Org. Biomol. Chem.* **2008**, *6*, 3899; (b) Tanaka, K.; Inafuku, K.; Chujo, Y. *Chem. Commun*. **2010**, *46*, 4378; (c) Tanaka, K.; Inafuku, K.; Adachi, S.; Chujo, Y. *Macromolecules* **2009**, *42*, 3489.

11. Tanaka, K.; Ohashi, W.; Kitamura, N.; Chujo, Y. *Bull. Chem. Soc. Jpn.* **2011**, *84*, 612.

12. Newkome, R. G.; Garbis, J. S.; Majestic, K. V.; Fronczek, R. F.; Chiari, G. *J. Org. Chem.* **1981**, *46*, 833.

13. Sun, Y.; Bi, S.; Song, D.; Qiao, C.; Mu, D.; Zhang, H. *Sensor Actuat. B* **2008**, *129*, 799.

14. (a) Gravel,M. C.; Zhang, C.; Dinderman, M.; Laine, R. M. *Appl. Organometal. Chem.* **1999**, *13*, 329; (b) Feher, F. J.; Wyndham*, K. D. *Chem. Commun.* **1998**, 323.

15. Davis, J. H.; Szostak, J. W. *Proc. Natl. Acad. Sci. USA* **2002**, *99*, 11616.

Chapter 7

Construction of Light-Driven Artificial Enzymes for Selective Oxidation of Guanosine Triphosphate Using Water-Soluble POSS Network Polymers

Chapter 7

Construction of Light-Driven Artificial Enzymes for Selective Oxidation of Guanosine Triphosphate Using Water-Soluble POSS Network Polymers

Abstract: The light-driven artificial enzymes were constructed to realize unnatural reactions concerning with bio-significant molecules. This chapter shows that the water-soluble POSS-based network polymers can enhance the selective recognition and oxidation of GTP. The author synthesized the water-soluble POSS network polymers containing the naphthyridine ligands to capture GTP inside the networks and ruthenium complexes to oxidize the captured GTP under light irradiation. Initially, the complexation of the naphthyridine ligands with the series of guanosine nucleotides was investigated, and it is shown that the POSS network should play a significant role in the stabilization of the complexes via hydrogen bonds. Next, the photo-catalytic activity of the ruthenium complex-modified POSS network polymers to guanosine nucleotides was investigated. Consequently, it was revealed that the modified polymers can decompose GTP efficiently under light irradiation.

GTP

Selective Recognition & Oxidation

Water-Soluble POSS Network Polymers

POSS Network/GTP Complexes
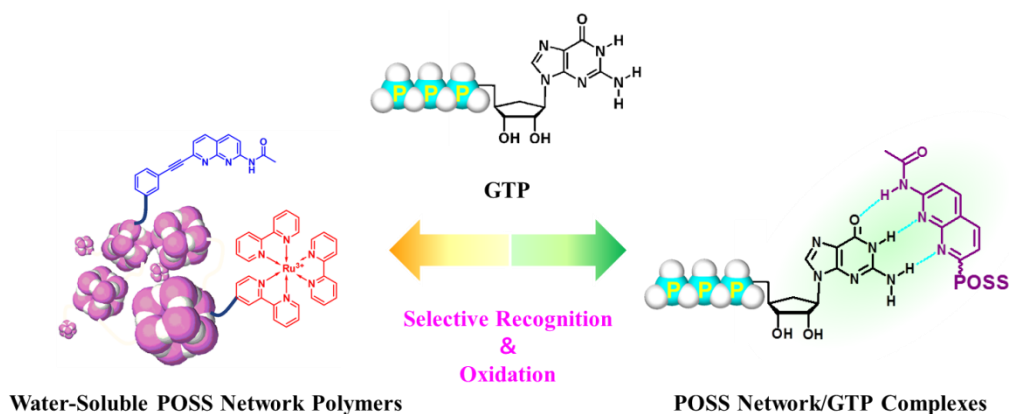
Introduction

The development of artificial enzymes is one of significant issues in biotechnology. Many researchers have aimed to develop materials and establish conventional systems to promote the biological reactions with higher efficiency than those by native enzymes or realize unnatural reactions concerning with biomolecules.[1-5] In particular, the usage of light irradiation as a trigger for the activation has several advantages: The time- and site-specificity can be readily received by modulating the timing and spot of light irradiation, respectively. Photo-activation can be achieved without further artifacts. Moreover, if the visible light is applicable for exciting the system, the influence of the light irradiation to vital organs should be negligible. Thus, light-driven artificial enzymes are promised to be an efficient tool to control the biological events as the author expects.[6-13]

Guanosine triphosphate (GTP) concerns a wide variety of biological events such as signal transduction, metabolism, and enzymatic reactions. In particular, GTP is a substrate of RNA polymerases in the RNA synthesis.[14] Therefore, the regulation of local concentrations of GTP is applicable for developing biosensors, drugs, and biotechnological tools. In vital bodies, the concentrations of GTP are regulated restrictedly by various kinds of GTP-related enzymes. There are classes of enzymes that can cause both of the GTP degradation and production. Moreover, most of the GTP degradation enzyme can catalyze the hydrolysis at the triphosphate moiety to convert to nucleoside, monophosphate, or other phosphate ester species. Thereby, even if these native enzymes are overexpressed for catalyzing GTP hydrolysis in the cells, it is difficult to induce the suppression of the GTP level at the local sites because the GTP synthetic enzymes would compensate the decrease. Thus, one of strategies for reducing the GTP concentrations is to decompose guanine base irreversibly.

The author has recently reported the selective encapsulation of GTP into the polyhedral oligomeric silsesquioxane (POSS)-core dendrimer via the complex formation with the

naphthyridine derivatives.[15] At the surface of the hydrophobic POSS core inside dendrimer, the complex stability via hydrogen bonds between the guanine moiety of GTP and the naphthyridine derivative was significantly improved. In addition, the negatively-charged compounds such as triphosphates of the nucleotides made a strong interaction with the ammonium groups at the surface dendrimer. As a result, although there is room to improve the binding affinity, only GTP can form the stable complex via hydrogen bonds with the naphthyridine derivatives inside the POSS-core dendrimer. Finally, the author established the selective encapsulation of GTP by the naphthyridine-modified POSS-core dendrimer complex. The author was inspired the application of the selective encapsulation with the POSS-based polymeric materials as a recognition unit for the artificial enzyme.

In this chapter, the author describes the light-driven artificial enzyme for GTP oxidation. The POSS-based water-soluble network polymers involving the naphthyridine ligands and the ruthenium complexes were synthesized. From the titration experiments with the series of guanosine nucleotides, the selectivity in the encapsulation for each guanosine nucleotide by the POSS network polymers in PBS was evaluated from the magnitude of binding affinity to the naphthyridine ligands. Next, the photo-triggered guanine oxidation was performed in the presence of the Ru complex-modified POSS network polymers. From the consumption rates of guanosine nucleotides during the photo reactions, the enzymatic ability of the POSS network polymers for guanine oxidation was quantitatively examined.

Experimental Section

General. ^{1}H NMR and ^{13}C NMR spectra were measured with a JEOL EX–400 (400 MHz for ^{1}H and 10 MHz for ^{13}C) spectrometer. ^{29}Si NMR spectra were measured with a JEOL JNM-A400 (80 MHz) spectrometer. Coupling constants (J value) are reported in Hertz. The chemical shifts are expressed in ppm downfield from tetramethylsilane, using residual chloroform ($\delta = 7.24$ in ^{1}H NMR, $\delta = 77.0$ in ^{13}C NMR) or residual DMSO ($\delta = 2.49$ in ^{1}H NMR, $\delta = 39.5$ in ^{13}C NMR) as an internal standard. MASS spectra were obtained on a JEOL JMS–SX102A. Emission from the samples was monitored using a Perkin Elmer LS50B at 25 °C using 1 cm path length cell. MASS spectra were obtained on a JEOL JMS–SX102A.

Synthesis of 1,8-naphthyridine ligands, 5.

The compound 1. The reaction mixture containing 9.07 g of malic acid (67.6 mmol) and 6.67 g of 2,6-diaminopyridine (61.1 mmol) was slowly added to 40 mL of 95 % H_2SO_4 at 0 °C. After stirring at 110 °C for 3 h, the solution was neutralized with NH_4OH, and the product was yielded as a precipitate. The title compound was separated by the filtration as a white powder (9.05 g, 92 %). ^{1}H NMR (DMSO-d_6) δ 11.85 (br, 2H), 7.64 (d, 1H, J=9.6 Hz), 7.63 (d, 1H, J=9.2 Hz), 6.32 (d, 1H, J=9.2 Hz), 6.01 (d, 1H, J=8.9 Hz). LRMS (NBA) [(M+H)$^+$] calcd. 162, found 162.

The compound 2. A suspension of compound **1** (30.0 g, 93.2 mmol) in 300 mL of acetic anhydride was heated at reflux for 3 h. The resulting mixture was cooled to room temperature, and the precipitate was collected by vacuum filtration, washed with diethyl ether, and air-dried to give 32 g (85 %) of the title compound as a yellow powder. ^{1}H NMR (DMSO-d_6) δ 11.90 (s, 1H, naphthyridinone NH), 10.50 (s, 1H, NH), 8.02 (d, 1H, H-4, J=8.4 Hz), 7.90 (d, 1H, H-3, J=8.4 Hz), 7.82 (d, 1H, H-5, J=9.2 Hz), 6.40 (d, 1H, H-6, J=9.2 Hz), 2.12 (s, 3H, CH_3). HRMS (NBA) [(M+H)$^+$] calcd. 203.0695, found 203.0694.

The compound 3. A mixture of compound **2** (20.0 g, 98.5 mmol) and $POCl_3$ (350 mL) was heated at 90–95 °C for 2 h. The resulting solution was cooled to room temperature, and excess $POCl_3$ was removed by kugelrohr distillation. The residue was dissolved in ice water, and the solution was made basic (pH = 8) with concentrated ammonium hydroxide, which prompted formation of a brownish green precipitate. The solid was collected by vacuum filtration, air-dried, and continuously extracted (Soxhlet extraction) with chloroform for 12 h. The solvent was removed *in vacuo*, and the crude product was purified by column chromatography (CH_3OH/CH_2Cl_2, 1:9 v/v) to give 13 g (60 %) of the title compound as golden needles. ^{1}H NMR (DMSO-d_6) δ 11.13 (s, 1H, NH), 8.40 (m, 3H, H-3, H-4, H-5), 7.54 (d, 1H, H-6, J=8.5 Hz), 2.16 (s, 3H, CH_3). ^{13}C NMR (DMSO-d_6) δ 170.41, 155.13, 154.18, 152.76, 140.42, 139.66, 121.46, 118.99, 115.13, 24.25. Anal. Calcd for $C_{10}H_8N_3ClO$: C, 54.19; H, 3.46; N, 18.96. Found: C, 54.07; H, 3.64; N, 18.88.

The compound 4. In a 25-mL round-bottom flask, 310 mg of compound **3** (1.4 mmol), 35 mg of $PdCl_2(PPh_3)_2$ (cat.) and 7.8 mg of CuI (cat.) were stirred in 10 mL of dry THF under argon. To the solution, 2 mL of triethylamine was slowly added through a syringe. The mixture was stirred at room temperature for 30 min and then 0.2 mL of 3-ethynylaniline (1.9 mmol) were added dropwise. The reaction was stirred at room temperature overnight. Upon removal of the volatiles under reduced pressure, the residue was dissolved in dichloromethane, passed through a plug of celite and then washed with ethyl acetate. The solvents were removed under reduced pressure and the crude product was dried under *vacuo*. Column chromatography in silica gel with an increasing gradient of methanol in dichloromethane (CH_2Cl_2/CH_3OH from 20:1 to 10:1) yielded 180 mg (31 %) of pure product. ^{1}H NMR (DMSO-d_6) δ 11.02 (s, 1H, NH), 8.43 (m, 3H), 7.65 (m, 1H), 7.11 (t, 1H, J=7.8 Hz), 6.84 (s, 1H), 6.79 (d, 1H, J=7.8 Hz), 6.69 (d, 1H, J=7.8 Hz), 5.32 (s, 2H, NH_2), 2.20 (s, 3H, CH_3). ^{13}C NMR (DMSO-d_6) δ 170.8, 155.4, 155.1, 149.4, 146.3, 139.7, 138.0, 129.9, 124.2,

121.7, 119.8, 116.9, 116.1, 115.7, 91.8, 88.8, 24.7.

The compound 5. Compound **4** (4.5 g, 15 mmol) was dissolved in 100 mL of dry methanol, and then succinic anhydride (4.0 g, 40 mmol) was added. The reaction mixture was stirred at room temperature for 6 h. After the reaction, the precipitate was collected by vacuum filtration, and the chloroform solution of the products were washed with methanol and dried over Na_2SO_4. After removing volatiles by evaporation, **5** was obtained as a brown powder (4.04 g, 67 %). ^{1}H NMR (DMSO-d_6) δ 11.07 (s, 1H, NH), 10.15 (s, 1H, NH), 8.43 (m, 3H), 7.99 (s, 1H), 7.72 (m, 1H), 7.60 (m, 1H), 7.42 (m, 1H), 7.33 (m, 1H), 2.58 (m, 4H, CH_2) 2.18 (s, 3H, CH_3). ^{13}C NMR (DMSO-d_6) δ 177.3, 173.7, 168.9, 157.6, 150.0, 143.6, 138.1, 136.9, 133.8, 128.6, 127.9, 126.4, 124.5, 122.9, 121.3, 115.8, 90.3, 86.5, 32.3, 30.7, 22.2. FABMS (NBA/CHCl$_3$) m/z 266 ([(M+H)$^+$]), HRMS (NBA) [(M+H)$^+$] calcd. 266.1657, found 266.1657.

Synthesis of 2,2-bipyridyl, 2.

4-(5-Cyanopentyl)-4′-methyl-2,2′-bipyridine, 1. To a solution of diisopropylamine (4.6 mL, 33 mmol) in THF (100 mL), n-butyllithium (1.6 M solution in hexane, 18.4 mL, 29.4 mmol) was added, and the reaction mixture was stirred at −78 °C for 15 min. After adding 4,4′-dimethyl-2,2′-bipyridine (5.16 g, 28 mmol) dissolved in THF (100 mL), the reaction mixture was stirred additionally for 1 h at −78 °C. 5-Bromovaleronitrile (3.6 mL, 31 mmol) in THF (5 mL) was subsequently added, and the reaction mixture was stirred for 2 h at 0 °C. The resulting mixture was diluted with water (100 mL), neutralized with 1 N HCl and extracted with ethyl acetate. The organic phase was washed with brine, dried over MgSO$_4$ and concentrated *in vacuo*. The crude product was purified by silica gel column chromatography (hexane : ethyl acetate = 10:1) to give 7.4 g (99 %) of the title compound as a brown powder. ^{1}H NMR (CDCl$_3$) δ 8.51 (dd, 1H, J=0.7, 5.1 Hz), 8.49 (dd, 1H, J=0.5, 4.9 Hz), 8.19–8.18 (m,

2H), 7.09–7.06 (m, 2H), 2.66 (t, 2H, J=7.7 Hz), 2.33 (s, 3H), 2.28 (t, 2H, J=7.0 Hz), 1.73–1.60 (m, 4H), 1.50–1.44 (m, 2H). ^{13}C NMR (CDCl$_3$) δ 155.9, 155.6, 151.6, 148.8, 148.6, 147.8, 124.4, 123.5, 121.7, 120.8, 119.3, 34.8, 29.2, 27.9, 24.9, 20.8, 16.7. FABMS (NBA/CHCl$_3$) m/z 266 ([(M+H)$^+$]), HRMS (NBA) [(M+H)$^+$] calcd. 266.1657, found 266.1657.

6-(4′-Methyl-2,2′-bipyridin-4-yl)hexanoic acid, 2. A mixture of bipyridine **1** (7.40 g, 27.9 mmol) and conc. HCl (35–37 %, 50 mL) was stirred at 100 °C overnight. The resulting mixture was adjusted the pH value to 4.0–4.5 with 6 N NaOH and extracted with chloroform. The organic phase was washed with brine, dried over MgSO$_4$ and concentrated *in vacuo* to yield bipyridine **2** (7.70 g, 97%) as a magenta powder. ^{1}H NMR (CDCl$_3$) δ 8.57 (d, 1H, J=0.7 Hz), 8.56 (d, 1H, J=0.7 Hz), 8.21 (s, 1H), 8.18 (d, 1H, J=0.7 Hz), 7.17 (ddd, 1H, J=0.7, 1.6, 5.1 Hz), 7.14 (dd, 1H, J=1.8, 5.1 Hz), 2.72 (t, 2H, J=7.7 Hz), 2.45 (s, 3H), 2.36 (t, 2H, J=7.3 Hz), 1.77–1.67 (m, 4H), 1.46-1.40 (m, 2H). ^{13}C NMR (CDCl$_3$) δ 177.7, 155.5, 152.8, 148.7, 148.6, 148.5, 124.7, 124.0, 122.6, 121.8, 35.1, 34.0, 29.7, 28.5, 24.5, 21.1. FABMS (NBA/CHCl$_3$) m/z 285 [(M+H)$^+$], HRMS (NBA) [(M+H)$^+$] calcd. 285.1603, found 285.1612.

Preparation of dichlorobis(4,4′-dimethyl-2,2′-bipyridine)ruthenium(II), Ru^{II}(bpy)$_2$-Cl$_2$. The mixture containing 4,4′-dimethyl-2,2′-bipyridine (1.417 g, 7.69 mmol), RuCl$_3$·3H$_2$O (1.0 g, 3.82 mmol), and lithium chloride (1.1 g, 25.9 mmol) in DMF (10 mL) were refluxed for 7 h. After the reaction, the resulting solution was poured into acetone (25 mL) and stored at 5 °C overnight to form the precipitate. The products were removed by filtration and washed with water (3 × 25 mL) and diethyl ether (3 × 25 mL) before drying in *vacuo* to yield the title compound as a black solid (1.72 g, 83%). The product was used directly in the next step.

Octaammonium POSS, POSS-[NH$_3$Cl]$_8$. (3-Aminopropyl)triethoxysilane (100 mL, 0.427

mol) and conc. hydrochloric acid (35–37 %, 135 mL) in methanol (800 mL) produced **7** as a white precipitate after 5 days at room temperature. The product was obtained after filtration, washing with cold methanol, and drying. The POSS-[NH$_3$Cl]$_8$ was spectroscopically pure in 30 % yield (18.8 g). ^{1}H NMR (DMSO-d_6) δ 8.23 (s, 24H), 2.76 (t, 16H), 1.71 (m, 16H), 0.72 (t, 16H). ^{13}C NMR (DMSO-d_6) δ 40.53, 20.13, and 7.96. ^{29}Si NMR (DMSO-d_6) δ –66.4 (s). MALDI–TOF [(M+H)$^+$] calcd. 880.41, found 879.42.

POSS derivative 1. In a 200-mL round-bottom flask, 14 g of bipyridine **2** (49 mmol), 7 mL of triethylamine (49 mmol) and 14 g of 4-(4,6-dimethoxy-1,3,5-triazin-2-yl)-4-methylmorpholinium chloride (DMT-MM, 90%) (56 mmol) were stirred in 100 mL of dry methanol until the solid had completely dissolved. To the mixture solution, 20 g of POSS-[NH$_3$Cl]$_8$ (17 mmol) was added. The mixture was stirred at room temperature under argon. After stirring for 24 h, the resulting mixture was evaporated to 20 mL and poured into acetonitrile containing 0.1% HCl. The precipitate was washed with acetonitrile. The POSS derivative containing the bipyridine **2** was obtained to yield (79%) as a yellowish powder after drying *in vacuo*.

POSS derivative 2. 1,8-Naphthyridine ligand **5** (9.9 g, 24.5 mmol), triethylamine (3.5 mL, 24.5 mmol) and DMT-MM (8.9 g, 37 mmol) were stirred in 50 mL of dimethyl sulfoxide (DMSO) until the solid had completely dissolved. To the mixture solution, 23 g of POSS derivative **1** (17 mmol) was added. The mixture was stirred at room temperature under argon. After stirring for 24 h, the resulting mixture was poured into acetonitrile containing 0.1 % HCl. The precipitate was collected by vacuum filtration, and washed with acetonitrile. The crude product was dissolved in water and filtrated, and the solvent was removed by rotary evaporator. The POSS derivative containing the bipyridine **2** and the 1,8-naphthyridine **5** was obtained as a darkish brown powder (43%).

Water soluble POSS network polymers containing the 1,8-naphthyridine ligands, POSS-N network polymers. The typical protocol for the polymerization reaction is described here. To a solution of POSS-[NH$_3$Cl]$_8$ (13.2 g, 11.2 mmol) and POSS derivative **2** (4 g, 2.2 mmol) in 20 mL of dry methanol, the premixed solutions containing 4.03 g of oxalic acid (44.8 mmol), 12.5 mL of triethylamine (89.6 mmol), 24.1 g of DMT-MM (0.1 mol) in dry methanol (100 mL) were added, and the reaction mixture was stirred at room temperature. After stirring for 24 h, the resulting mixture was poured into acetonitrile containing 0.1 % HCl, and the precipitate was washed with acetonitrile. The crude product was dissolved in water and filtrated, and the solvent was removed by rotary evaporator. The title compound was obtained as a darkish red powder (57%) after drying *in vacuo*.

Water soluble POSS network polymers containing the Ru-complexes, POSS-Ru network polymers. 1g of POSS-N network polymer (bipyridine unit; 14.5 mg, 0.0508 mmol) and Ru^{II}(bpy)$_2$Cl$_2$ (27.4 mg, 0.0508 mmol) were heated at reflux in water (20 mL) for 24 h. The resulting solution was poured into acetonitrile containing 0.1% HCl, and the precipitate was collected by vacuum filtration, washed with acetonitrile. The crude product was dissolved in water and filtrated, and the solvent was removed by rotary evaporator. The title compound was obtained as a blackish powder (93%).

POSS network polymers and guanosine nucleotides. General procedure for the complexation of guanosine nucleotides by the POSS network polymers are described here. The stock solutions of the POSS-N network polymers (x10) and guanosine nucleotides (x10) were mixed at room temperature, and then the 500 μL of the samples were prepared by adding the PBS buffer (pH 7.4) solution. The complexation with POSS-Ru network polymers was also prepared with the same procedure in PBS buffer solution containing potassium ferricyanide (K$_3$[Fe(CN)$_6$]).

Fluorescence measurements of the complexes. The fluorescence emission of the 1,8-naphthyridine ligand **5** (20 μM of naphthyridine on POSS-N network polymer and 10 μM of naphthyridine on POSS-Ru network polymer) in the presence and absence of the guanosine nucleotides under excitation at 424 nm were monitored using a Perkin Elmer LS50B at 25 °C using 1 cm path length cell. The excitation bandwidth was 1 nm. The emission bandwidth was 1 nm. The quantum yields were determined as an absolute value with an integral sphere.

Stern-Volmer plots. The data were analyzed in terms of the Stern-Volmer equation:

$$\frac{I_0}{I} = 1 + K_{SV}[Q]$$

The emission intensities were plotted according to a Stern-Volmer equation, reporting I_0/I versus the concentrations of guanosine nucleotides [Q], where I_0 is the intensity in the absence of quencher and I is the intensity in the presence of a quencher concentration. K_{SV} is the Stern-Volmer quenching constant. A plot of I_0/I versus [Q] yields an intercept of one and a slope equals to K_{SV}.

Binding constants calculation. If the non-emissive complex formation between the 1,8-naphthyridine receptor and guanosine nucleotides occurs, the binding constant (K_A) can be calculated with the number of the binding molecules (*n*) from the following equation:

$$\log\frac{I_0-I}{I} = \log K_A + n\log[Q]$$

Figure 5 represents the plots for evaluating the K_A values of the 1,8-naphthyridine ligands to GDP and GTP.

Results and Discussion

The principle of molecular recognition of guanosine nucleotides is based on the complexation that can occur among native nucleotide bases. The hydrogen bonding is mimicked by the naphthyridine ligands in the POSS network polymers and the guanosine nucleotides. Novel naphthyridine-type fluorescent molecular sensors can be designed for the guest molecules of guanosine nucleotides to address three major issues; (i) to incorporate an additional binding site into the existing triple hydrogen bonding motif of 2-amino-1,8-naphthyridine derivative to enhance the binding affinity, (ii) to develop the selective fluorescence detection of guanosine nucleotides by novel fluorescent sensors conjugated with the 1,8-naphthyridine ligands, and (iii) to demonstrate the enzyme reaction using the complexes of the naphthyridine ligands in the POSS network polymers with guanosine nucleotides by photo-triggering system.

The author designed the novel fluorescent sensor using the water-soluble POSS network polymers composed of the naphthyridine ligands and the bipyridine moieties as shown in Figure 1. The author expected that the hydrophobicity of POSS core inside the network polymers can enhance the affinity between the naphthyridine ligands and the guanine moiety of guanosine nucleotides via hydrogen bonding in the aqueous solution. In addition, the ammonium groups at the surface of the network polymers can assist to recruit the guanosine nucleotides around the POSS network polymers by electrostatic interaction with the phosphate groups. The incorporation of the naphthyridine ligands leads to the introduction of a fluorescent moiety to the POSS network polymers. When the naphthyridine ligands in the network polymers come in contact with guanosine nucleotides, the fluorescence emission is changed. This can be observed by the fluorescence quenching as a consequence of electron transfer from the naphthyridine ligands to the guanosine nucleotides through the hydrogen

153

bonds. In other words, the decrease of the emission represents the complex formation of the naphthyridine ligands with guanosine nucleotides inside the network polymers. Thereby, the binding constants can be calculated with the Stern–Volmer equation in the case of the non-emissive complex model. These optical properties of the naphthyridine ligands in the POSS network polymers can make possible to quantitatively assess the stability of the complexes of the naphthyridine ligands with guanosine nucleotides.
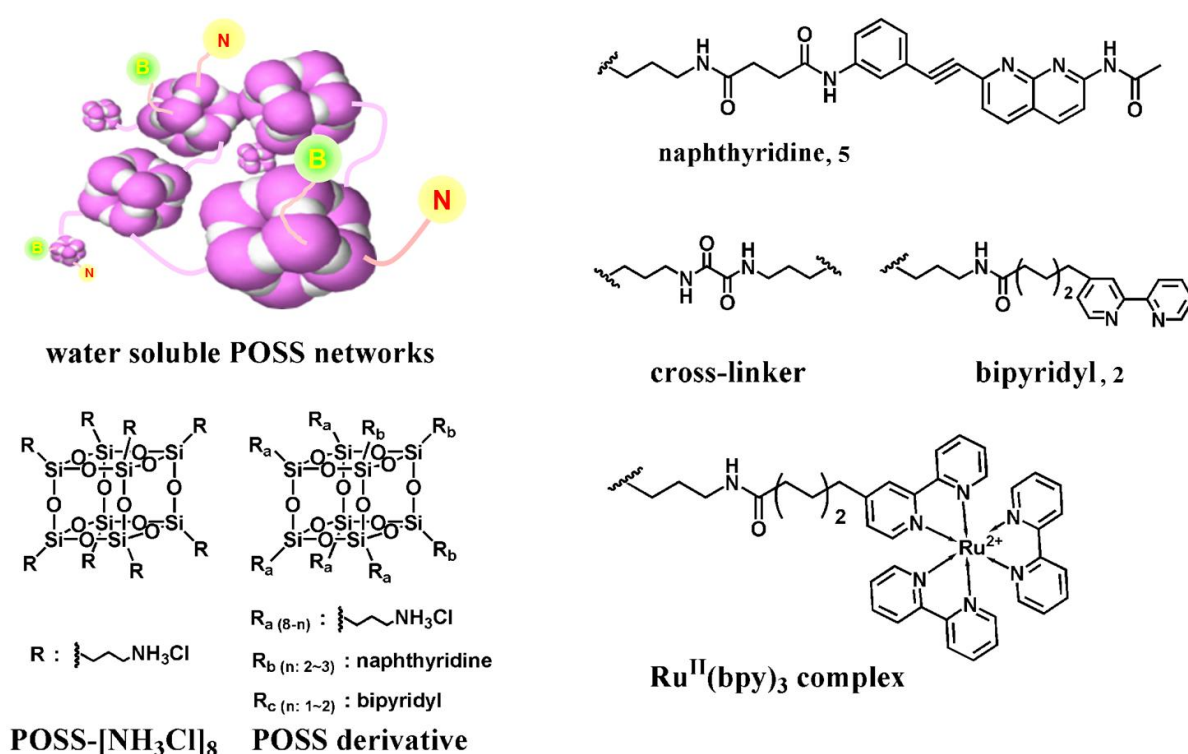

Figure 1. Chemical structures of water-soluble POSS network polymers.

Initially, the author investigated the changes of fluorescence emission from the naphthyridine ligands in the POSS-N network polymers by adding the series of the guanosine nucleotides. The emission spectra were obtained from PBS buffer solution (pH 7.4) containing 20 μM naphthyridine ligands in the POSS network polymers and various concentrations of guanosine nucleotides (0 to 400 μM) with the excitation light at 364 nm

(Figure 2). The strong fluorescence emission with the peak around 424 nm was observed from the naphthyridine ligand in PBS buffer solution. Thus, the author can evaluate the selectivity of the naphthyridine ligand by changing fluorescence emission at 424 nm in data sets obtained from the complexes of the POSS-N network polymer with the guanosine nucleotides. The addition of guanosine triphosphate (GTP) caused the significant quenching of the emission from the naphthyridine ligand as shown in Figure 2. Moreover, the emission with the peak at 424 nm was gradually reduced by the addition of up to 400 μM GTP. In particular, fluorescence emission of the naphthyridine ligands was dramatically quenched by 85% after addition of 400 μM GTP. This result indicates that the naphthyridine ligands can efficiently capture GTP by the complex formations between the POSS-N network polymers and GTP. The quenching is most likely due to electron transfer from the naphthyridine ligand to GTP enabled by the triple hydrogen bonding.

To examine the selectivity of the fluorescent sensor as the POSS network polymers containing the naphthyridine ligands, the author chose various kinds of nucleotides which can be divided into two groups. The first consists of nucleoside triphosphate with different purine base (ATP), and the second is composed of guanosine with varying numbers of phosphate groups (rG, GMP, cGMP, and GDP). The first group was chosen to test the fluorescent sensor in order to evaluate the influence of the triphosphate group on the emission property of the naphthyridine ligands, and the second group was chosen for examining the influence of the number of phosphate groups to the binding affinity with the 1,8-naphthyridine ligands. The binding of the naphthyridine ligands with the guanosine derivatives such as guanosine (rG), guanosine monophosphate (GMP), and cyclic guanosine monophosphate (cGMP) was very weak since no apparent change in the fluorescence spectra was observed even with the addition of excess amounts of the guanosine derivatives (e.g., 20 equiv) (Figure 3). In

contrast, the naphthyridine ligands showed the significant quenching of the emission by adding GDP. By the addition of GDP (400 μM), the emission was quenched by 41 %. These results clearly show the influence of the phosphate groups on the complex formations with the naphthyridine ligands. POSS network polymers can highly improve the local concentrations of the guanosine derivatives containing large numbers of phosphate groups around the naphthyridine ligands by electrostatic interaction between the terminal ammonium groups of the network polymers and the phosphate groups. Then the naphthyridine ligands can efficiently form the complexes with GTP via hydrogen bonds.
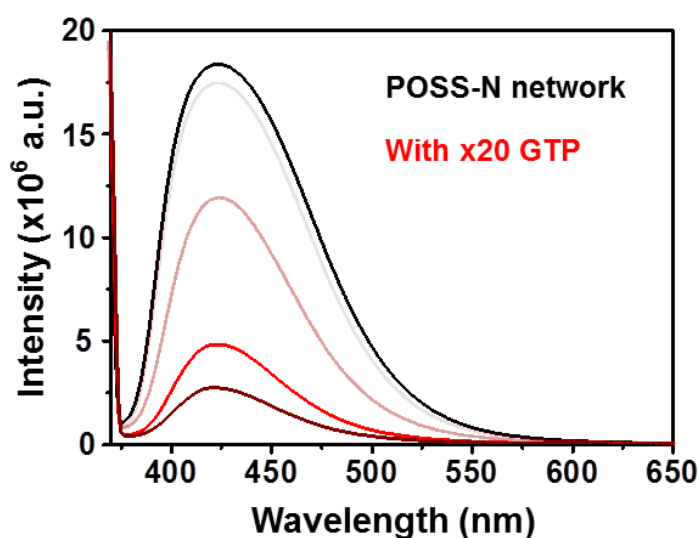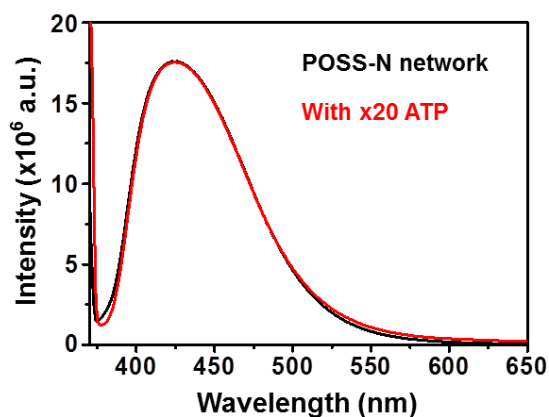

Figure 2. Emission changes of 20 μM naphthyridine ligands in the POSS-N network polymers by adding guanosine triphosphate (GTP) (0 to 400 μM) in PBS buffer solution (pH 7.4) at 25 °C. Excitation wavelength was 364 nm.
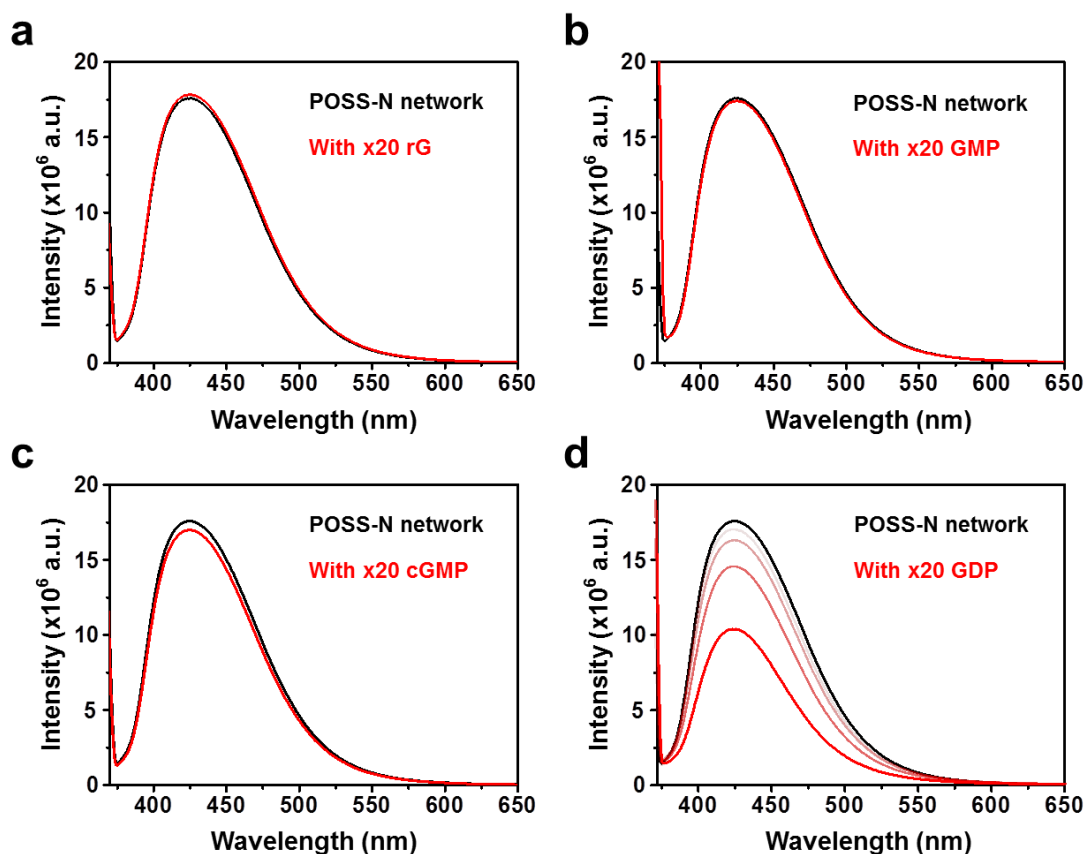
Figure 3. Emission changes of 20 μM naphthyridine ligands in the POSS-N network polymer by adding (a) rG, (b) GMP, (c) cGMP, and (d) GDP (0 to 400 μM) in PBS buffer solution (pH 7.4) at 25 °C. Excitation wavelength was 364 nm.

The fluorescence measurements were also carried out with adenosine triphosphate (ATP), and it was found that the emission was hardly changed even with the addition of excess amounts of ATP (e.g., 20 equiv.) (Figure 4). This result suggests that the triphosphate groups of ATP should less influence on the emission property of the naphthyridine ligands, and the emission of the naphthyridine ligand was quenched by forming complex with guanine moiety of nucleotide via hydrogen bonds.

Figure 4. Emission change of 20 μM naphthyridine ligands in the POSS-N network polymer by adding 400 μM of adenosine triphosphate (ATP) in PBS buffer solution (pH 7.4) at 25 °C. Excitation wavelength was 364 nm.

The author prepared the Stern–Volmer plots with guanosine derivatives as a quencher (Figure 5a). Based on the formation of a non-emissive complex model, the binding constants were calculated as shown in Figure 5b. The optical properties, quenching constants, and the binding constants of the POSS-N network polymers to the guanosine derivatives are listed in Table 1. All plots obtained from the titration of GDP and GTP were fitted on the line, and the binding constants can be determined. It was found that the POSS network polymers can enhance the binding affinity of the naphthyridine ligands with GTP approximately 10^4-times larger than that with GDP. It was confirmed that the naphthyridine ligand can selectively recognize GTP, and complex stability via hydrogen bonds between the naphthyridine ligand and GTP are significantly improved in PBS buffer solution by the strong hydrophobicity of POSS core inside the network polymers and by the interaction between the negative charge of phosphate groups of GTP and the ammonium groups at the surface of the POSS network polymers.
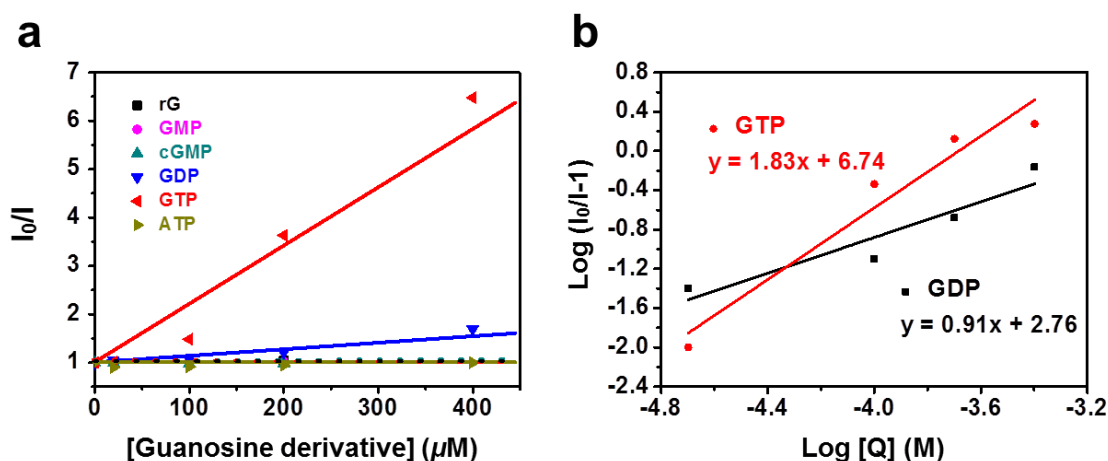
Figure 5. (a) Stern–Volmer plots with the solution containing 20 μM naphthyridine ligands in the POSS-N network polymers by adding various kinds of guanosine nucleotides. (B) The plots for determining the binding constants between the naphthyridine ligands in the POSS-N network polymers and guanosine nucleotides according to the above equation. The slopes represent the number of the binding guanosine nucleotides. The y-intercepts represent the logK_A values. The lines were prepared with the least-square method. R^2 is determination coefficient.

Table 1. Optical properties and the binding constants of the 1,8-naphthyridine moiety in the POSS network polymers[a]

Nucloetides[a]	Φ[b]	K_{SV} [x10^3 mol L^{-1}][c]	n[d]	K_A [M^{-1}][d]
None	0.35	n.d.[e]	n.d.[e]	n.d.[e]
rG	0.35	n.d.[e]	n.d.[e]	n.d.[e]
GMP	0.35	n.d.[e]	n.d.[e]	n.d.[e]
cGMP	0.34	n.d.[e]	n.d.[e]	n.d.[e]
GDP	0.29	1.33	0.91	5.8x10^2
GTP	0.22	12.05	1.83	5.5x10^6

[a]Procedures and conditions are described in the Experimental.

[b]400 μM solutions.

[c]Determined as an absolute value.

[d]Quenching constants were determined with the slopes of the fitting line in the Stern–Volmer plots.

[e]Calculated according to the reference 16.

[f]n.d. = not determined because of too weak interaction.

The photo-triggering reaction was observed by changing the emission of the naphthyridine ligands into the complex consisted of the POSS-Ru network polymers with GTP. The emission spectra were obtained from 10 μM of the naphthyridine ligands in the POSS-Ru network polymers with 100 μM of potassium ferricyanide ($K_3[Fe(CN)_6]$) by adding 200 μM of GTP in PBS buffer solution (pH 7.4) with the excitation light at 364 nm as shown in Figure 6a. The strong fluorescence emission of the POSS-Ru network polymers was observed around 424 nm. This result indicates that the Ru-complexes in the POSS network polymers should be less influenced on the emission property of the naphthyridine ligands. The addition of GTP caused the significant quenching of the emission from the naphthyridine ligands in the POSS-Ru network polymers. The emission of the naphthyridine ligands was quenched by 75 % after addition of 200 μM GTP. This result suggests that the naphthyridine ligands can capture GTP, and the POSS-Ru network/GTP complexes should be formed even after incorporation of the $Ru^{II}(bpy)_2Cl_2$ to the bipyridine moieties on POSS network polymers. Next, the author demonstrated the UV-triggered release of GTP from the complexes with the POSS-Ru network polymers by fluorescence imaging of the naphthyridine ligands in the POSS-Ru network polymers loaded with GTP. The irradiation of UV light with the 365 nm wavelength induced to change of the emission from the naphthyridine ligands in the complexes. The fluorescence emission of the naphthyridine ligands at 424 nm increased gradually corresponding with the increase of the UV irradiation time. Figure 6b simply shows the change of emission intensity observed from the naphthyridine ligands at 424 nm by different intervals of time. From this result, the author calculated the amount of the released GTP by changing emission intensity before and after UV irradiation. Importantly, GTP was released as 55 % from the complexes with the POSS-Ru network polymers after UV irradiation for 2 h. From this result, the author suggests that the UV irradiation at the complexes can be obtained with the decomposition of GTP by electron transferring between

the $Ru(bpy)_3^{3+}$ on the POSS network polymers and GTP, and then affinity of the 1,8-naphthyridine ligands to GTP was changed. Therefore, GTP was separated from the complexes and subsequently restored the emission intensity of the naphthyridine ligand on the POSS-Ru network polymers.
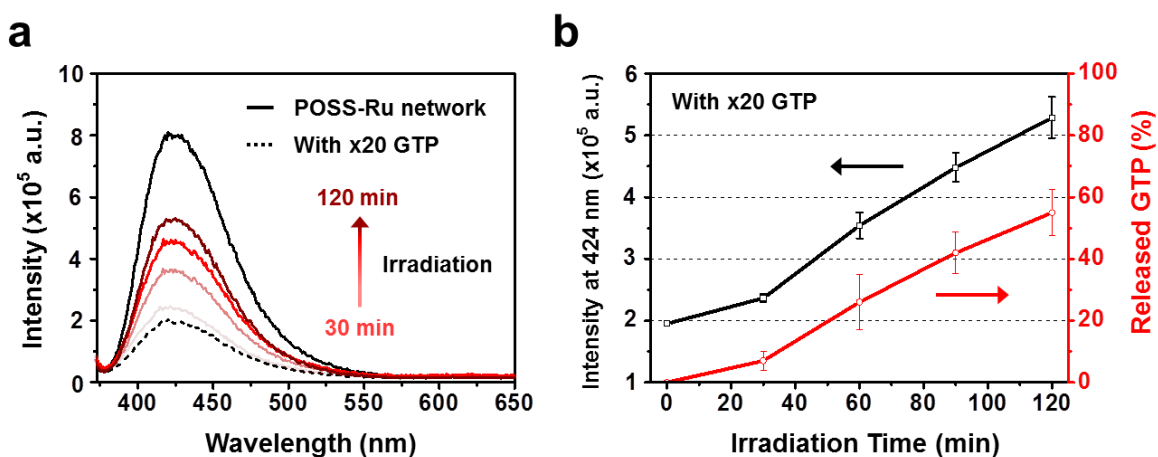
Figure 6. (a) Emission changes of 10 μM naphthyridine ligands in the POSS-Ru network polymers by adding 200 μM guanosine triphosphate (GTP) with 100 μM $K_3[Fe(CN)_6]$ in PBS buffer solution (pH 7.4) at 25 °C. Excitation wavelength was 364 nm. Photolysis was performed for 120 min at 25 °C with a 4 W UV-Lamp (365 nm). (b) Release profile in PBS buffer solution for the GTP in POSS-Ru/GTP complex under UV irradiation.

The electron transfer oxidation properties to the guanosine derivatives are examined by the photoinduced electron transfer reactions with one electron oxidants such as $Ru(bpy)_3^{2+}$ in the POSS-Ru network polymers in the presence of $Fe(CN)_6^{3-}$ in PBS buffer solution. Figure 7a shows the changes of absorbance obtained from the complexes of the POSS-Ru network polymers with GTP by UV irradiation. The peak of 250 nm clearly increased in the absorbance by the addition of 20 equivalent of GTP and continually enhanced with the increase of the UV irradiation time. These data indicate that the change of absorbance at 250 nm should be originated from the oxidized GTP after electron transfer reaction under UV exposure. Based on these results, the author estimated the amount of oxidized GTP from the

comparison of the absorbance between the POSS-Ru network/GTP complexes and the Ru^{II}(bpy)$_3$/GTP complexes by UV irradiation as shown in Figures 7b and 8.
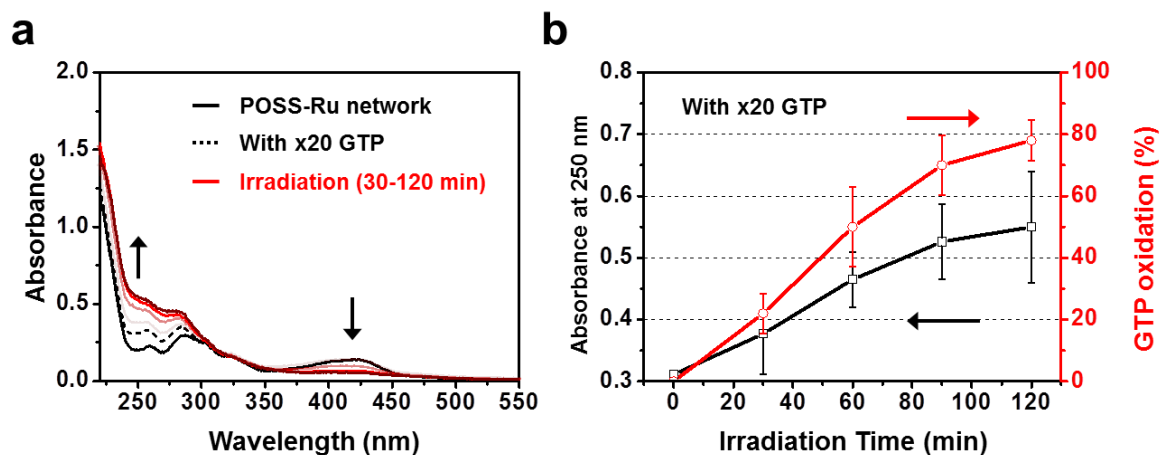
Figure 7. (a) UV-vis spectral changes of 10 μM naphthyridine ligands in the POSS-Ru network polymers by adding 200 μM guanosine triphosphate (GTP) with 100 μM K$_3$[Fe(CN)$_6$] in PBS buffer solution (pH 7.4) at 25 ^{o}C. Photolysis was performed for 120 min at 25 ^{o}C with a 4 W UV-Lamp (365 nm). (b) Oxidation ability of the POSS-Ru network polymers to GTP was determined from the intensity ratio of the Ru^{II}(bpy)$_3$/GTP to the POSS-Ru/GTP in UV-vis spectra at 250 nm.

The Ru^{II}(bpy)$_3$/GTP complexes were prepared by the mixing of 10 μM Ru^{II}(bpy)$_3\cdot$6H$_2$O and 200 μM GTP in PBS buffer solution (pH 7.4) containing 100 μM K$_3$[Fe(CN)$_6$] (Figure 8). First, the author examined the influence of Ru^{II}(bpy)$_3$ on the absorbance of GTP under UV irradiation. As shown in Figure 8b, the absorption peak at 250 nm was enhanced by adding GTP. The peak was highly improved by UV irradiation for 2 h. This result indicates that the GTP can be oxidized by electron transfer reaction in the PBS buffer solution containing Ru^{II}(bpy)$_3$ with K$_3$[Fe(CN)$_6$] and subsequently show the change in absorbance of GTP. For the evaluation of the amount of the oxidized GTP, the author determined the consumption rate of the Ru^{II}(bpy)$_3$/GTP complex by HPLC with increasing gradient of water in acetonitrile (CH$_3$CN/H$_2$O from 19:1 to 0:100) before and after of UV exposure. Before the measurement

of HPLC, the complex solution was mixed with the thymidine as a standard. The intensity ratio (I_G/I_T value) gradually decreased corresponding with the increase of the irradiation time. This result indicates that the structure of GTP was changed by oxidation, and then the peak position in the HPLC profiles should be changed. From this result, the author evaluated the amount of the oxidized GTP by the complexes of POSS-Ru network polymers.
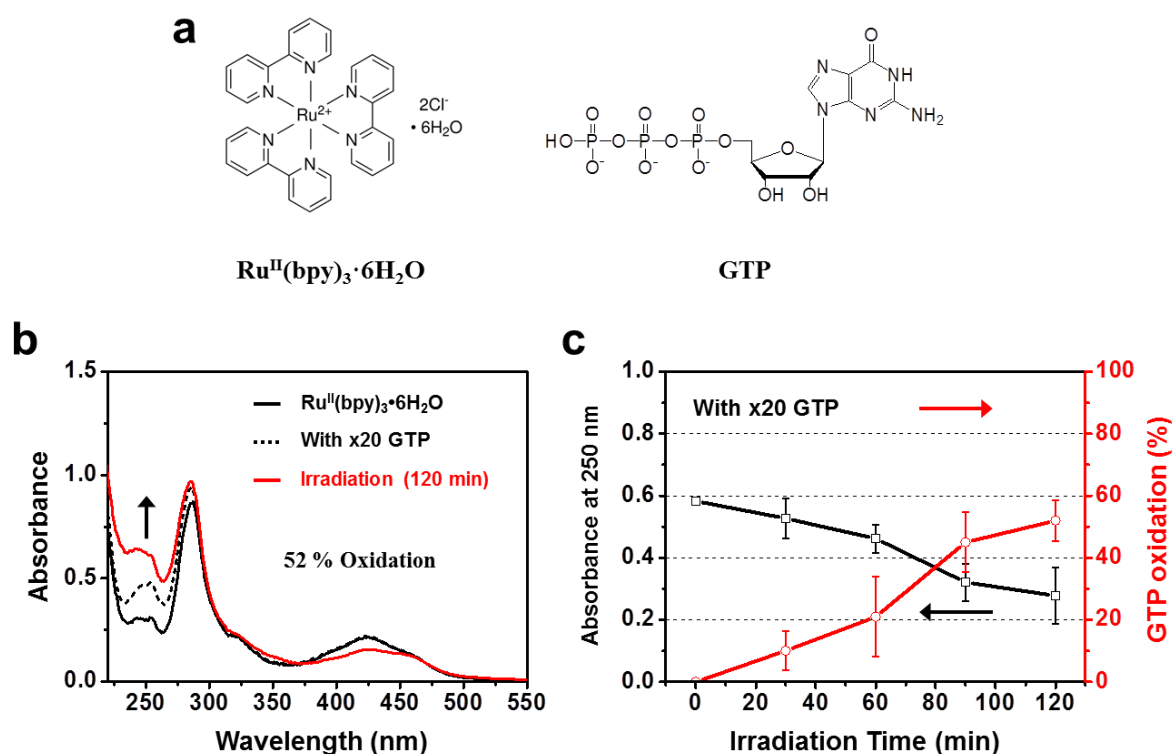
Figure 8. (a) Chemical structures of $Ru^{II}(bpy)_3$ and GTP used in this study for the comparison to evaluate the oxidation degree of GTP by the POSS-Ru network polymers. (b) UV–vis spectra of 10 μM $Ru^{II}(bpy)_3 \cdot 6H_2O$ by adding 200 μM GTP with 100 μM $K_3[Fe(CN)_6]$ in PBS buffer solution (pH 7.4) at 25 °C. Photolysis was performed for 120 min at 25 °C with a 4 W UV-Lamp (365 nm). (C) Oxidation ability of $Ru^{II}(bpy)_3$ to GTP was evaluated from the results of gradient HPLC measurement (CH_3CN/H_2O form 19:1 to 0:100) (I_G; intensity of GTP, I_T; intensity of thymidine, total concentration of GTP and thymidine was fixed).

It was found that 55% of GTP in the mixture with $Ru^{II}(bpy)_3$ was oxidized by UV irradiation for 2 h. Using these results, the author evaluated approximately the amount of

oxidized GTP in the complexes with the POSS-Ru network polymers as shown in Figure 7b. The amount of oxidized GTP gradually increased corresponding with the increase of the irradiation time, and finally 78 % of the GTP was oxidized after irradiation for 2 h. This result clearly indicates that the Ru-complexes on the network polymers can well oxidize GTP due to the efficient electron transferring. Because the interaction between the terminal ammonium groups in the network polymers and the phosphate groups improved local concentration of GTP inside the network polymers, GTP could be efficiently oxidized by the POSS-Ru network polymers. In addition, the author examined the oxidation ability of the POSS-Ru network polymers to different nucleobases such as rG, GMP, cGMP, and GDP as shown in Figure 9. In contrast, the degradation can slightly proceed. These results also supported that the Ru-complexes can selectively oxidize GTP with the POSS-Ru network polymers due to the high local concentration of GTP around the network polymers.
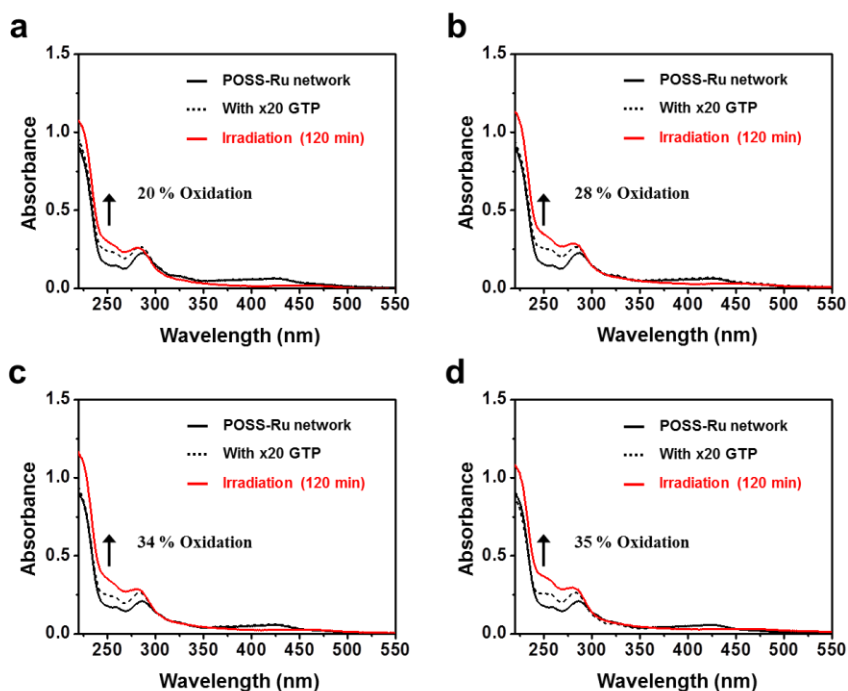
Figure 9. UV–vis spectral changes of 10 μM naphthyridine ligands in the POSS-Ru network polymers by adding 200 μM of (a) rG , (b) GMP, (c) cGMP, and (d) GDP with 100 μM K$_3$[Fe(CN)$_6$] in PBS buffer solution (pH 7.4) at 25 ^{o}C. Photolysis was performed for 120 min at 25 ^{o}C with a 4 W UV-Lamp (365 nm).

Conclusion

The author has demonstrated the guanosine triphosphate (GTP)-selective oxidation using the network polymers composed of POSS. The water-soluble POSS network polymers containing the naphthyridine ligands to capture GTP inside the networks and ruthenium complexes to oxidize the captured GTP under light irradiation were successfully synthesized. Initially, the naphthyridine-modified POSS network polymers show highly selective binding to GTP in the series of the guanosine derivatives. Accordingly, the complex with GTP showed the significant binding affinity ($K_a = 5.5 \times 10^6$ M^{-1}) with the naphthyridine ligands into network polymers. Next, the photo-catalytic activity of the complexes with GTP and the ruthenium complex-modified POSS network polymers were investigated. Consequently, it was revealed that the modified network polymers can decompose GTP efficiently under the light irradiation. This is the first example, to the best of the author's knowledge, to offer not only the GTP-selective host polymers with high affinity but also the light-driven artificial enzymes for GTP oxidation.

References

1. Strack, G.; Bocharova, V.; A. Arugula, M.; Pita, Marcos.; Halámek, J.; Katz, E. *J. Phys. Chem. Lett.* **2010**, *1*, 839.

2. Ho, M. Y. K.; Rechnitz, G. A. *Anal. Chem.* **1987**, *59*, 536.

3. Yu, T.; Wang, W.; Chen, J.; Zeng, Y.; Li, Y.; Yang, G.; Li, Yi. *J. Phys. Chem. C* **2012**, *116*, 10516.

4. Orozco, J.; García-Gradilla, V.; D'Agostino, M.; Gao, W.; Cortés, A.; Wang, J. *ACS Nano*

2013, *7*, 818.

5. Gharibi, H.; Moosavi-Movahedi, Z.; Javadian, S.; Nazari, K.; A. Moosavi-Movahedi, A. *J. Phys. Chem. B* **2011**, *115*, 4671.

6. E. Evans, S.; Grigoryan, A.; A. Szalai, V. *Inorg. Chem.* **2007**, *46*, 8349.

7. Chakrabarti, M. H.; Roberts, E. L. *J. Chem. Soc. Pak.* **2008**, *30*, 817.

8. Langmaier, J.; Saměc, Z.; Samcová, E.; Hobza, P.; Řeha, D. *J. Phys. Chem. B* **2004**, *108*, 15896.

9. D. A. Stemp, E.; K. Barton, J. *Inorg. Chem.* **2000**, *39*, 3868.

10. R. Holcomb, D.; A. Ropp, P.; C. Theil, E.; Thorp, H. H. *Inorg. Chem.* **2010**, *49*, 786.

11. E. Evans, S.; Grigoryan, A.; A. Szalai, V. *Inorg. Chem.* **2006**, *45*, 3124.

12. Stemp, E. D. A.; Arkin, M. R.; Barton, J. K. *J. Am. Chem. Soc.* **1997**, *119*, 2921.

13. Fukuzumi, S.; Miyao, H.; Ohkubo, K.; Suenobu, T. *J. Phys. Chem. A* **2005**, *109*, 3285.

14. Westover, K. D.; Bushnell, D. A.; Kornberg, R. D. *Cell* **2004**, *119*, 481.

15. Tanaka, K.; Murakami, M.; Jeon, J-H.; Chujo, Y. *Org. Biomol.Chem.* **2012**, *10*, 90.

16. Newkome, R. G.; Garbis, J. S.; Majestic, K. V.; Fronczek, R. F.; Chiari, G. *J. Org. Chem.* **1981**, *46*, 833.

Chapter 8

Synthesis of Water-Soluble POSS Network Polymers and Its Application for Selective Complex Formation between the Designed Ligands and a Nucleobase

Chapter 8

Synthesis of Water-Soluble POSS Network Polymers and Its Application for Selective Complex Formation between the Designed Ligands and a Nucleobase

Abstract: The recognition systems for ATP, TTP, and CTP are demonstrated based on the water-soluble polyhedral oligomeric silsesquioxane (POSS) network polymers. The series of ligands were designed and conjugated into the POSS-based network polymers. From the titration experiments, the selective recognition of each triphosphate can be observed. Accordingly, POSS network polymer/nucleoside triphosphate interactions showed the significant values (K_a = POSS-G network/CTP, 3.5×10^8 M^{-1}; POSS-U network/ATP, 1.6×10^3 M^{-1}; POSS-A network/UTP, 1.9×10^{-7}, respectively). With other nucleoside including diphosphates and monophosphates, the complexation was hardly detected. These results indicate that the complex formation with nucleoside triphosphate should occur inside POSS network polymers. Next, the binding selectivity and affinity of the ligands in the POSS network polymers for each target base were examined. Consequently, it was revealed that the POSS network polymers can effectively capture only the target base molecules based on their hydrogen bonding motifs.
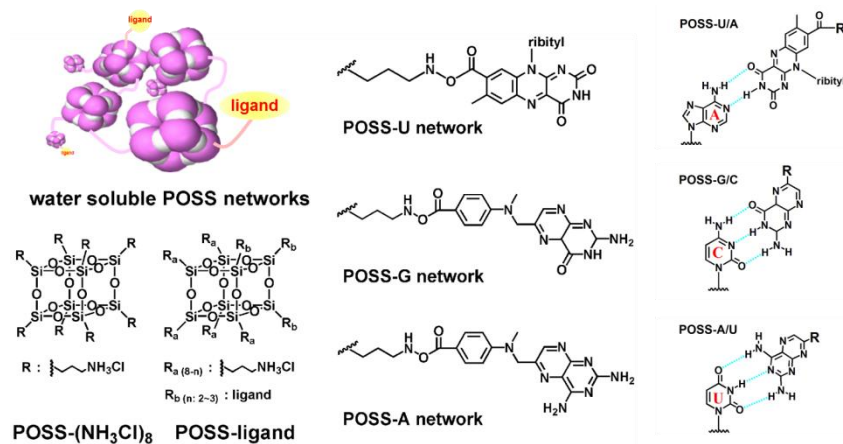
Introduction

Triphosphates play crucial roles in a wide variety of biological events such as RNA synthesis, signal transduction, metabolism, and enzymatic reactions.[1–5] Therefore, the regulation of local concentrations of triphosphates is applicable for developing biosensors, drugs, and biotechnological tools. For example, in the active tumor region, the production of the nucleic acids is relatively-vigorous comparing to the normal organs. Therefore, if the concentration of the triphosphate can be reduced, the activity of the tumor should be suppressed. This strategy can be also applied for the inhibition of the virus replications. In the HIV-infected cells, the production of RNA is active to construct the virus. To prohibit the RNA production, the addition of the artificial nucleobase such as azidothymidine is conventionally used as the anti-virus drugs.[6–9] However, these drugs can critically influence on the native metabolism in the normal cells, leading to the heavy side reactions. As one of solves to overcome dilemma, novel strategy should be required.

Recently, the author found the selective encapsulation of GTP into the polyhedral oligomeric silsesquioxane (POSS)-based polymers via the complex formation with the naphthyridine derivatives.[10] At the surface of the hydrophobic POSS core inside network polymers, the complex stability via hydrogen bonds between the guanine moiety of GTP and the naphthyridine derivative was significantly enhanced. In addition, the negatively-charged compounds such as nucleotide triphosphates made a strong interaction with the ammonium groups inside the polymers. As a result only GTP can form the stable complex via hydrogen bonds with the naphthyridine derivative inside the POSS-based network polymers. Finally, the author established the selective encapsulation of GTP. Furthermore, the light-driven artificial enzyme for GTP oxidation can be developed. These results suggest the possibility that the site- and time-specific control of GTP can be obtained. However, these systems were applicable only for the discrimination of guanosine nucleotides. To extend the feasibility, the

recognition of other nucleobases should be needed.

Herein, the recognition systems for ATP, TTP, and CTP are demonstrated. The series of ligands were designed and introduced into the POSS-based network polymers. From the titration experiments, the selective recognition of each triphosphate can be observed. The selectivity by changing the number of the phosphate unit and the base moiety was evaluated with each nucleoside and nucleotide.

Experimental Section

General. ^{1}H NMR and ^{13}C NMR spectra were measured with a JEOL EX-400 (400 MHz for ^{1}H and 100 MHz for ^{13}C). ^{29}Si NMR spectra were measured with a JEOL JNM-A400 (80 MHz) spectrometer. Coupling constants (J value) are reported in Hertz. The chemical shifts are expressed in ppm downfield from tetramethylsilane, using residual chloroform ($\delta = 7.24$ in ^{1}H NMR, $\delta = 77.0$ in ^{13}C NMR) or residual DMSO ($\delta = 2.49$ in ^{1}H NMR, $\delta = 39.5$ in ^{13}C NMR) as an internal standard. Masses were determined with a MALDI-TOF mass spectroscopy (acceleration voltage 21 kV, negative mode) with 2,5-dihydroxybenzoic acid (DHB) as a matrix.   Emission from the samples was monitored using a Perkin Elmer LS50B at 25 °C using 1 cm path length cell. MASS spectra were obtained on a JEOL JMS-SX102A.

Synthesis of the 8-carboxyriboflavin, U. U-ligand was synthesized according to the previous report.[11] The characterization was executed according to B. McCormick *et al*. The typical protocol for the modification of riboflavin is described here:

The compound U1. To the suspension containing 2.5 g of riboflavin in 200 mL of glacial acetic acid-acetic anhydride (1:1), 0.5 mL of 70% perchloric acid was added dropwise. After stirring for 30 minutes at 40 °C, the reaction mixture was cooled in an ice bath and diluted

with an equal volume of cold water. The diluted solution was extracted twice with 200 mL of chloroform, and the combined organic layer was washed twice with 100 mL of water and dried over anhydrous sodium sulfate. After the filtration, the volatile was removed under reduced pressure at 50 °C to yield 3.5 g (95%) of the **U-1** with a melting point of 250–252 °C.

The compound U2. The mixture containing tetraacetylriboflavin (**U-1**) (3.5 g) and 2.5 mL of bromine in 25 mL of warm dioxane and 2.5 mL of pyridine was refluxed for 2 h and evaporated. A small aliquot of this crude mixture stirred into acetone and diethyl ether gave a reddish-brown precipitate which by analysis contained 31.60% bromine and was in reasonable agreement for a 1:1 molecular complex of tetraacetyldibromoriboflavin with dibromopyridine which would contain 30.88% bromine. The entire mixture was then stirred into 250 mL of chloroform and shaken briefly with an equal volume of 0.5 N hydrochloric acid. Then, the organic phase was washed twice with 250 mL portions of water. The chloroform solution was dried over anhydrous sodium sulfate, and the volume was reduced to about 10 mL by evaporation under reduced pressure. The concentrated solution provided the product as a precipitate by stirring into 100 mL of ether. The precipitate was collected by filtration, resuspended in 5 mL of methanol and 45 mL of ether, again collected by filtration, rinsed with ether, and dried to give 2.5 g (50%) of the tetraacetyldibromoriboflavin (**U-2**).

The compound U3. Tetraacetyldibromoriboflavin (**U-2**) (2.5 g) was dissolved in 50 mL of warm 6 N hydrochloric acid, and the mixture was refluxed for 1 h. The solution was evaporated to near dryness, stirred with 10 mL of water and allowed to stand at room temperature overnight. The precipitate was collected by filtration, rinsed with methanol and ether, ground up in 25 mL of warm chloroform, again collected by filtration and rinsed with methanol and ether, and dried to give 1.2 g (90%) of the formylriboflavin (**U-3**).

The compound U. The formylriboflavin (**U-3**) was readily oxidized to the carboxylic acid derivative by several conventional methods including dilute aqueous potassium permanganate or even periodic acid. This latter reagent must be carefully limited to avoid oxidative cleavage of the D-ribityl side chain. For this periodic acid procedure, 225 mg of periodic acid in 1 mL of water was added dropwise to a cold saturated solution containing 40 mg of formylriboflavin. With stirring, the carboxyflavin (**U**) precipitated from solution and was collected by filtration, rinsed with a small quantity of cold water, and dried to give 25 mg (60%).

Synthesis of the 4-[[(2-amino-3,4-dihydro-4-oxo-6-pteridinyl)methyl]methylamino]-benzoic acid, G. A stirred mixture of 4-[[(2,4-diamino-6-pteridinyl)methyl]methylamino]-benzoic acid (**A**) (6.60 g, 16.8 mmol) and 0.2 N NaOH (1.2 L) was refluxed under N_2 gas for 1.5 h. The cooled and filtered (Norit, Celite) solution was treated with 3 N HCl to lower the pH to 3.5, and the yellow precipitate was collected by centrifugation, suspended in H_2O (1 L), and redissolved by adding the required amount of 1 N NaOH. The precipitation process described above was repeated, and the compound **G** was first collected by centrifugation, then suspended in H_2O and collected by filtration (70%). Spectral data (^{1}H NMR and UV) agreed with reported results.[12] ^{1}H NMR (CDCl$_3$) δ 8.57 (d, 1H, J=0.7 Hz), 8.56 (d, 1H, J=0.7 Hz), 8.21 (s, 1H), 8.18 (d, 1H, J=0.7 Hz), 7.17 (ddd, 1H, J=0.7, 1.6, 5.1 Hz), 7.14 (dd, 1H, J=1.8, 5.1 Hz), 2.72 (t, 2H, J=7.7 Hz), 2.45 (s, 3H), 2.36 (t, 2H, J=7.3 Hz), 1.77–1.67 (m, 4H), 1.46–1.40 (m, 2H). ^{13}C NMR (CDCl$_3$) δ 177.7, 155.5, 152.8, 148.7, 148.6, 148.5, 124.7, 124.0, 122.6, 121.8, 35.1, 34.0, 29.7, 28.5, 24.5, 21.1. FABMS (NBA/CHCl$_3$) m/z 285 [(M+H)$^+$], HRMS (NBA) [(M+H)$^+$] calcd. 285.1603, found 285.1612.

Octaammonium-POSS, POSS-(NH$_3$)$_8$. (3-Aminopropyl)triethoxysilane (100 mL, 0.427 mol)

and conc. HCl (35–37 %, 135 mL) in methanol (800 mL) produced title compound as a white precipitate after 5 days at room temperature. The product was obtained after filtration, washed with cold methanol, and dried. The title compound was spectroscopically pure in 33% yield (18.8 g). ^{1}H NMR (DMSO-d_6) δ 8.23 (s, 24H), 2.76 (t, 16H), 1.71 (m, 16H), 0.72 (t, 16H). ^{13}C NMR (DMSO-d_6) δ 40.53, 20.13, and 7.96. ^{29}Si NMR (DMSO-d_6) δ −66.4 (s). MALDI-TOF [(M+H)$^{+}$] calcd. 880.41, found 879.42.

POSS-G ligands. In a 100-mL round-bottom flask, 0.14 g of the compound **G** (0.44 mmol), 0.06 mL of triethylamine (0.44 mmol) and 0.15 g of 4-(4,6-dimethoxy-1,3,5-triazin-2-yl)-4-methylmorpholinium chloride (DMT-MM, 90%) (0.6 mmol) were stirred in 50 mL of dry methanol until the solid had completely dissolved. To the mixture solution, 1.0 g of POSS-(NH$_3$)$_8$ (0.87 mmol) was added. The mixture was stirred at room temperature under argon. After stirring for 24 h, the resulting mixture was evaporated to 10 mL and poured into acetonitrile containing 0.1% HCl. The precipitate was washed with acetonitrile. The title compound was obtained to yield (79%) a yellow powder after drying *in vacuo*.

POSS-U ligands and POSS-A ligands. POSS-U and POSS-A ligands were prepared with the same procedures as described above. [POSS-U ligands, dark brown color]: The compound **U** (0.18 g, 0.44 mmol), POSS-(NH$_3$)$_8$ (1 g, 0.87 mmol), triethylamine (0.06 mL, 0.44 mmol), and DMT-MM (0.15 g, 0.6 mmol). [POSS-A ligands, yellow color]: The compound **A** (0.15 g, 0.44 mmol), POSS-(NH$_3$)$_8$ (1 g, 0.87 mmol), triethylamine (0.06 mL, 0.44 mmol), and DMT-MM (0.15 g, 0.6 mmol).

POSS network polymers containing the designed ligands. The typical protocol for the polymerization reaction is described here. To a solution of POSS-(NH$_3$)$_8$ (5 g, 4.4 mmol) and

POSS ligands (POSS-G, POSS-U, and POSS-A) (0.87 mmol) in 20 mL of dry methanol, the premixed solutions containing 0.99 g of oxalic acid (11 mmol), 3.1 mL of triethylamine (22 mmol), 6.6 g of DMT-MM (27.5 mmol) in dry methanol (50 mL) were added, and the reaction mixture was stirred at room temperature. After stirring for 24 h, the resulting mixture was poured into acetonitrile containing 0.1% HCl, and the precipitate was washed with acetonitrile. The crude product was dissolved in water and filtrated, and the solvent was removed by rotary evaporator. The water-soluble POSS network polymers were obtained (POSS-G network polymers, 57%, bright yellow color; POSS-U network polymers, 61%, dark brown color; POSS-A network polymers, 59%, yellow color) after drying in *vacuo*.

Complexation with the POSS network polymers containing the designed ligands. General procedure for the complexation of the designed ligand-modified POSS network polymers and the various kinds of the nucleotides are described here. The stock solutions of the POSS network polymers ($\times 10$) and the nucleotides ($\times 10$) were mixed at room temperature, and then the 500 μL of the samples were prepared by adding the PBS buffer (pH 7.4) solution.

Fluorescence measurements of the complexes. The fluorescence emissions of 20 μM designed ligands in the POSS network polymers in the absence and presence of the nucleotides under excitation (POSS-G network: λ_{ex} 367 nm, POSS-U network: λ_{ex} 445 nm, POSS-A network: λ_{ex} 373 nm) were monitored using a Perkin Elmer LS50B at 25 °C using 1 cm path length cell. The excitation bandwidth was 1 nm. The emission bandwidth was 1 nm. The quantum yields were determined as an absolute value with an integral sphere.

Stern-Volmer plots. The data were analyzed in terms of the Stern-Volmer equation:

$$\frac{I_0}{I} = 1 + K_{SV}\,[Q]$$

The emission intensities were plotted according to a Stern-Volmer equation, reporting I_0/I versus the concentrations of the nucleotides $[Q]$, where I_0 is the intensity in the absence of quencher and I is the intensity in the presence of a quencher concentration. K_{SV} is the Stern-Volmer quenching constant. A plot of I_0/I versus $[Q]$ yields an intercept of one and a slope equals to K_{SV}.

Binding constants calculation. If the non-emissive complex formation between the designed ligands and nucleobases occurs, the binding constant (K_A) can be calculated with the number of the binding molecules (n) from the following equation:

$$\log\frac{I_0\text{-}I}{I} = \log K_A + n\log[Q]$$

From the plots, the K_A values of the designed ligands in the POSS network polymers to nucleoside diphosphate and nucleoside triphosphate were calculated.
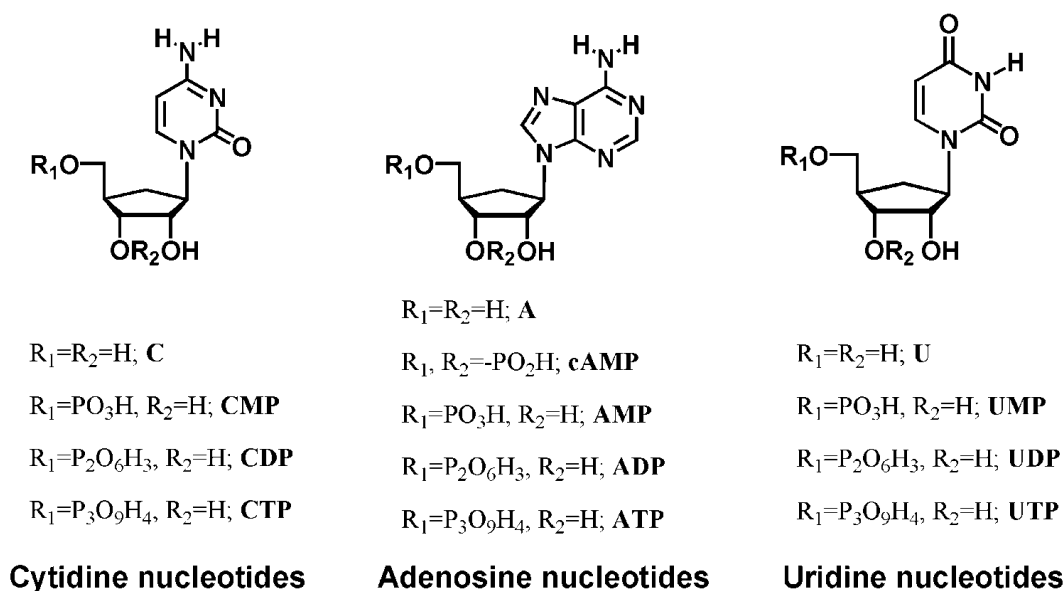
Results and Discussion

The author designed new fluorescent ligands such as POSS-U, POSS-G, and POSS-A network polymers as shown in Figure 1. From the previous reports[1], the author expected that strong hydrophobicity around the POSS cores inside the network polymers can enhance the affinity between the designed ligands and the target base molecules. In addition, the ammonium groups in the network polymers can significantly improve the selectivity for the nucleoside triphosphates (NTPs) by the electrostatic interaction with the negatively charged phosphate groups of the nucleotides. To exploit the possible use of the ligand-modified POSS network polymers as a new class of fluorescent sensor for detection of the target base molecules, the author examined the binding of non-fluorescent nucleotides to the ligand-
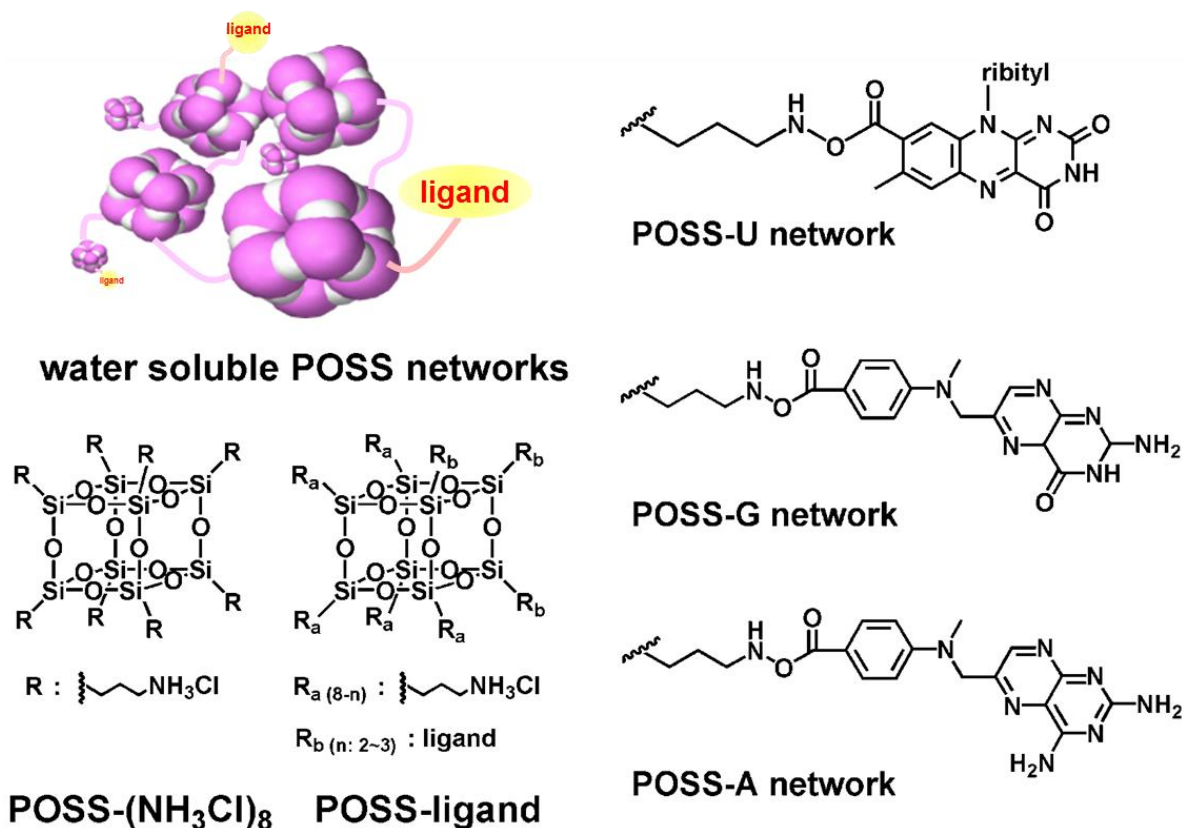
Figure 1. Chemical structures of various kinds of the POSS network polymers containing the base-selective fluorescent ligands used in this study.
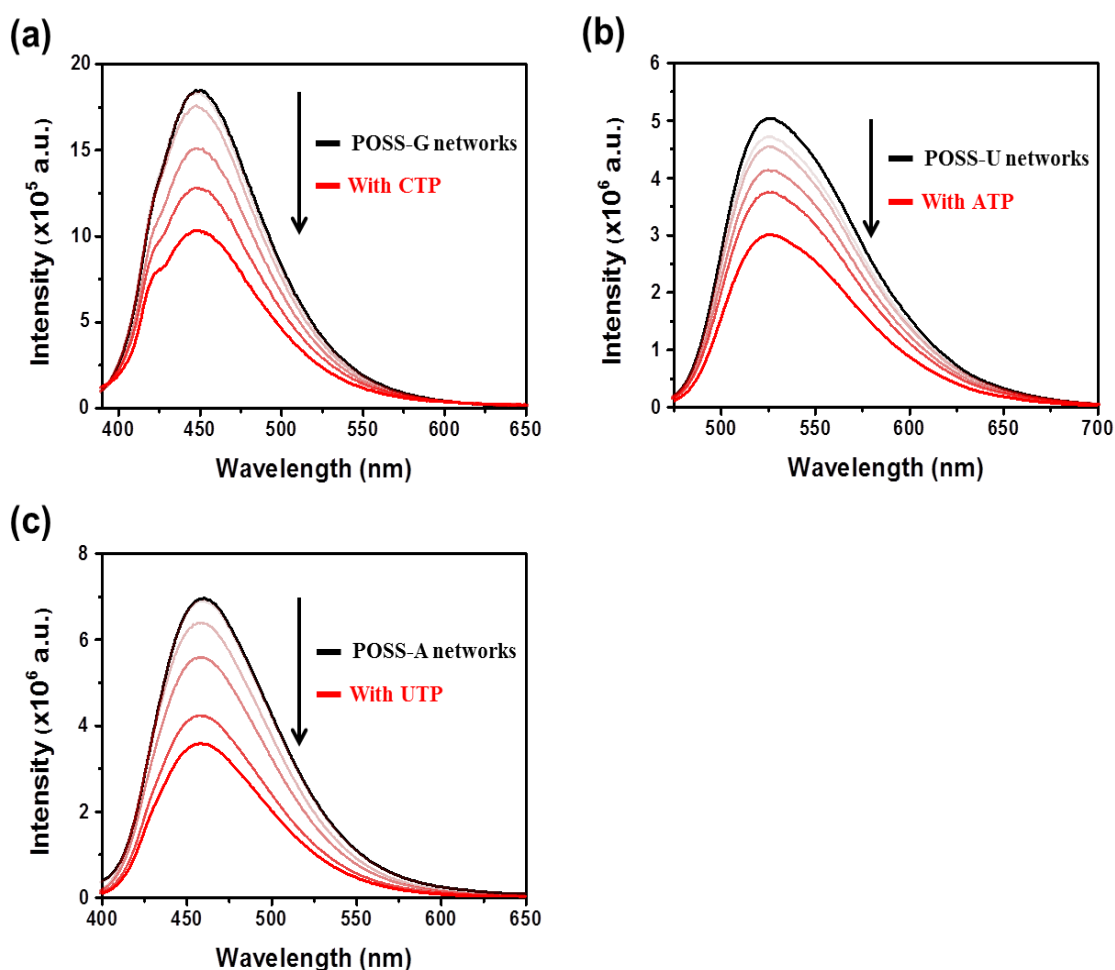
modified POSS network polymers (Figure 2). The water-soluble POSS network polymers containing a series of base-selective fluorescent ligands can bind to a specific base, resulting in the fluorescence quenching.

$R_1=R_2=H$; **C**
$R_1=PO_3H$, $R_2=H$; **CMP**
$R_1=P_2O_6H_3$, $R_2=H$; **CDP**
$R_1=P_3O_9H_4$, $R_2=H$; **CTP**

Cytidine nucleotides

$R_1=R_2=H$; **A**
R_1, $R_2=$-PO_2H; **cAMP**
$R_1=PO_3H$, $R_2=H$; **AMP**
$R_1=P_2O_6H_3$, $R_2=H$; **ADP**
$R_1=P_3O_9H_4$, $R_2=H$; **ATP**

Adenosine nucleotides

$R_1=R_2=H$; **U**
$R_1=PO_3H$, $R_2=H$; **UMP**
$R_1=P_2O_6H_3$, $R_2=H$; **UDP**
$R_1=P_3O_9H_4$, $R_2=H$; **UTP**

Uridine nucleotides

Figure 2. Chemical structures of the target base molecules used in this study.

Initially, the author investigated the binding behaviors of the base-selective fluorescent ligands in the POSS network polymers to NTPs by fluorescence titration experiments as shown in Figure 3. Cytosine-selective POSS-G network polymers, adenine-selective POSS-U network polymers, and uracil-selective POSS-A network polymers were used as fluorescent reporter molecules for the detection of the binding of cytidine triphosphate (CTP), adenosine triphosphate (ATP), and uridine triphosphate (UTP), respectively. The fluorescence emissions of the ligand-modified POSS network polymers were quenched by adding NTPs. Moreover, the fluorescence intensities of the ligand-modified POSS network polymers were depended
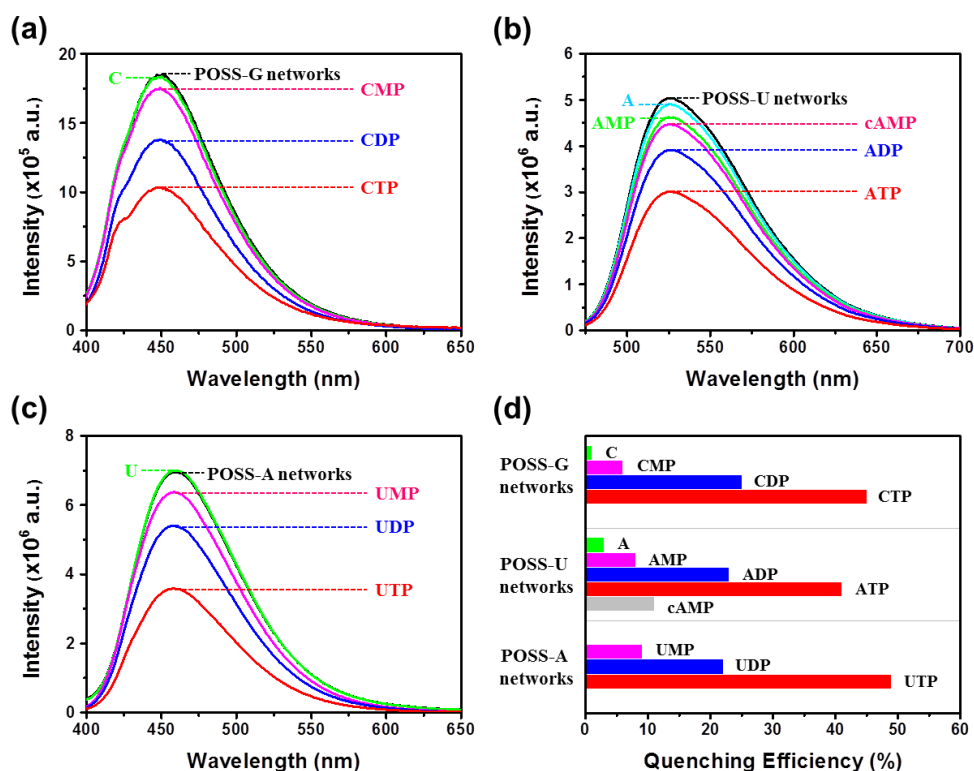
Figure 3. Fluorescence spectra of the ligand-modified POSS network polymers in the absence and presence of NTPs in PBS buffer solution (pH 7.4). (a) POSS-G network polymers (20 μM of G-ligand) upon addition of CTP (0-200 μM); λ_{ex} = 367 nm. (b) POSS-U network polymers (20 μM of U-ligand) upon addition of ATP (0-200 μM); λ_{ex} = 445 nm. POSS-A network polymers (20 μM of A-ligand) upon addition of UTP (0-200 μM); λ_{ex} = 373 nm.

on the concentrations of NTPs such as CTP, ATP, and UTP. Figure 3 shows the changes of fluorescence emissions from the ligand-modified POSS network polymers by adding NTPs. The emission spectra were obtained from PBS buffer solution (pH 7.4) containing 20 μM base-selective fluorescent ligands in the POSS network polymers and various concentrations

of each NTPs (0 to 200 μM) with the excitation light at 367 nm (CTP), 445 nm (ATP), and 373 nm (UTP), respectively. Black lines show the fluorescence spectra of the ligand-modified POSS network polymers in the absence of NTPs. By the addition of NTPs, fluorescence emissions were remarkably quenched (red color line, quenching efficiencies: 45%, 41%, and 49% for POSS-G network, POSS-U network, and POSS-A network polymers at base-selective fluorescent ligand/NTP concentrations of 20 μM/200 μM, respectively).

To study the selectivity of the ligand-modified POSS network polymers, the author chose a variety of nucleotides such as nucleoside (C, A, and U), nucleoside monophosphate (CMP, AMP, and UMP), cyclic nucleoside monophosphate (cAMP), and nucleoside diphosphate (CDP, ADP, and UDP) (Figure 4). As shown in Figure 4a, the POSS-G network polymers exhibited the decreases of the fluorescence intensity corresponded to the complexation with the target cytosine base. The quenching efficiency was in the order of C < CMP < CDP < CTP. By the complexation with the target nucleobases, the fluorescence alterations of POSS-U and POSS-A network polymers showed higher quenching efficiencies with NTPs with the similar behaviors to the POSS-G polymers (POSS-U network polymers: A < AMP < cAMP < ADP < ATP, POSS-A network polymers: U < UMP < UDP < UTP, Figure 4b-d). From these data, highly selective detection of NTPs (CTP, ATP, and UTP) over other nucleoside can be achieved by using the water-soluble POSS network polymers. The fluorescence quenching efficiencies of the ligand-modified POSS network polymers depended on the number of the phosphate groups in the nucleotides. The negatively-charged triphosphates should made a strong interaction with the ammonium groups in the POSS network polymers. Thereby, the ligand-modified POSS network polymers can effectively capture NTPs.

Figure 4. Fluorescence spectra of 20 μM base-selective fluorescent ligands in the POSS network polymers in the absence and presence of different flanking nucleotides (200 μM) in PBS buffer solutions (pH 7.4) and (d) their quenching efficiencies. (a) POSS-G network/cytidine nucleotides, (b) POSS-U network/adenosine nucleotides, (c) POSS-A network/uridine nucleotides.

The author prepared the Stern–Volmer plots with the nucleotides as a quencher. Based on the formation of a non-emissive complex model, the binding constants were calculated as shown in Figure 5. The optical properties, quenching constants, and the binding constants of the designed ligands in the POSS network polymers to the variety of nucleotides are listed in Table 1. All plots obtained from the titration of NDPs and NTPs were fitted on the line, and the binding constants can be determined. The interaction of the base-selective fluorescent ligands in the POSS network polymers with nucleosides and nucleoside monophosphates were very weak, and the binding constants at the concentration range examined in this study

were not obtained. Accordingly, the binding constant for the POSS-G network/CTP complex is 3.49×10^8 M^{-1} and about 2550-times higher than that with the POSS-G network/CDP complex. Furthermore, the binding of the POSS-U network/ATP and POSS-A network/UTP complexes showed higher values than those of the POSS-U network/ADP and POSS-A network/UDP interactions, respectively. These data indicate that the water-soluble POSS network polymers can enhance the binding affinity of the base-selective fluorescent ligands to the target base molecules as NTPs. The complex formation with NTPs should occur inside the POSS network polymers by electrostatic interaction between the ammonium groups of the POSS network polymer and triphosphate, and hydrogen bonding could be enhanced by strong hydrophobicity of the POSS core as described in the previous chapters.

Table 1. Optical properties and the binding constants of the designed ligands in the POSS network polymers[a]

Ligands[b]	Nucleotides[c]	K_{SV} [x10^3 mol L^{-1}][e]	n[f]	K_A [M^{-1}][f]
POSS-G network	C	n.d.[g]	n.d.[g]	n.d.[g]
	CMP	n.d.[g]	n.d.[g]	n.d.[g]
	CDP	1.51	1.52	1.37x10^5
	CTP	3.18	2.31	3.49x10^8
POSS-U network	A	n.d.[g]	n.d.[g]	n.d.[g]
	cAMP	n.d.[g]	n.d.[g]	n.d.[g]
	AMP	n.d.[g]	n.d.[g]	n.d.[g]
	ADP	1.61	0.78	1.94x10^2
	ATP	2.97	0.95	1.63x10^3
POSS-A network	U	n.d.[g]	n.d.[g]	n.d.[g]
	UMP	n.d.[g]	n.d.[g]	n.d.[g]
	UDP	1.28	1.48	8.80x10^4
	UTP	3.81	1.94	1.54x10^7

[a]Procedures and conditions are described in the Experimental.

[b]20 μM solutions.

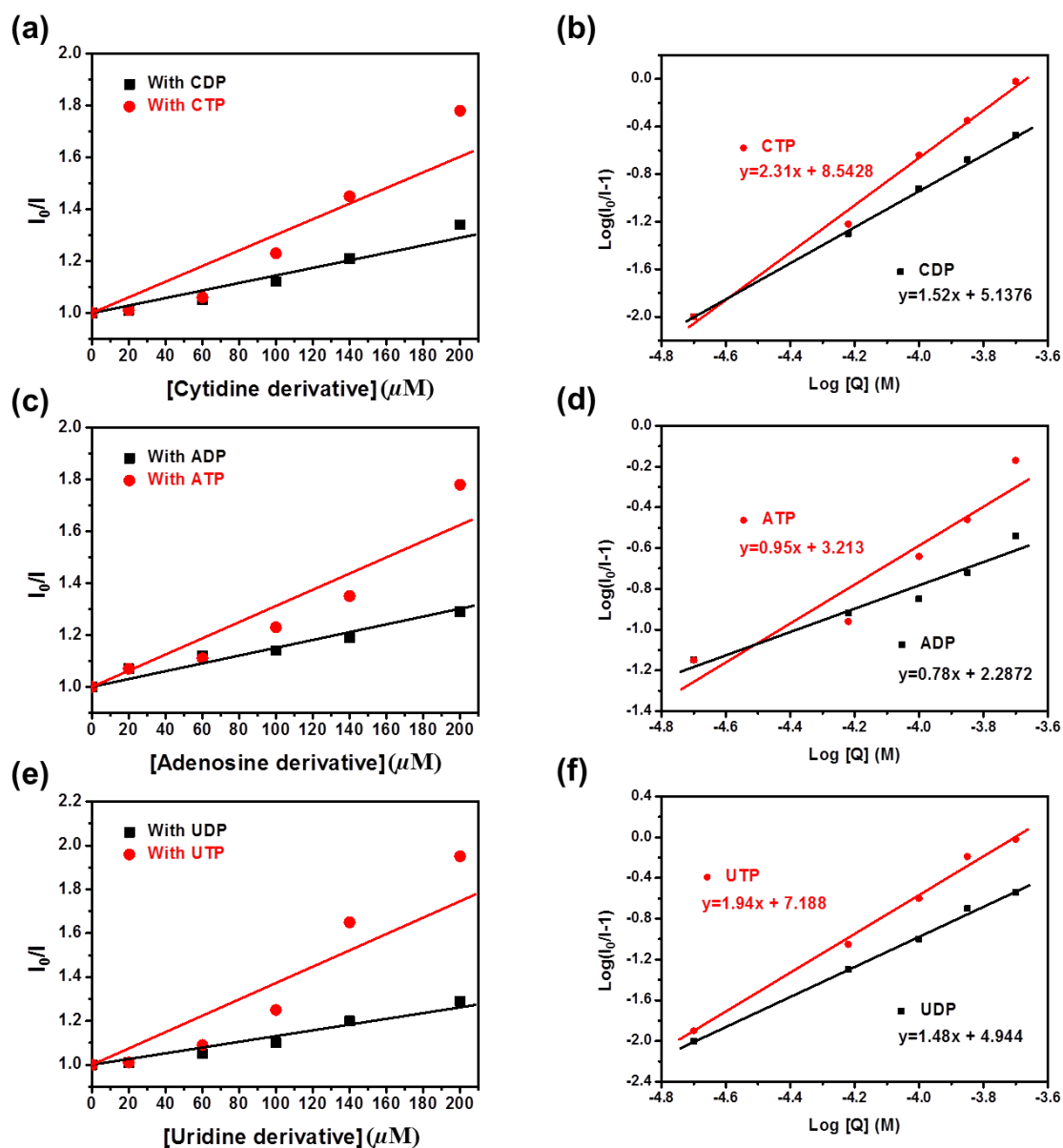[c]200 μM solutions.

[d]Determined as an absolute value.

[e]Quenching constants were determined with the slopes of the fitting line in the Stern-Volmer plots.

[f]Calculated according to the reference 13.

[g]n.d. = not determined because of too weak interaction.

Figure 5. Stern-Volmer plots with the solution containing 20 μM base-selective fluorescent ligands in the POSS network polymers (POSS-G network (a), POSS-U network (c), and POSS-A network (e)) by adding various kinds of nucleotides. The plots for determining the binding constants between the ligands (POSS-G network (b), POSS-U network (d), and POSS-A network (f)) and nucleobases according to the above equation. The slopes represent the number of the binding nucleotides. The y-intercepts represent the logK_A values. The lines are prepared with the least-square method.

The binding selectivity and affinity of the ligand-modified POSS network polymers for a particular target base were evaluated by fluorescence titration experiments (Figure 6). The POSS-G networks exhibited significant decreases of fluorescence emissions by the complex formations with the GTP and CTP, whereas slight changes in the fluorescence intensity of the ligands were observed with UTP and ATP (Figure 6a). The quenching efficiencies were depended on the target base with the order of CTP > GTP > ATP > UTP (Figure 6b). In contrast, strong fluorescence quenching of the POSS-U networks was observed in the presence of ATP, while hardly changes of the ligands in the fluorescence intensity were observed for the GTP, CTP, and UTP (Figure 6c). In addition, fluorescence of POSS-A networks was greatly quenched by UTP, and slight quenching was induced by CTP and ATP as shown in Figure 6d. These enhanced discrimination abilities of POSS-G, POSS-U, and POSS-A network polymers are likely because the introduction of the specific ligands having the different hydrogen-bonding sites to the POSS network polymers can enhance the selectivity of the recognition to the target base molecules. However, it should be mentioned that the quenching efficiency of the designed ligands to the target molecules was greatly improved by the water-soluble POSS network polymers. For instance, the quenching efficiency of POSS-G network for CTP was 45%. Moreover, the efficiencies of POSS-U network/ATP and POSS-A network/UTP were 41% and 49%, respectively.
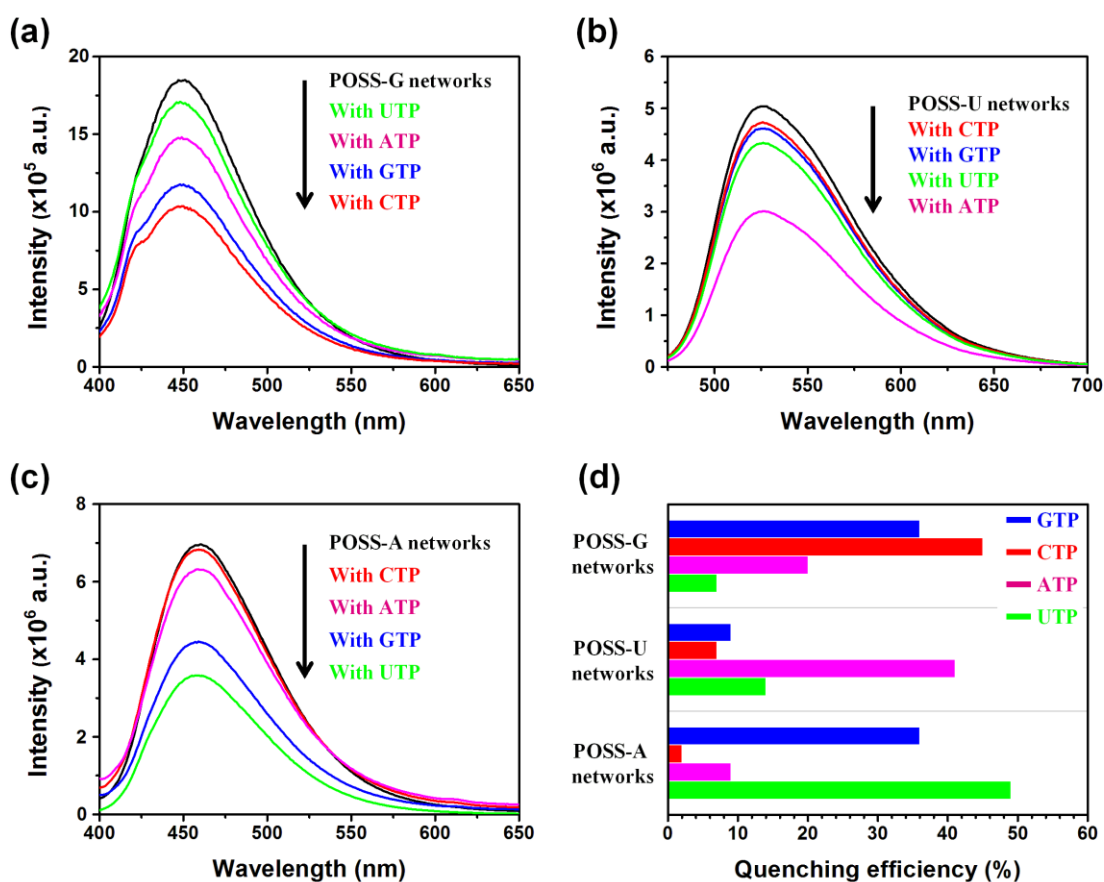
Figure 6. Fluorescence spectra of (a) POSS-G networks, (b) POSS-U networks, and (c) POSS-A networks in the absence and presence of different flanking nucleotides. (d) Comparison of fluorescence quenching efficiencies of POSS network ligands in the absence and presence of nucleobases. [Ligand] = 20 μM, [Nucleobase] = 200 μM in PBS buffer solution (pH 7.4) at 25 °C.

Conclusion

The recognition systems for ATP, CTP, and UTP can be obtained using the water-soluble POSS network polymers. By the enhancement effect originated from the hydrophobic spaces of POSS, the precise and robust complexation via hydrogen bonds between the ligand and the target nucleobase can be observed. Finally, the selectivity can be tuned by replacing the

ligand inside the network polymers. These materials might be directly applicable for producing the recognition unit in artificial receptors or enzymes as demonstrated in the previous chapters. Moreover, based on this strategy, other bio-significant molecules could be captured, leading to the development of the novel biotechnological tools or drugs.

References

1. Strack, G.; Bocharova, V.; A. Arugula, M.; Pita, Marcos.; Halámek, J.; Katz, E. *J. Phys. Chem. Lett.* **2010**, *1*, 839.

2. Ho, M. Y. K.; Rechnitz, G. A. *Anal. Chem.* **1987**, *59*, 536.

3. Yu, T.; Wang, W.; Chen, J.; Zeng, Y.; Li, Y.; Yang, G.; Li, Yi. *J. Phys. Chem. C* **2012**, *116*, 10516.

4. Orozco, J.; García-Gradilla, V.; D'Agostino, M.; Gao, W.; Cortés, A.; Wang, J. *ACS Nano* **2013**, *7*, 818.

5. Gharibi, H.; Moosavi-Movahedi, Z.; Javadian, S.; Nazari, K.; A. Moosavi-Movahedi, A. *J. Phys. Chem. B* **2011**, *115*, 4671.

6. Zhang, L.; Zhang, L.; Luo, T.; Zhou, J.; Sun, L.; Xu, Y. *ACS Comb. Sci.* **2012**, *14*, 108.

7. Gao, Y.; Katsuraya, K.; Kaneko, Y.; Mimura, T.; Nakashima, H.; Uryu, T.; *Macromolecules* **1999**, *32*, 8319.

8. Tong, W.; Lu, C-D.; K. Sharma, S.; Matsuura, S.; G. So, A.; A. Scott, Walter. *Biochemistry* **1997**, *36*, 5749.

9.   Giacalone, G.; Bochot, A.; Fattal, E.; Hillaireau, H. *Biomacromolecules* **2013**, *14*, 737.

10. Tanaka, K.; Murakami, M.; Jeon, J-H.; Chujo, Y. *Org. Biomol.Chem.* **2012**, *10*, 90.

11. McCormick, D. B. *J. Heterocyclic Chem.* **1970**, *7*, 447.

12. R. Piper, J.; A. Montgomery, J. *J. Org. Chem.* **1977**, *42*, 208.

13. Newkome, R. G.; Garbis, J. S.; Majestic, K. V.; Fronczek, R. F.; Chiari, G. *J. Org. Chem.* **1981**, *46*, 833.

List of Publications

Chapter 1

POSS Ionic Liquid Crystals

Kazuo Tanaka, Fumiyasu Ishiguro, Jong-Hwan Jeon, Tatsuhiro Hiraoka, and Yoshiki Chujo

To be submitted.

Chapter 2

POSS Fillers for Modulating Thermal Properties of Ionic Liquids

Jong-Hwan Jeon, Kazuo Tanaka, and Yoshiki Chujo

RSC Adv. **2013**, *3,* 2422-2427.

Chapter 3

Synthesis of Sulfonic Acid-Containing POSS and Its Filler Effects for Enhancing Thermal Stabilities and Lowering Melting Temperatures of Ionic Liquids

Jong-Hwan Jeon, Kazuo Tanaka, and Yoshiki Chujo

To be submitted.

Chapter 4

Rational Design of POSS Fillers for Simultaneous Improvements of Thermomechanical Properties and Lowering Refractive Indices of Polymer Films

Jong-Hwan Jeon, Kazuo Tanaka, and Yoshiki Chujo

J. Polym. Sci. Part A: Polym. Chem. **2013**, *51*, in press.

Chapter 5

Enhancement of Optical Properties of Dyes for Bioprobes by Freezing Effect of Molecular Motion Using POSS-Core Dendrimers

Kazuo Tanaka, Jong-Hwan Jeon, Kenichi Inafuku, and Yoshiki Chujo

Bioorg. Med. Chem. **2012**, *20*, 915-919.

Chapter 6

Enhancement of Affinity in Molecular Recognition via Hydrogen Bonds by POSS-Core Dendrimer and Its Application for Selective Complex Formation between Guanosine Triphosphate and 1,8-Naphthyridine Derivatives

Kazuo Tanaka, Masahiro Murakami, Jong-Hwan Jeon, and Yoshiki Chujo

Org. Biomol. Chem. **2012**, *10*, 90-95.

Chapter 7

Construction of Light-Driven Artificial Enzymes for Selective Oxidation of Guanosine Triphosphate Using Water-Soluble POSS Network Polymers

Jong-Hwan Jeon, Kazuo Tanaka, and Yoshiki Chujo

To be submitted.

Chapter 8

Synthesis of Water-Soluble POSS Network Polymers and Its Application for Selective Complex Formation between the Designed Ligands and a Nucleobase

Jong-Hwan Jeon, Kazuo Tanaka, and Yoshiki Chujo

To be submitted.

Other publications not included in this thesis

Polyhedral Oligomeric Silsesquioxane (POSS)-Based Fluorescent ON-OFF Probes for the Detection of a Nucleobase

Jong-Hwan Jeon, Kazuo Tanaka, and Yoshiki Chujo

To be submitted.

Preparation of Inorganic/Organic Hybrid Polymers Based on Polyhedral Oligomeric Silsesquioxanes and Its Application for Simultaneous Improvements of Thermomechanical Properties and Lowering Refractive Indices of Polymer Films

Jong-Hwan Jeon, Kazuo Tanaka, and Yoshiki Chujo

To be submitted.

Thermomechanical Properties of Polypropylenes Containing Tethered and Untethered Polyhedral Oligomeric Silsesquioxanes (POSSs)

Jong-Hwan Jeon, Kazuo Tanaka, and Yoshiki Chujo

To be submitted.

Adamantane Ionic Liquids

Kazuo Tanaka, Tatsuhiro Hiraoka, Jong-Hwan Jeon, and Yoshiki Chujo

To be submitted.

Hypoxic Condition-Selective Upconversion via Triplet-Triplet Annihilation Based on POSS-Core Dendrimer Complexes

Kazuo Tanaka, Hiroshi Okada, Wataru Ohashi, Jong-Hwan Jeon, Kenichi Inafuku, and Yoshiki Chujo

Bioorg. Med. Chem. **2013**, *21*, 2678-2681.

Selective Complex Formation between Guanosine Triphosphate and Naphthyridine-Modified POSS

Kazuo Tanaka, Jong-Hwan Jeon, and Yoshiki Chujo

Photomed. Photobiol. **2012***, 34,* 57-58.

Synthesis and Characterization of Hybrid Nanocomposites of Pd Nanoparticles Containing POSS(Pd-POSS) and Poly(acrylic acid) via Ionic Interactions

Jong-Hwan Jeon, Jung-Hyurk Lim, Yoshiki Chujo, and Kyung-Min Kim

Polymer (Korea) **2009**, *33*, 615-619.